January 2014

A Study Of Bench Scale, Pressurized, Continuous Flow Thermal Cracking Of Crop Oil

Blake Sander

A STUDY OF BENCH SCALE, PRESSURIZED, CONTINUOUS FLOW THERMAL CRACKING OF CROP OIL

by

Blake Sander
Bachelor of Science, North Dakota State University, 1994

A Thesis
Submitted to the Graduate Faculty
of the
University of North Dakota
in partial fulfillment of the requirements
for the degree of
Master of Science

Grand Forks, North Dakota
May
2014

This thesis, submitted by Blake Sander in partial fulfillment of the requirements for the Degree of Master of Science from the University of North Dakota, has been read by the Faculty Advisory Committee under whom the work has been done and is hereby approved.

Dr. Wayne Seames
Chair

Dr. Evguenii Kozliak
Committee Member

Dr. Robert Wills
Committee Member

This thesis meets the standards for appearance, conforms to the style and format requirements of the Graduate School of the University of North Dakota, and is hereby approved.

Dr. Wayne Swisher
Dean of the School of Graduate Studies

April 28, 2014
Date

PERMISSION

Title	A Study of Bench Scale, Pressurized, Continuous Flow Thermal Cracking of Crop Oil
Department	Chemical Engineering
Degree	Master of Science

In presenting this thesis in partial fulfillment of the requirements for a graduate degree from the University of North Dakota, I agree that the library of this University shall make it freely available for inspection. I further agree that permission for extensive copying for scholarly purposes may be granted by the professor who supervised my thesis work or, in his absence, by the chairperson of the department or the dean of the Graduate School. It is understood that any copying or publication or other use of this thesis or part thereof for financial gain shall not be allowed without my written permission. It is also understood that due recognition shall be given to me and to the University of North Dakota in any scholarly use which may be made of any material in my thesis.

Blake Sander
06 March 2014

TABLE OF CONTENTS

LIST OF FIGURES

Figure Page

LIST OF TABLES

ACKNOWLEDGMENTS

I would like to express my appreciation and thanks to my advisor Dr. Wayne Seames, you have challenged me immensely. I will draw upon this life changing accomplishment as a source of personal strength and pride for the remainder of my lifetime, thank you for that.

I would also like to thank Dr. Evguenii Kozliak and Dr. Robert Wills for serving as my committee members. Dr. Kozliak, I appreciated the chemistry insight. Dr. Wills, thanks for taking the time to be on my committee. Thank you both for your comments and suggestions.

I also want to thank the Chemical Engineering Department's ingenious shop staff, David Hirschmann and Joe Miller. You guys were instrumental in building the reactor system, and a joy to work with, much thanks to you both.

I also wish to acknowledge the assistance provided by Dr. Alena Kubatova and the UND Chemistry Department. Their analytical chemistry expertise was an essential component to this work.

Lastly, I want to acknowledge the assistance provided by Inna Sakodinskaya, and the summer interns from Cal Poly Pomona; Robert Mota, Elizabeth Scott, and David Rodriguez.

To Abby

You are greatly missed.

ABSTRACT

This study builds upon previous research at UND which demonstrated that crop oils are a potential renewable alternative to select petroleum based products. The crop oils investigated for this study include soybean, canola, and jojoba oil. The processing method utilized was a non-catalytic cracking process.

The goal of this work was to build a new bench-scale continuous flow thermal cracking reactor system capable of being operated under high pressure, and also to use this reactor to explore the effects of pressure, temperature, and feed rate during non-catalytic cracking on the yield and composition of the liquid and gas products produced from the three crop oil feedstocks studied.

The reactor developed for this work was a 9.7 L bench scale, continuous stirred tank unit. The continuous flow and scale of this design is significant, as published research into the thermal cracking of crop oils has focused on utilization of batch reactors and lab scale continuous flow reactors.

A split-plot full factorial experimental design was used to study the effects of pressure, temperature and feed rate on soybean oil feedstock. For these experiments, pressures ranged from 1.38 to 2.76 MPa gauge (200 to 400 psig), temperatures ranged from 400 to 420°C, and feed rates were 4.0 to 7.0 L/hr (0.41 to 0.72 liquid hourly space velocity (LHSV)). In addition, a side by side comparison among soybean, canola, and

jojoba oil feedstocks at thermal cracking conditions of 1.38 MPa gauge (200 psig), 420°C, and 4.0 L/hr were conducted.

Design of Experiments (DOE) response measurements included with this work are liquid distillate yields, liquid product acid number, gas product constituent yields, and gas product constituent molar concentrations.

The DOE significant findings showed that soybean oil middle distillate (150 to 250°C) product yield was favored at lower pressure (1.38 MPa gauge (200 psig)), higher temperature (420°C), and lower feed rate (4L/hr), and that all three variables were significant factors per the DOE. Acid number testing did not correlate with the level of liquid product decarboxylation, and ethylene was the only gas product yield identified with pressure as a significant factor per the DOE. A non-DOE finding suggests that pressure can be used to favor alkane over alkene products

The side by side comparison of soybean, canola, and jojoba oil feedstock showed that the predominate C_{42} wax esters of jojoba oil proved much less responsive to thermal degradation than the predominant C18:2 polyunsaturated fatty acids of soybean oil and C18:1 mono unsaturated fatty acids of canola oil.

CHAPTER I
INTRODUCTION

Researchers at UND have been working on developing a means to convert crop oils to liquid fuel grade products, as a renewable alternative to traditional petroleum based liquid fuels. The method being explored is a cracking process, where high molecular weight organic compounds are cleaved into smaller organic chemicals. The petroleum industry developed the cracking process post World War I, and use it extensively to upgrade the physical and chemical properties of heavy petroleum oil feed stocks.

Prior UND research has demonstrated that both thermal cracking and catalytic cracking processes can be used to upgrade vegetable oil to aviation grade liquid fuels [1] [2] through the use of 500 mL and 1 L batch reactors. Also, a bench scale plug flow reactor (PFR) study was initiated during the summer of 2007 to build upon the success of the previous batch reactor studies, but the PFR study unexpectedly produced a liquid product that was high in olefins (alkenes), which are undesirable in liquid fuels due to poor thermal stability and tendency to readily combine to form gum.

This work was initiated to try and address problems with olefin product generation in the previous UND PFR study. The previous PFR reactor was operated at low pressures, typically less than 0.34 MPa gauge (50 psig), and it was postulated that olefins generated during liquid phase cracking lacked sufficient gas phase residence time

under these low pressure conditions to further react to alkanes and aromatics, which are more desirable liquid fuel compounds.

The goal of this work was to build a new reactor system capable of being operated under high pressure (3.45 MPa gauge (500 psig)), and explore the thermal cracking effects of pressure, temperature, and feed rate on the characterization of the liquid and gas products generated from crop oil feed stocks. The continuous flow and bench scale design of this work was significant, as published research into the thermal cracking of crop oils has focused on utilization of batch and lab scale continuous flow reactors. Another significant aspect of this work was to examine the effects of pressure on the thermal cracking of crop oils, an area of study void of published research.

Chapter II presents the background of the study conducted, which includes information about crop oil chemical properties, world crop oil production statistics, and preliminary research work carried out prior to this study.

Chapter III presents a literature review on published crop oil thermal cracking research. This chapter takes a look at the proposed thermal cracking reaction schemes offered by the authors, and summarizes the observed effects of temperature, residence time, pressure, and oil chemistry on the reaction products.

Chapter IV provides the information of the experimental set up, and details the procedures and calculations used in performing the experimental runs. This chapter also covers the physical and chemical analysis procedures used on the products generated under this work.

Chapter V covers the statistically guided experimental design used in this study, and presents the results from the statistical analysis. This work used a split-plot full

factorial experimental design, and studied the effect of pressure, temperature, and feed rate on the thermal cracking of soybean oil. This chapter also presents finds on how the thermal cracking behavior of soybean, canola, and jojoba oil compare and differ.

Finally, Chapter VI presents a summary of the findings and conclusions.

CHAPTER II
BACKGROUND

Crop Oils

A triglyceride, also commonly referred to as a crop oil molecule, consists of three fatty acid groups attached to a single glycerol group as illustrated in Figure 1. The most common oil molecules are mixed triglycerides, in which a single oil molecule is constructed with up to three different fatty acid groups.

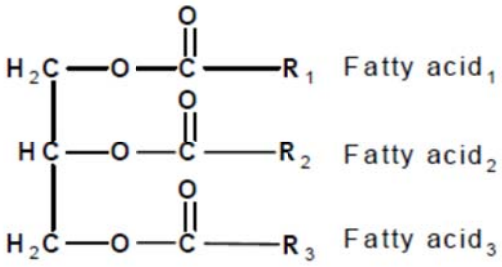

Figure 1. Typical crop oil (mixed triglyceride) molecule [3]

The fatty acid moieties are classified by carbon content and the number of carbon-carbon double bonds present. Saturated fatty acids contain only single carbon - carbon bonds, whereas unsaturated fatty acids contain one (monounsaturated) or more (polyunsaturated) carbon - carbon double bonds. Saturated and unsaturated carbon bonds are illustrated in Figure 2.

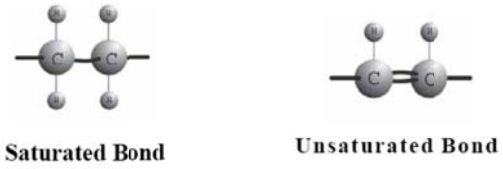

Figure 2. Structure of a saturated and unsaturated fatty acid [3]

For common crop oil fatty acids with two or more double bonds, the double bond locations will occupy non-conjugated positions as illustrated in Figure 3. For example, linoleic acid ($C_{18:2}$), listed in Table 1 contains two double bond sites located at the 9 and 12 carbon positions.

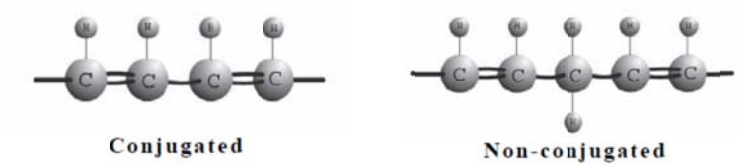

Figure 3. Polyunsaturated fatty acid bond positions [3]

In addition to the relative position of the multiple double bond sites, the carbon-carbon double bonds can take on one of two isomer forms, cis or trans, as illustrated in Figure 4.

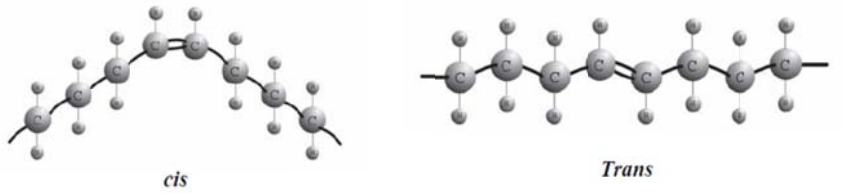

Figure 4. Carbon double bond configurations [3]

Following the previous example, linoleic acid listed in Table 1 contains a cis double bond structure. The cis structure exists in most naturally occurring unsaturated fatty acids, and is the reason for a triglyceride's liquid state at room temperature.

Table 1. Chemical name and structure of common fatty acids

Systematic Name	Common Name	Structure $C_{a:b}$
Butanoic	Butyric	$C_{4:0}$
Hexanoic	Caproic	$C_{6:0}$
Octanoic	Caprylic	$C_{8:0}$
Decanoic	Capric	$C_{10:0}$
cis 9-Decenoic	Caproleic	$C_{10:1}$
Dodecanoic	Lauric	$C_{12:0}$
cis 9-Dodecenoic	Lauroleic	$C_{12:1}$
Tetradecanoic	Myristic	$C_{14:0}$
cis 9-Tetradecenoic	Myristoleic	$C_{14:1}$
Hexadecanoic	Palmitic	$C_{16:0}$
cis 9-Hexadecenoic	Palmitoleic	$C_{16:1}$
Octadecanoic	Stearic	$C_{18:0}$
cis 9-Octadecenoic	Oleic	$C_{18:1}$
cis 9-cis 12-Octadecadienoic	Linoleic	$C_{18:2}$
cis 9-cis 12-cis 15-Octadecatrienoic	Linolenic	$C_{18:3}$
Eicosanoic	Arachidic	$C_{20:0}$
cis 9-Eicosenoic	Gadoleic	$C_{20:1}$
Docosanoic	Behenic	$C_{22:0}$
cis 13-Docosenoic	Erucic	$C_{22:1}$

a – number of carbon atoms
b – number of double bonds

As previously mentioned, crop oils are mixed triglycerides, composed of two or more different fatty acid types in varying degrees of composition. A listing of the fatty acid makeup for the most popular crop oils produced in the world is provided in Table 2.

Table 2. Typical fatty acid composition of major world crop oils (mole % of total fatty acids) [3]

	Caproic	Caprylic	Capric	Lauric	Myristic	Palmitic	Stearic	Arachidic	Behenic	Lignoceric	Palmitoleic	Oleic	Gadoleic	Linoleic	Linolenic
	Saturated										Mono Unsaturated			Poly Unsaturated	
*	6:0	8:0	10:0	12:0	14:0	16:0	18:0	20:0	22:0	24:0	16:1	18:1	20:1	18:2	18:3
Coconut	1	8	6	47	18	9	3					6		2	
Cottonseed					1	22	3				1	19		54	1
Olive						13	3	1			1	71		10	
Palm					1	45	4					40		10	
Palm Kernel		3	4	48	16	8	3					15		2	
Peanut						11	2	1	3	2		48	2	32	
High Oleic Canola						4	2					75		17	2
Soybean						11	4					24		54	
Sunflower						7	5					19		68	1

*number of carbon atoms : number of double bonds

The leading vegetable oil types produced in the world are illustrated in Figure 5. Palm, soybean, and canola oil combined accounted for roughly 76% of world vegetable oil production in 2009-10. Indonesia and Malaysia are the lead producers of palm oil, accounting for 21.0 and 17.8, respectively of 44.8 million metric tons (MMT), or a combined 87% of world palm oil production in 2009-10 [4].

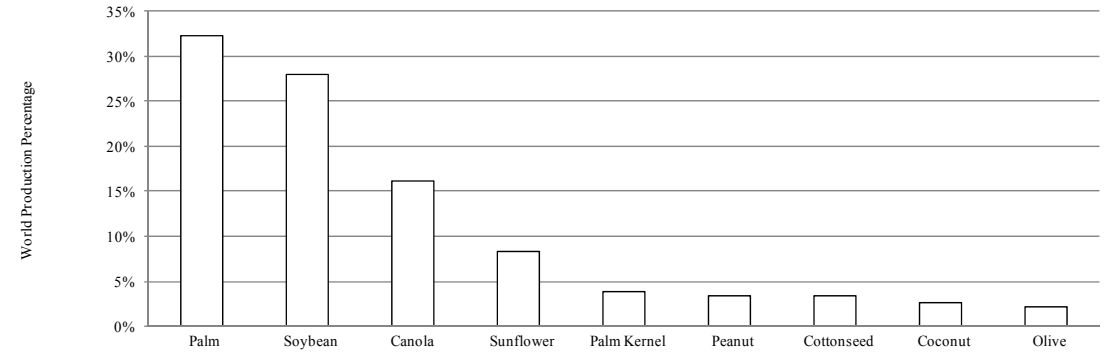

Figure 5. Major vegetable oils world annual production (2009-10) [4]

In the United States, soybean oil is of interest for the production of bio-based hydrocarbon products due to its domestic availability. Figure 6 shows that the United States led the world in 2009-10 soybean production at 91.4 MMT, or about 35% of world production, followed by Brazil at 69.0 MMT (26.5%) and Argentina at 54.5 MMT (21.0%).

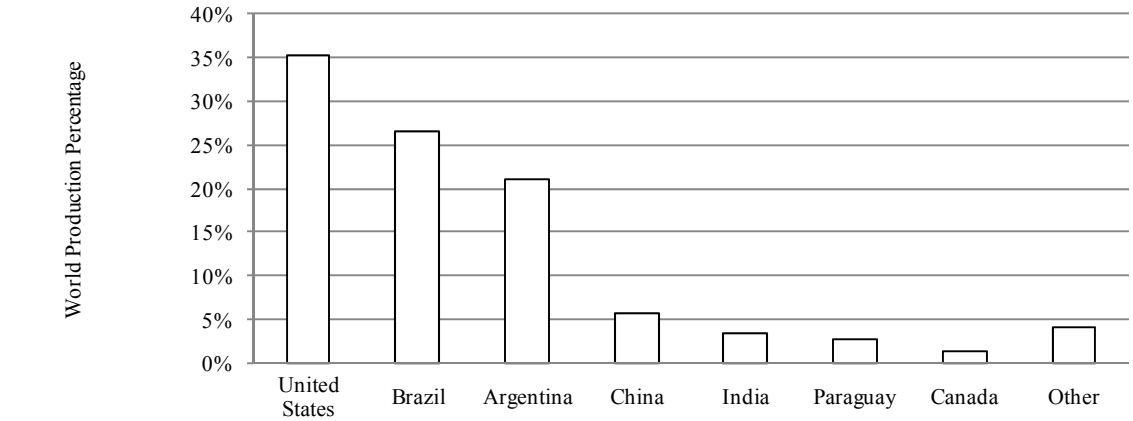

Figure 6. World soybean production [4]

In addition to being a top soybean producer, the United States is a major soybean processor. Figure 7 shows that the United States produced 8.90 MMT of soybean oil in 2009-10, or 23.0% of the world soybean oil supply. China, the top soybean importer, was a close second in soybean oil production at 8.70 MMT.

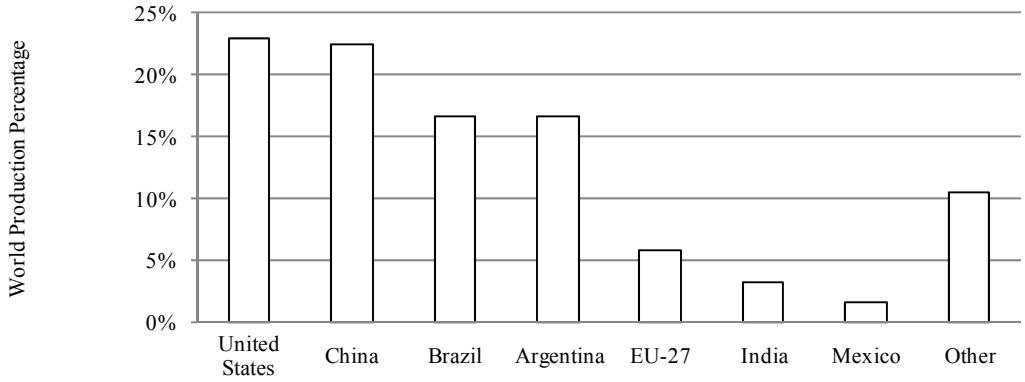

Figure 7. World soybean oil production [4]

Canola, the third leading crop oil produced in the world, is of regional interest to North Dakota. Figure 8 shows that the United States accounted for only 0.7 MMT, or 1.1% of world canola production in 2009-10. Canola however is regionally produced with North Dakota accounting for about 90% of the United States domestic supply. Couple this with North Dakota's close proximity to the number three world producer in Canada, and canola is an attractive regionally available crop oil source.

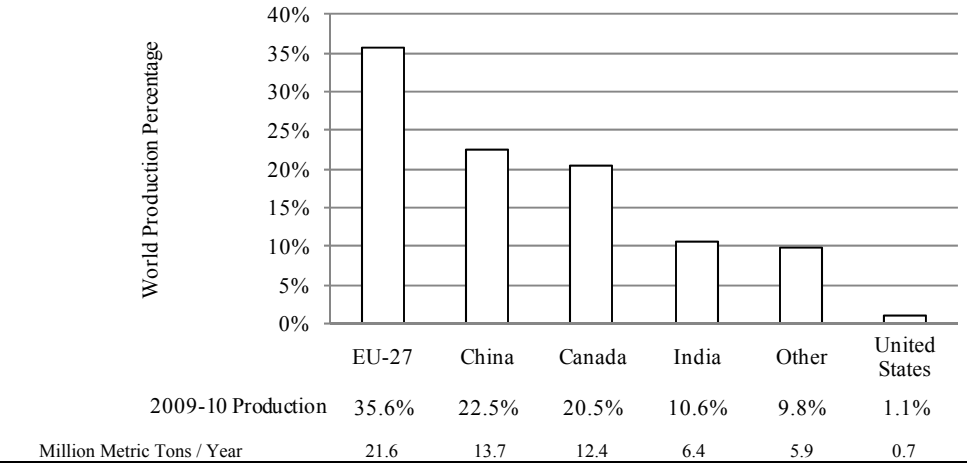

Figure 8. World canola production [4]

Vegetable oils are an energy dense product. For example, the typical heat content of raw crop oil products is approximately 80-90% of No. 2 diesel fuel [5]. This high energy density along with their liquid nature make vegetable oils an attractive energy source. The commercialization of vegetable oil fuels however has been hindered by inferior fuel properties including low volatility, high viscosity, and poor stability. To overcome these disadvantages, vegetable oils require processing to change their chemical makeup and improve their physical properties [5].

Currently, the most popular processing method to improve the physical properties of crop oils for use as a fuel or petrochemical feedstock is transesterification. The transesterification process illustrated in Figure 9 involves the reaction of one triglyceride molecule with three alcohol molecules, typically methanol or ethanol, in the presence of a strong base catalyst, producing a mixture of alkyl esters and glycerol. Although an improvement over the properties of straight vegetable oils, the alkyl ester liquid fuels exhibit poor cold flow properties, and the presence of oxygen is detrimental to the fuel's heat content and stability [5].

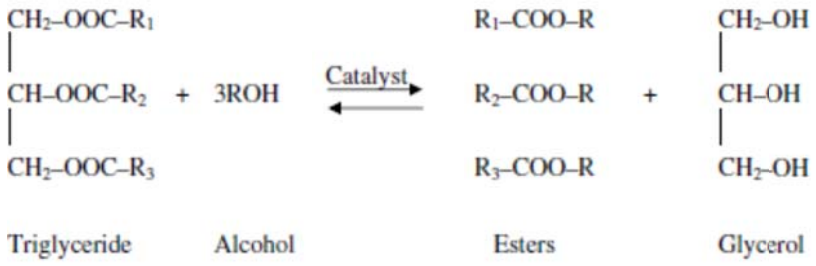

Figure 9. Transesterification of a triglyceride molecule with alcohol [6]

The thermal cracking process is an alternative method being examined by UND researchers for the purpose of upgrading vegetable oil for use in liquid fuel and chemical

applications. The thermal cracking process involves the application of heat energy to hydrocarbon based molecules, resulting in molecular decomposition by way of carbon-carbon bond cleavage.

The thermal cracking process was developed for use in the petroleum industry post World War I to meet increased gasoline demand. Prior to the thermal cracking process, gasoline fraction hydrocarbons were produced by single pass distillation of crude oil feedstocks. This single pass distillation of crude oil produced a highly marketable light fraction for generating gasoline, but also a heavy oil fraction with little market demand or value. To meet the growing need for gasoline grade distillates, refiners incorporated the thermal cracking process to upgrade the heavy oil fraction from higher molecular weight materials to lower molecular weight products. The result was an increase in gasoline yield from a barrel of crude oil, and superior automobile engine performance due to the chemical changes in the hydrocarbon structure that took place during the thermal cracking process. World War II brought about additional petroleum oil refinery advancements through the use of the catalytic cracking process, making further improvements to the quality and supply of transportation liquid fuels [7].

Researchers at UND have demonstrated that both thermal cracking and catalytic cracking processes can be used to upgrade vegetable oil to aviation grade liquid fuels [1] [2]. This promising research was carried out with 500 mL and 1 L batch reactors.

Prior research at UND also included construction of a bench scale plug flow reactor (PFR) during the summer of 2007 to build upon the success of the batch reactor results. Unexpectedly, the liquid products from the PFR were high in olefins, which are

undesirable in liquid fuels due to poor thermal stability and tendency to readily combine to form gum.

The previous PFR reactor was operated at low pressures, typically less than 0.34 MPa gauge (50 psig), and it was postulated that olefins generated during liquid phase cracking lacked sufficient gas phase residence time under these low pressure conditions to further react to alkanes and aromatics, which are more desirable liquid fuel compounds. This reasoning correlates with recognized practice in the oil refining industry where it has been established that olefinic products are produced at lower pressures (<200 psia), and that paraffinic liquid fuel grade products are produced at high pressures (350-1500 psia) [7].

Based on this assumption that pressure may help address the problem with olefin products with the PFR reactor, a revised continuous stirred tank reactor CSTR reactor design was pursued in the fall of 2008. The objective was to build a CSTR capable of being operated at pressures up to 3.45 MPa gauge (500 psig). The new CSTR reactor also incorporated design changes to overcome operational shortcomings with the previous PFR reactor such as poor feed rate control, poor temperature control, leakage issues, coking, and maintenance shortcomings that hindered experimental efforts and long term continuous operation.

A preliminary experiment comparing the PFR and CSTR was conducted in December 2008. An analysis of the liquid product was performed that compared linear C9-C18 alkane products, and linear C9-C18 alkene products with double carbon bonds in the terminal position. Under identical conditions of 420°C, 0.7 liquid hourly space velocity (LHSV), and 0.34 MPa gauge (50 psig), the new CSTR design produced a liquid

product with an 87% increase in C9-C18 alkane yield (by weight), and 30% reduction in C9-C18 alkene yield (by weight). A second comparison with the PFR at 0.34 MPa gauge (50 psig) vs the CSTR at 2.07 MPa gauge (300 psig), with both run under identical temperature of 420°C and LHSV of 0.7/hr, indicated a 210% increase in C9-C18 alkane yield and 65% reduction in C9-C18 alkene yield by weight with the CSTR.

These preliminary results with the new CSTR reactor appeared to support the hypothesis that reactor design and pressure could be used to reduce olefinic liquid products, and led to the work presented in this thesis.

CHAPTER III
LITERATURE REVIEW

Research into the thermal cracking of crop oils for the production of renewable fuels and chemicals lags bio-oil and bio-diesel research. However, political and economic factors over the past three decades have revived interest in the thermal cracking process as a means to convert vegetable oils to renewable fuel and chemical products [5]. The use of flow reactors for studies involving the thermal cracking of vegetable oils is limited, and Idem et al. claimed in 1996 to be the first to report such work [8]. Past cracking studies have been typically carried out in batch reactors, at temperatures from 300-500°C, and at atmospheric pressure. Areas of opportunity in thermal cracking research include fatty acid cracking behavior, reaction optimization, detailed characterization of reaction products, reaction product properties, and scale-up [5].

Thermal Cracking Reaction Mechanisms

Rice and Kossiakoff (R-K) examined high temperature (>600°C) and low pressure (atmospheric) hydrocarbon pyrolysis in 1943. They proposed a free radical reaction mechanism for hydrocarbon pyrolysis known as the R-K mechanism. The R-K mechanism predicts that alkyl radicals undergo successive unimolecular decomposition by β-scission. For example, with n-hexadecane as the parent molecule, the R-K mechanism predicts that decomposition by β-scission will result in methane, ethane, and C_2 to C_{15} α-olefins products. It has been shown that radical decomposition reactions are favored at higher temperatures and lower pressure [9].

Fabuss, Satterfield, and Smith (FSS) examined the thermal cracking of n-hexadecane at elevated temperature (550-600°C) and pressure (1-7 MPa) in 1962. They observed C_2 to C_{14} n-alkane products, which the R-K mechanism does not predict. They proposed modification to the R-K mechanism to account for the generation of alkane products, illustrated in Figure 10. The proposed one-step FSS mechanism accounts for n-alkane products by participation of n-alkyl radicals in hydrogen abstraction reactions, as illustrated in equation (3). For example, with n-C_{16} as the parent molecule, the FSS mechanism predicts equimolar distribution for n-alkanes and α-olefins. It has been observed that high pressure favors the bimolecular reactions of both radical addition and hydrogen abstraction [10].

$$\text{n-}C_{16} + R_1\bullet \rightarrow R_1H + \text{n-}C_{16}\bullet \quad (1)$$

$$\text{n-}C_{16}\bullet \rightarrow \text{1-}C_jH_{2j} + \text{n-}C_iH_{2i+1}\bullet \quad (2)$$

$$\text{n-}C_iH_{2i+1}\bullet + \text{n-}C_{16} \rightarrow \text{n-}C_iH_{2i+2} + \text{n-}C_{16}\bullet \quad (3)$$

Figure 10. FSS thermal cracking mechanism [10]

Chang and Wan studied the thermal cracking of the saturated triglyceride, tung oil, and proposed a reaction scheme in 1947 to account for their work. The scheme includes 16 reactions and is illustrated in Figure 11. They estimated that a large part of the fatty acids, acrolein and ketenes generated in reaction (1) are quickly decomposed in reaction (2) and reaction (3), and that hydrocarbon products compatible with gasoline fractions are generated in reactions (6) through (11) [5].

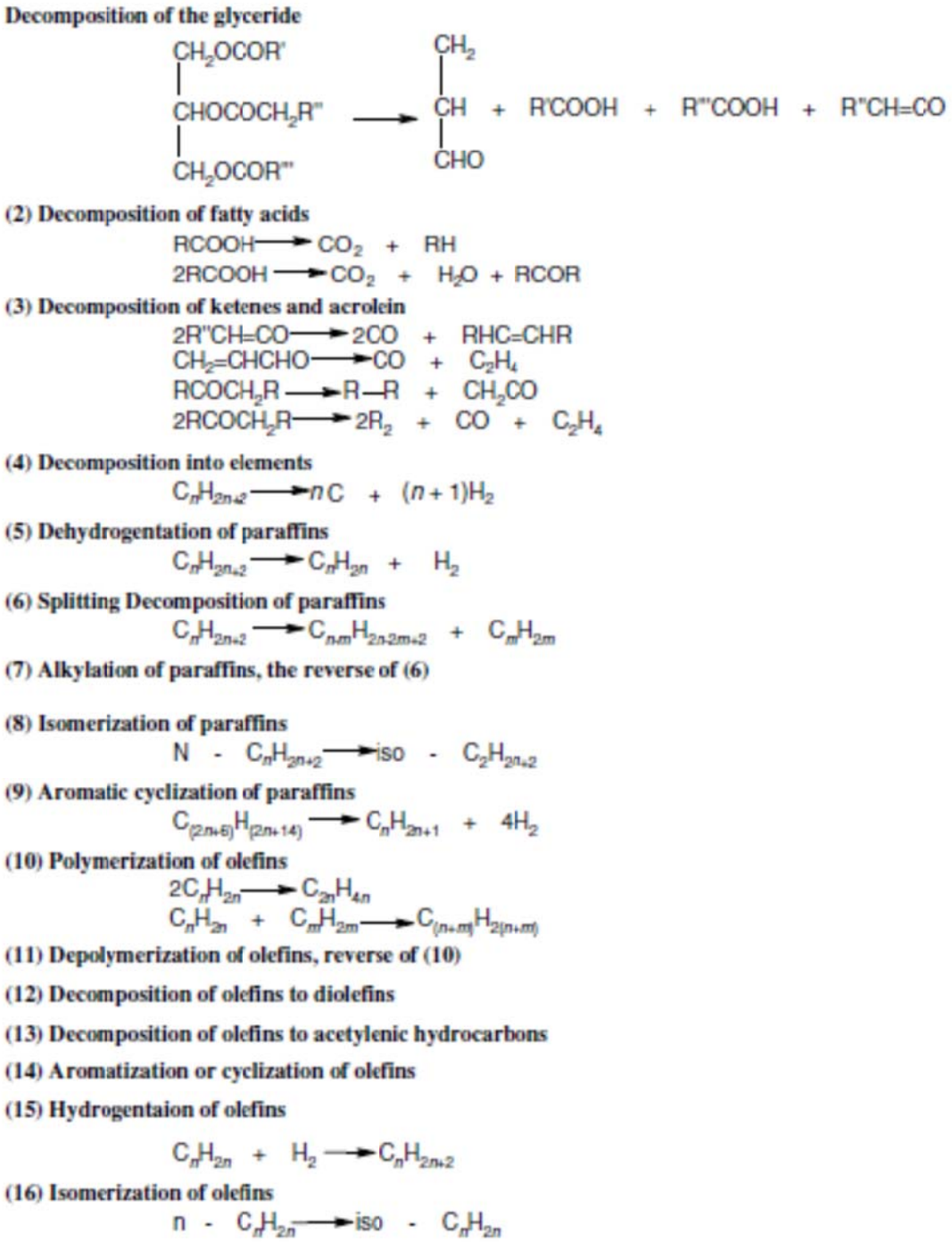

Figure 11. Reaction scheme for thermal cracking of a saturated triglyceride by Chang and Wan [11]

Alencar et al. [12] proposed a thermal cracking scheme for their work with saturated triglycerides in 1983, based on the reaction scheme put forward by Chang and Wan. They carried out cracking reactions from 300-500°C and at atmospheric pressure, utilizing saturated oils of babassu, piqui, and palm oil. The scheme by Alencar et al. is presented in Figure 12.

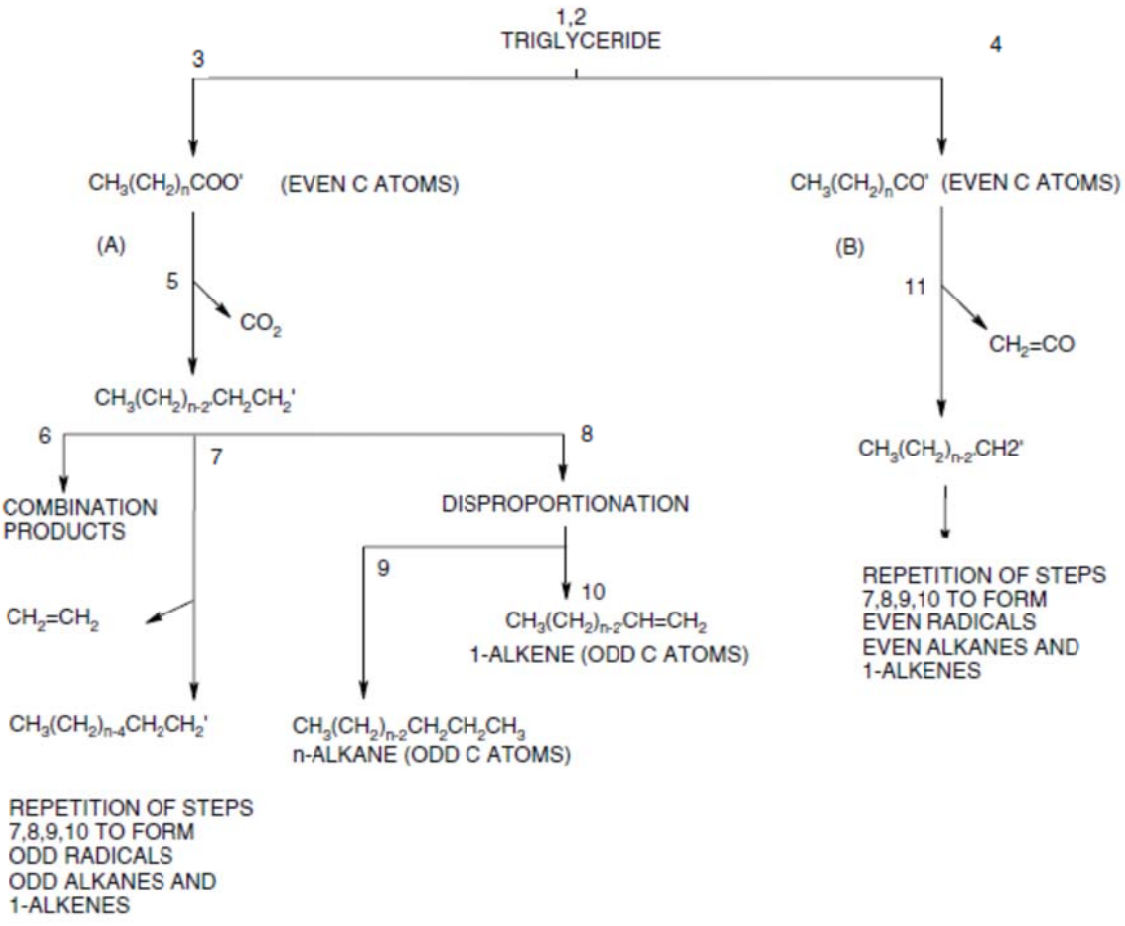

Figure 12. Reaction scheme for thermal cracking of a saturated triglyceride by Alencar et al. [12]

Referring to Figure 12, Alencar et al. predicted that triglyceride cracking produces free radicals (A) and (B), with decarboxylation of radical (A) resulting in odd n-alkanes

and 1-alkenes, and that the loss of a ketene from radical (B) would result in the formation of even alkanes and 1-alkenes. Both paths would be followed by ethylene elimination, and the chain termination step of disproportionation, meaning the transfer of a hydrogen atom from the beta position of one radical to another radical, resulting in the formation of an alkane and an alkene.

Schwab et al. [13] published their work with unsaturated triglycerides in 1988 and proposed a mechanism to address the formation of alkanes, alkenes, alkadienes, aromatics, and carboxylic acids products. The scheme is presented in Figure 13.

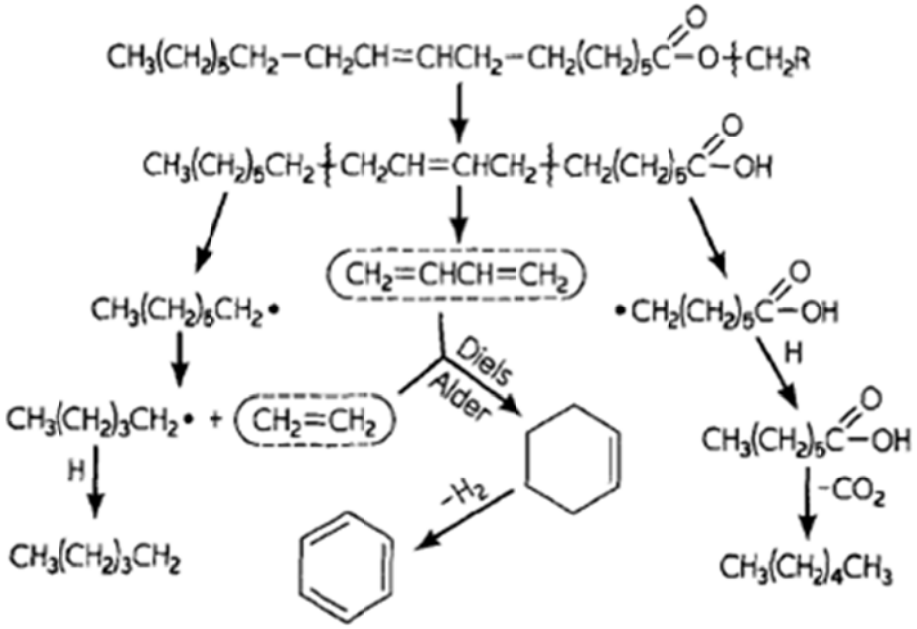

Figure 13. Reaction scheme for thermal cracking of an unsaturated triglyceride by Schwab et al. [13]

Based on the mechanism proposed by Schwab, thermal decomposition of fatty acids proceeds through either a free radical or carbonium ion mechanism, and for the most part follows the R-K mechanism previously mentioned. Triglyceride thermal

cracking results through the generation of an RCOO• radical, by cleavage of the fatty acid group from the triglyceride molecule, followed by decarboxylation. Unsaturated sites on the fatty acid enhance cleavage at the double bond β position, and is a dominate reaction. Schwab et al. accounted for aromatic formation by Diels-Alder ethylene addition to a conjugated diene.

Idem et al. [8] built upon the schemes of Alencar et al. and Schwab et al. to address their work on the continuous flow thermal cracking of canola oil in 1996. The reaction scheme is presented in Figure 14, and accounts for both saturated and unsaturated fatty acids. In this scheme, decarboxylation and decarbonylation can occur before or after C-C bond cleavage.

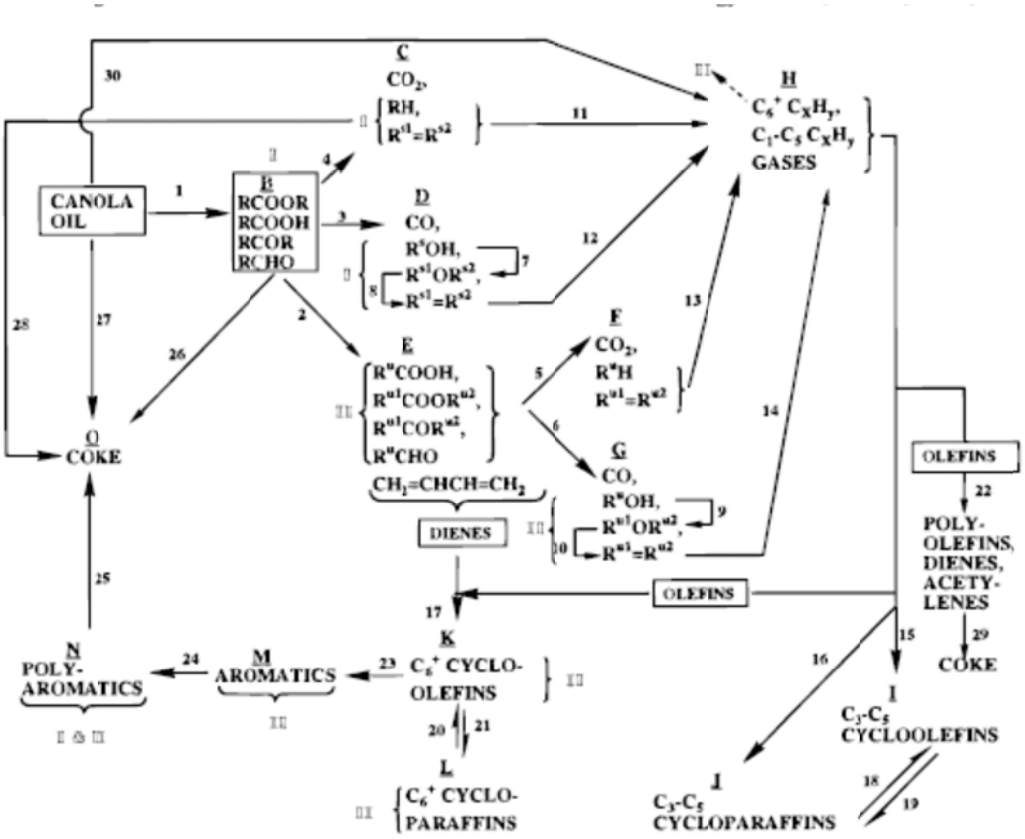

Figure 14. Reaction scheme for the thermal cracking of saturated and unsaturated triglycerides by Idem et al. [8]

Idem et al. identified decarboxylation, decarbonylation, and ketene elimination as dominant steps in the cracking of a triglyceride molecule (steps 3, 4, 5, and 6). Saturated fatty acids would favor decarboxylation, decarbonylation, and ketene elimination (steps 3 and 4) followed by C-C bond cleavage (11 and 12). Unsaturated fatty acids would favor C-C bond cleavage (step 2) followed by decarboxylation, decarbonylation, and ketene elimination (steps 5 and 6).

Idem et al. accounted for aromatic generation (step 23) by the elimination of hydrogen from C6+ cycloolefins at high temperatures.

A recent study by Kubatova et al. [14] with unsaturated triglycerides in 2012 provides an alternative cyclic product reaction scheme to the bimolecular Diels-Alder mechanism proposed by Schwab et al. The scheme is presented in Figure 15, and accounts for the formation of cyclic products via intramolecular cyclization of alkenyl radicals. Kubatova et al. observed that a depletion of alkenes was coupled by an accumulation of corresponding monocyclic hydrocarbons of identical carbon count.

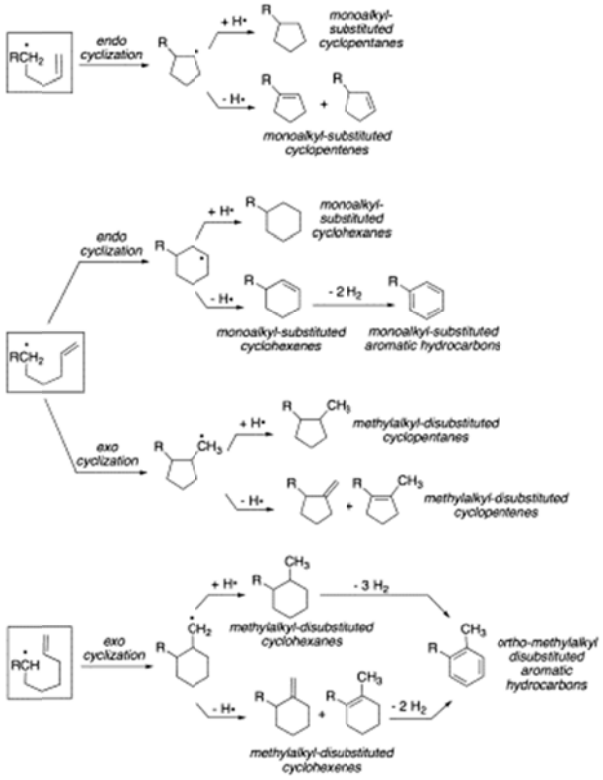

Figure 15. Cyclic product thermal cracking reaction scheme by Kubatova et al. [14]

Thermal Cracking Temperature Effects

In alkane thermal cracking studies, an increase in temperature favored radical forming decomposition reactions over bimolecular reactions. This was accounted for by

the difference in activation energies for the two competing pathways. Radical decomposition reactions tend to have higher activation energies than bimolecular reactions, and are therefore favored at higher temperatures. Higher temperatures were also shown to increase the generation rate of H_2 [10] [15].

Fatty acid thermal cracking studies showed that an increase in temperature has a positive effect on the conversion of the fatty acid feedstocks, and lead to the production of products with lower carbon numbers [16].

Individual gas phase products increased in yield with cracking temperature, also implying that the reactions that led to their formation are endothermic [8].

An increase in temperature has a positive effect on the generation of aromatics [16] [8]. It was also observed that dehydrogenation, a key reaction in the aromatization process, increases with temperature. Conversely, hydrogenation processes such as stabilization of hydrocarbon radicals, hydrogenation of alkenes to alkanes and cycloolefins to cycloparaffins become less pronounced with an increase in temperature [8].

It has also been reported that the initial decomposition of vegetable oils to heavy oxygenated hydrocarbons begins at temperatures in the range 240 to 300°C [8]. Also, Maher and Bressler established through computer simulation that cleavage between the glycerol backbone and the fatty acid begins at 288°C, and that C-C bond scission reactions are initiated at 400°C [5].

Residence Time Effect

Initial decomposition of triglyceride molecules into oxygenated hydrocarbons is not affected significantly by higher oil space velocity (lower residence times), although secondary cracking of these intermediate oxygenated hydrocarbons is affected negatively [8].

Higher residence times are favorable for subsequent decomposition of intermediate products (i.e. heavy oxygenated hydrocarbons), and have been shown to lower the carbon number of reaction products, leading to increased production of noncondensable gases, aromatics, and insoluble solids [16] [8]. In addition, reaction steps required for the formation of C6+ aliphatic hydrocarbons appear late in the reaction sequence, and increase with increased residence times [8].

Pressure Effect

Wu et al. reported that during the thermal cracking of n-hexadecane, the probability of bimolecular reactions, which favor alkane products, increases at higher pressures. They also reported that pressure has an effect on the rate and selectivity of alkane cracking. Bimolecular reaction rate increases faster than the unimolecular reaction rate as pressure is increased [15].

Farhad and Gray also carried out pressurized thermal cracking of n-hexadecane. They reported that high pressure favors bimolecular reactions (radical addition and hydrogen abstraction) over unimolecular radical decomposition. At high pressure (>10MPa) and relatively moderate temperatures (400°C), free radicals generated from decomposition of the parent radical are stabilized much faster by hydrogen abstraction than by decomposition via β-scission, resulting in equimolar distribution of n-alkanes and

low selectivity for gases. Low pressure favors the R-K mechanism, and ethylene is a major product in low-pressure pyrolysis of alkanes. They also proposed that under high density conditions, i.e. liquid phase reactions, addition reactions involving lower alkyl radicals are suppressed due to a cage effect [10].

Liquid / Gas Phase Effect

Wu et al. examined liquid versus gas phase thermal cracking of n-hexadecane. They found that cracking products are strongly dependent on reactant concentrations. They reported that reactant densities in liquid phase thermal cracking can be two orders of magnitude higher than gas phase densities, and thermal cracking products have been found to be dependent on reactant concentrations.

Wu et al. observed that liquid phase cracking favors free radical stabilization by bimolecular hydrogen abstraction over free radical decomposition via β-scission. Liquid phase cracking resulted in an equimolar distribution of alkanes to alkenes at low conversion, and a higher distribution of alkanes to alkenes at high conversion, respectively [15]. Khorasheh and Gray postulated that under high-density conditions, lower alkyl radical addition reactions may be suppressed due to a cage effect, and these radicals favor stabilization by way of hydrogen abstraction [10].

Wu et al. also observed that gas phase cracking favored alkene product generation to that of alkane products, indicating that gas phase cracking favors decomposition of large radicals by the unimolecular β-scission process [15].

Oil Effect

Maher and Bressler reported that the degree of fatty acid unsaturation has a significant effect on the cracking behavior of triglycerides [5]. For example, the initial reactions of decarboxylation and decarbonylation of a fatty acid can occur before or after C-C bond cleavage. They proposed that for unsaturated triglycerides, C-C bond cleavage most likely occurs before decarboxylation and decarbonylation. Conversely, saturated triglycerides will favor decarboxylation and decarbonylation prior to C-C bond cleavage reactions.

CHAPTER IV
EXPERIMENTAL

Oil Feedstock

Soybean oil, high-oleic canola oil, and jojoba oil were used as thermal cracking feedstock for this study. Soybean oil was used in performing the DOE part of this study, and the three oil types were thermally cracked under identical conditions of 4 L/hr, 420°C, and 1.38 MPa gauge (200 psig), for a three way comparison of the different oil types thermal cracking behavior.

The soybean oil used in this study was Sun Brand Salad Oil, Lot # I0427BA, purchased from Columbus Oils of Chicago, Illinois. The high-oleic canola oil was Clear Valley 75 High Oleic Canola Oil, Lot # 053008/285 from Cargill of Minneapolis, Minnesota. The jojoba oil was Jojoba Oil – Golden, Lot # 191288, purchased from Jedwards International, Inc. of Quincy Massachusetts. Fatty acid composition of the three oil types used in this study are illustrated in Figure 16.

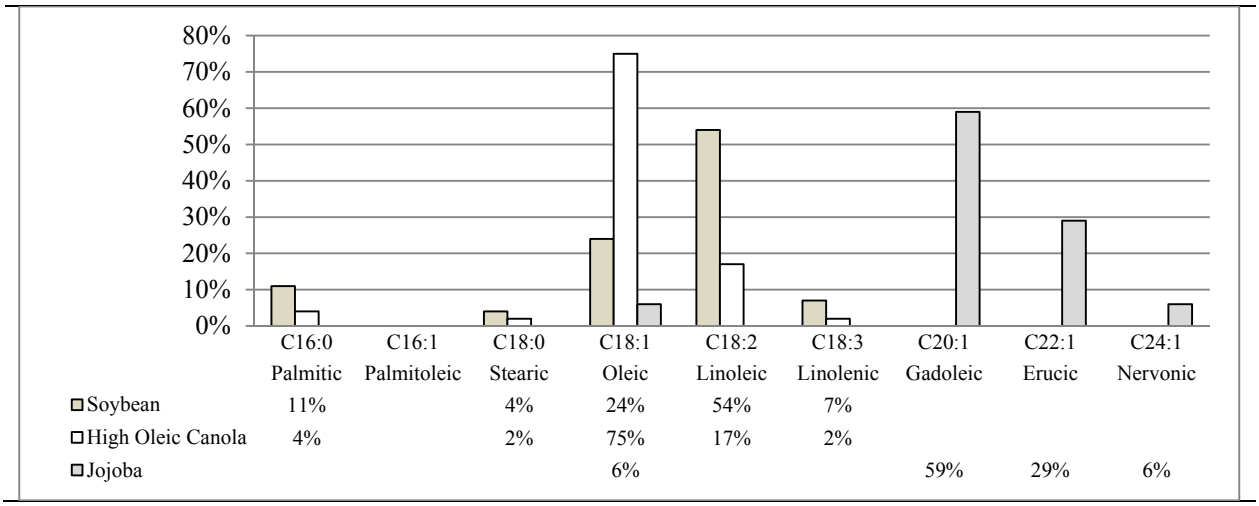

Figure 16. Fatty acid composition of soybean oil, high oleic canola oil, and jojoba oil

Experimental Apparatus

The apparatus used in these experiments is a bench scale, continuous flow, thermal cracking system, illustrated in Figure 17. The main system components includes a 68 L (18 gallon) feedstock storage tank, variable feed rate diaphragm pump, oil feed line preheater, 9.7 L reactor with three independently controlled external ceramic heaters, water cooled condensing unit, and a condensed liquid product storage tank.

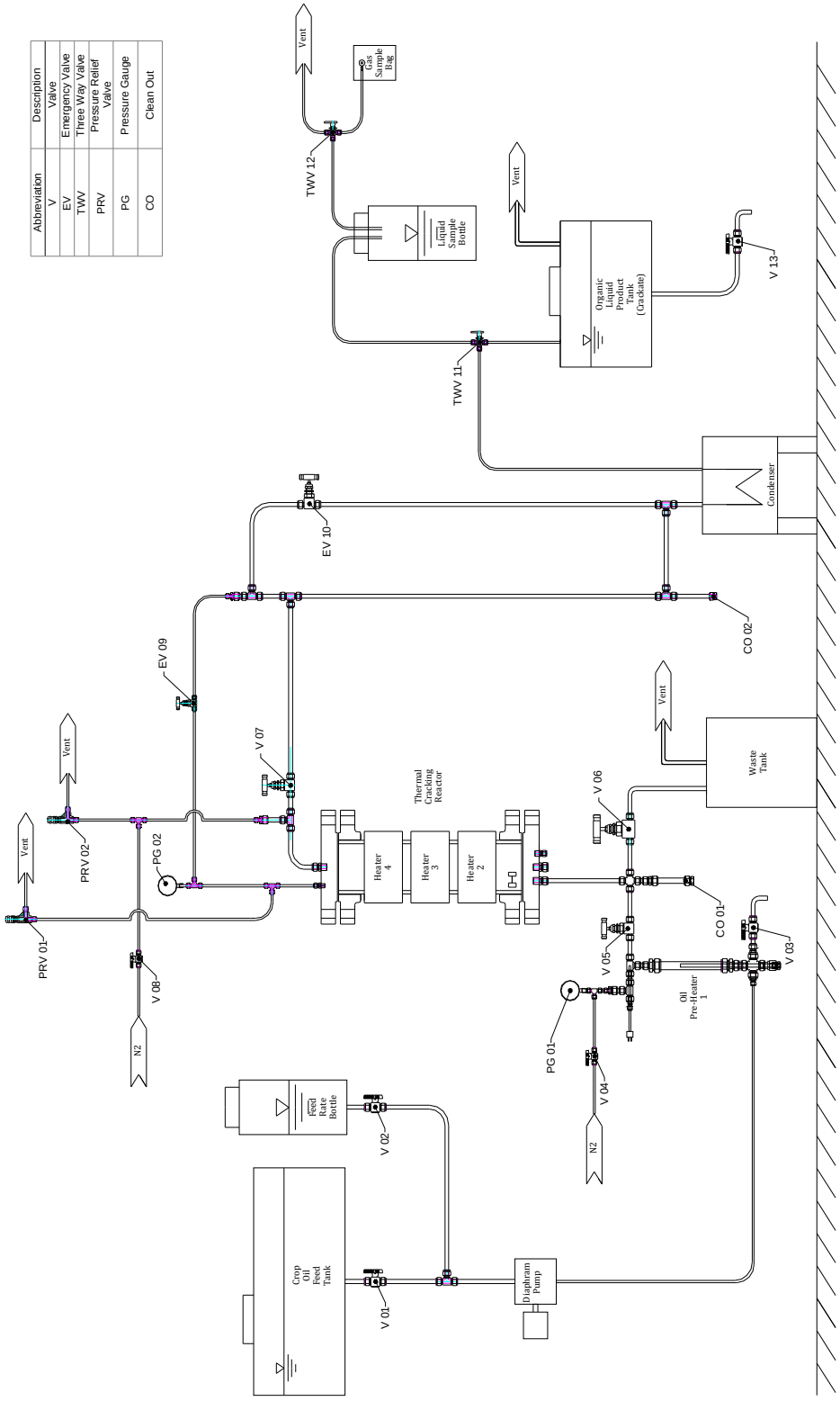

Figure 17. Thermal cracking apparatus

The apparatus was designed to operate at a feed rate of 4 L/h, with a maximum temperature of 450°C and maximum pressure of 3.45 MPa gauge (500 psig). Refer to Appendices A and B for reactor and heater design discussion and calculations.

Reactor Heating and Temperature Control

The thermal cracking reactor heating and temperature control system is illustrated in Figure 18. The system incorporates four thermal couples and three independently controlled external ceramic heaters. Thermal couples B, C, and D were used to independently monitor and control one of three external ceramic heaters, and thermal couple A was employed to monitor temperature at the bottom of the reactor, with no controlling function.

The thermocouples were positioned to help ensure the most accurate temperature readings and maintain proper heating control. The tips of thermal couples B, C, and D were located slightly above (higher than) the heater they were used to control, within the narrow neutral zone between heaters. With reactor fluid flow from bottom to top, temperature measurement above the heater will help minimize overheating of the reactor products. Also, temperature measurement in the neutral zone should help limit the effect of radiation energy coming from the heaters.

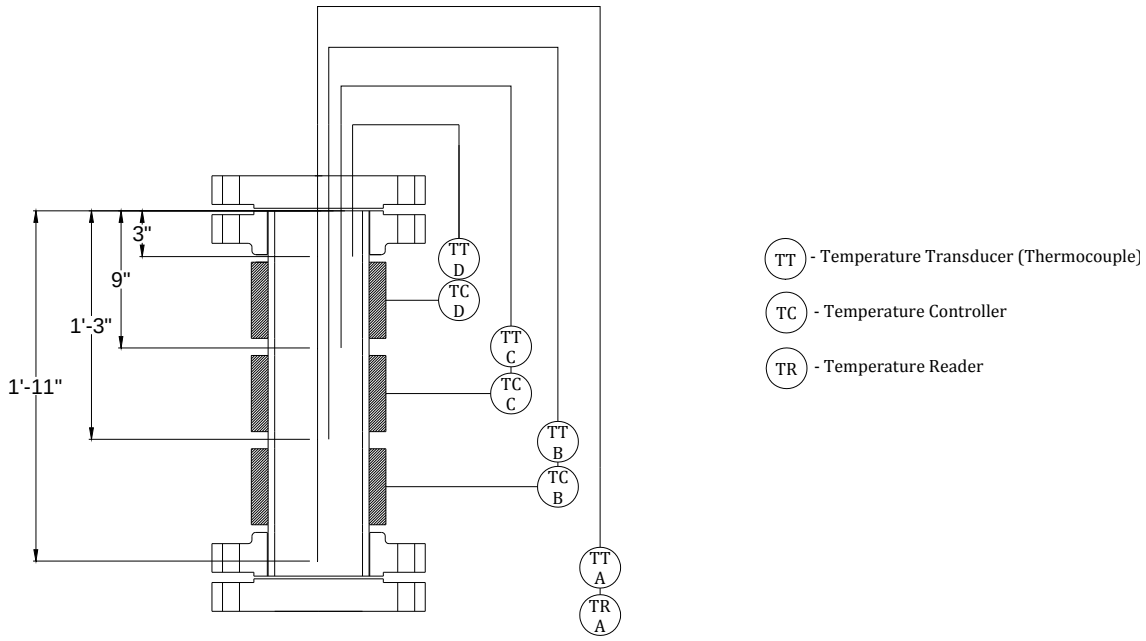

Figure 18. Reactor heating and temperature control

Due to external heating of the reactor, it can be assumed that the radial temperature profile within the reactor is not uniform. The radial temperature profile will be highest at the reactor walls and lowest at the center of the reactor. To compensate for this non-uniformity, all thermal couples were placed half way (approximately 1.5”) between the higher temperature inside wall and the cooler center of the reactor as shown in Figure 19. This placement of the thermocouples should provide a mean temperature measurement, and compensate for variability in the radial temperature profile.

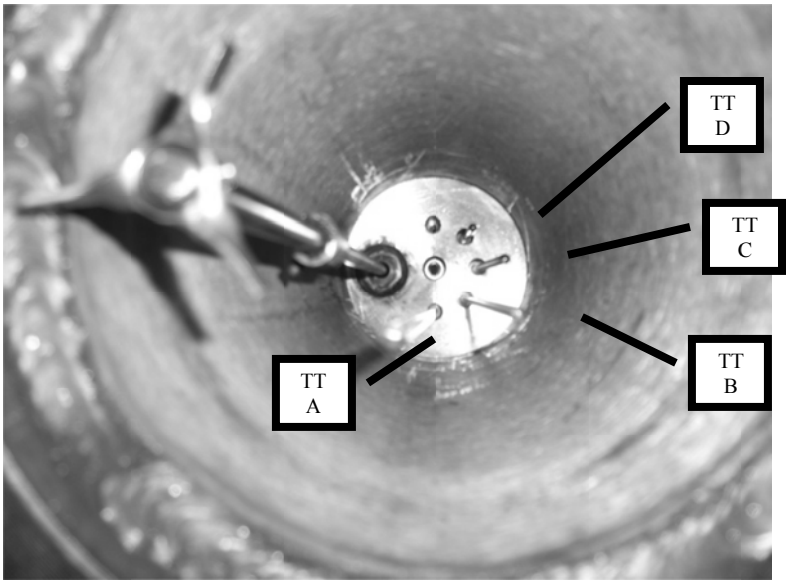

Figure 19. Reactor bottom up view – thermal couple placement

A magnetic mixer was also incorporated into the reactor to help maintain uniform heat distribution of liquid phase contents. Referring to Figure 19, the mixer included one impeller at the bottom of the reactor and a second impeller (not shown in this figure) 4" above the impeller shown. The magnetic mixer was also located off center to minimize vortexing of the reactors liquid phase contents.

Four temperature controllers were used on this apparatus, including one for the preheater, and three for the thermal cracking reactor heaters. Each temperature controller was individually auto tuned to establish appropriate PID settings to achieve temperature stability. Two PID settings, one for each flow rate level of the DOE, were established for each controller. One set of PID settings was established to accommodate the lower level oil feed rate of 4L/hr and the second set was established for the higher level feed rate of 7L/hr. The controller PID settings used in this study are listed in Appendix H.

Reactor Operating Conditions

The thermal cracking reactor was operated in a liquid and gas phase combination during these experiments. The liquid phase accounted for roughly 60% of the lower reactor volume, while the gas phase accounted for the upper remaining 40%. The reactor was operated in this fashion due to the observation that the existence of a liquid phase during the thermal cracking process greatly reduced coke generation, where control of coking is critical to the operational efficiency of this process and is required for runs of long duration. Figure 20 illustrates an earlier run during commissioning of the new CSTR reactor where no liquid phase was maintained within the reactor. The absence of a liquid phase, resulted in considerable generation of coke products after a run time of only 2 hours.

Figure 20. Post run – coke accumulation (2 hour run time)

Alternatively, Figure 21 illustrates the results from operating the reactor with a liquid phase present. The top view into the reactor after this run of 16 hours shows an

absence of heavy solids accumulation as compared to Figure 20. The presence of the liquid phase was postulated based upon observed temperature readings within the reactor during the run, and confirmed post run by the existence of a liquid boundary line within the reactor approximately 10" from the top of the reactor.

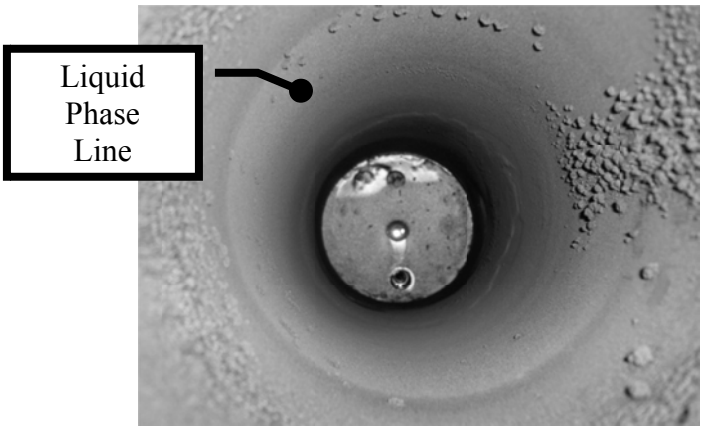

Figure 21. Post run – liquid and gas phase solids accumulation (16 hour run time)

In order to achieve and maintain a liquid phase in the reactor during these experiments, the reactor was operated at two different temperatures. Referring to Figure 22, heater B was operated at 370°C, while heaters C and D were operated at the temperature level of the experimental design (400 or 420°C).

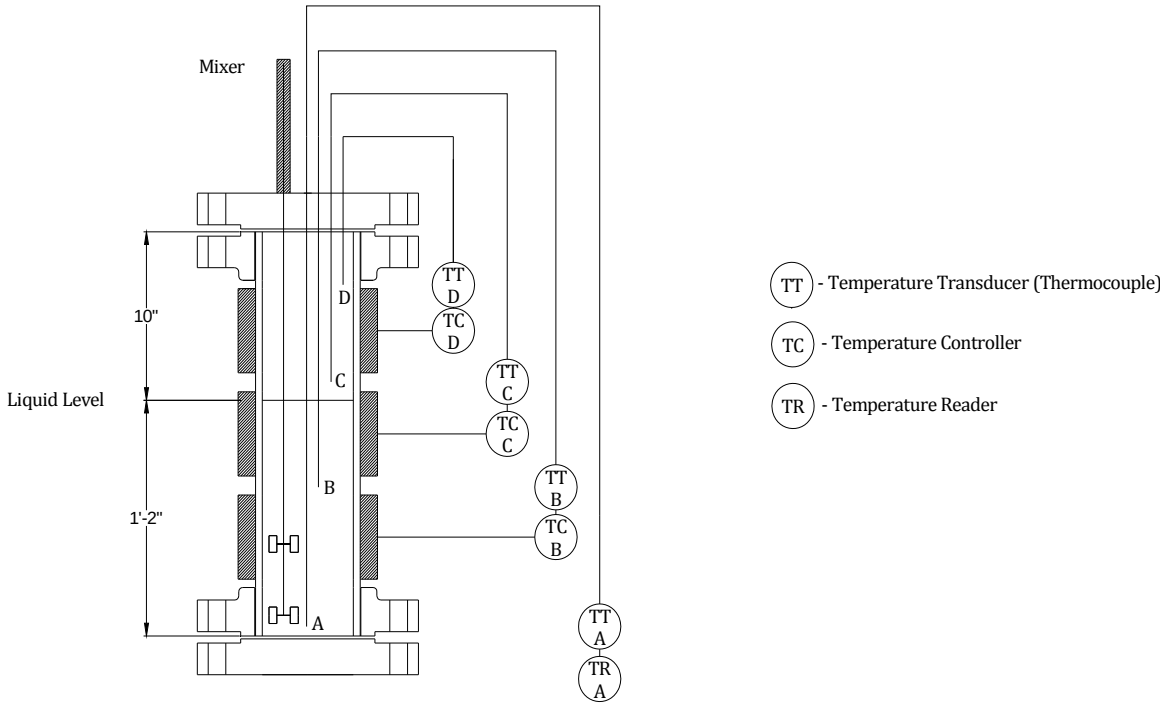

Figure 22. Reactor liquid phase operation

The bottom zone temperature set point of 370°C was established by trial and error on previous runs. At temperatures much above this, the liquid phase would dissipate. This observation was based upon the monitoring of thermocouples A and B during the run. In the presence of a liquid phase, the thermocouple A and B temperature readings did not vary from each other by more than a 2 to 3°C. Loss of the liquid phase was apparent when the temperature readings between these two thermocouples diverged, with thermocouple A temperature remaining steady, and the temperature of thermocouple B approaching the higher operating temperature of thermocouples C and D.

Flow Rate Measurements and Product Yields

Product yields were calculated based upon flow rate measurements and a simple mass balance of the thermal cracking process. The following sections describe that procedure.

Mass Balance Procedure

Mass balance closure was conducted around the thermal cracking process for the purpose of calculating product yields. The thermal cracking process, illustrated in Figure 23, consisted of one input stream, two output streams, and an accumulation term. The mass balance was carried out by measuring the oil feed input stream and liquid product output stream during each run. The solids accumulation term was measured during cleaning of the reactor at the conclusion of eight runs. The gas product was calculated by closing the mass balance.

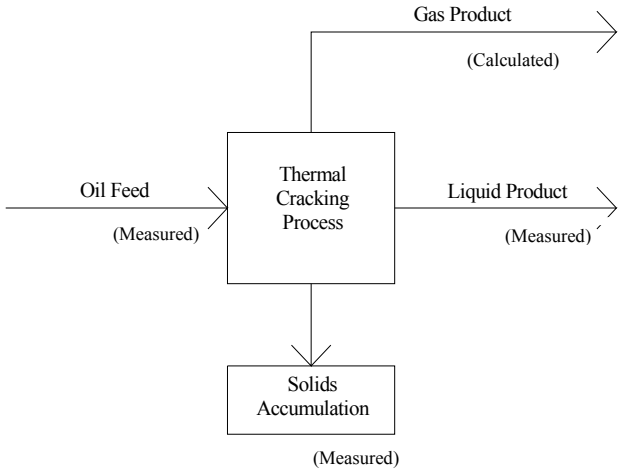

Figure 23. Process mass balance

Oil Feed Measurement

The oil feed system, illustrated in Figure 24, consists of a metering diaphragm pump that is gravity fed from a 68 L (18 gallon) vegetable oil storage tank, and a 1 L container used to measure and verify the volumetric oil feed rate during each experimental run. The calibration curve for the metering diaphragm pump is provided in Appendix H.

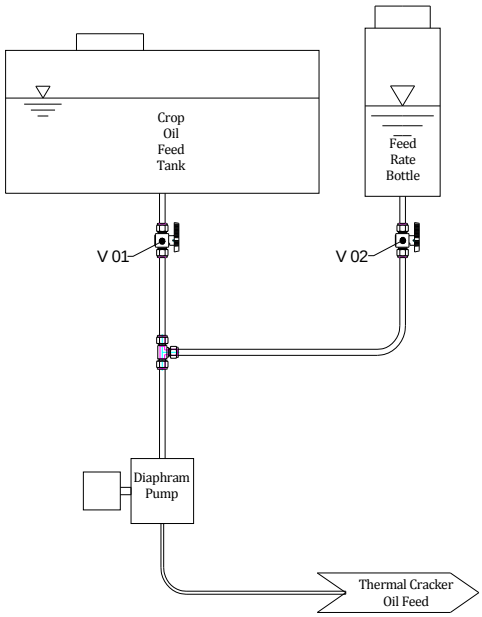

Figure 24. Oil feed system

During normal operation, valve 01 was open, valve 02 was closed, and the system was fed from the 68 L (18 gallon) tank. The oil feed rate measurement was initiated by filling the feed rate bottle with approximately 1 L of oil. The feed rate bottle was graduated at 0.25, 0.50, 0.75, and 1.0 L increments. Valve 02 was opened and valve 01 was closed, in that order and in close succession to prevent starving and air locking the diaphragm pump. When the feed rate bottle liquid level dropped to the 0.75 L mark,

timing began and continued until the liquid level reached the 0.25 L mark. The time required for the pump to draw 0.5L of oil from the feed rate bottle was used to calculate the volumetric feed rate (EQ 1). The mass feed rate was determined by multiplying the previously calculated volumetric feed rate by the density of the vegetable oil feedstock (EQ 2).

$$\dot{V}_{Oil\ Feed} = \frac{0.75 - 0.25}{t} \cdot \frac{Liters}{Hour} \qquad \text{EQ 1}$$

$$\dot{m}_{Oil\ Feed} = \rho_{Oil} \dot{V}_{Oil\ Feed} \qquad \text{EQ 2}$$

Liquid Product Yield

After the cracking process, the products are cooled in a condensing unit, resulting in a combined liquid products and non-condensable gas products stream. Both phases enter a 38 L (10 gallon) holding tank, where the liquid products are collected and gas products are vented off as illustrated in Figure 25.

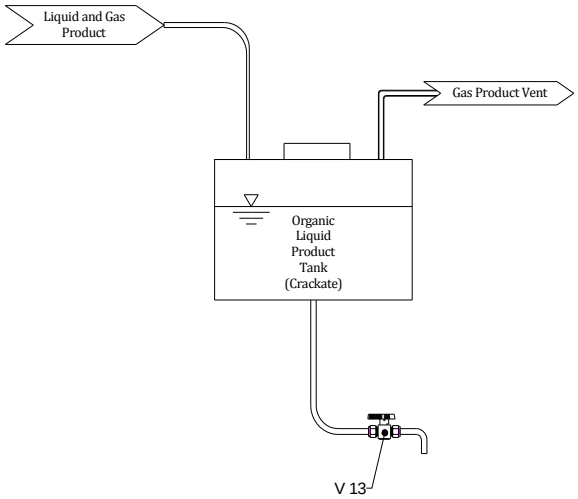

Figure 25. Product collection system

The liquid product rate was measured over the entire duration of each experimental run, typically 30 minutes, by measuring the mass of liquid product collected in the liquid product tank over a given time period (EQ 3).

$$\dot{m}_{Liquid\ Product} = \frac{m_{Liquid\ Product}}{t_{run}} \qquad \text{EQ 3}$$

The procedure included the following steps. Immediately prior to each run, the liquid products tank was completely drained down by opening valve 13. Once the liquid product tank was empty, valve 13 was closed and timing was started. At the end of each run, the liquid product was drained by way of valve 13 into a tared container. After complete drainage of the liquid product tank, timing was stopped at the instant valve 13 was closed.

The oil feed rate (EQ 2) and liquid product rate (EQ 3) were used to calculate the liquid product yield for the particular runs (EQ 4).

$$Yield_{Liquid\ Product} = \frac{\dot{m}_{Liquid\ Product}}{\dot{m}_{Oil\ Feed}} \quad \text{EQ 4}$$

Solids Yield

Solids accumulation was measured post experiment, at the conclusion of a single day operation of the reactor (total of eight runs per experiment). Ideally, the solids yield would have been measured at the conclusion of each experimental run. This however was impractical, as it would have required a total of 16 dismantling and assembly procedures of the reactor, a process that would have added over a month to the DOE.

Since eight runs were conducted prior to reactor tear down and cleaning, the solids accumulation term represents an average measurement over these eight runs, and no distinction was made on solids accumulation among the individual runs.

Solids yield was obtained by dividing the total solids collected upon post run cleaning of the reactor by the total oil fed during the entire duration of the eight runs (EQ 5). The average solids yield over 8 runs was only 0.5%, and it was assumed that any variability of solids yield between runs was insignificant.

$$Yield_{Solids\ Accumulation} = \frac{m_{Solids\ Accumulation}}{m_{Oil\ Feed}} \quad \text{EQ 5}$$

Gas Product Yield

The gas product yield was not measured, but rather calculated by substituting the previously measured liquid product yield (EQ 4) and solids accumulation yield (EQ 5) into EQ 6. Note, there may be a limited amount of error introduced into the gas product

yield calculation due to the use of a solids accumulation term that was an average measurement over eight runs.

$$Yield_{Liquid\ Product} + Yield_{Solids\ Accumulation} + Yield_{Gas\ Product} = 100\% \qquad \text{EQ 6}$$

Sample Collection

A liquid and gas sample was collected during each experimental run. Figure 26 illustrates the product collection apparatus after the thermally cracked products have been condensed. Under normal operating conditions, three way valve 11 directs the combined liquid and gas product stream to the 38 L (10 gallon) tank, where only the liquid product is collected, and the gas product is vented. Turning the three way valve 11 diverts the liquid and gas product stream for sample collection. Sample collection was initiated approximately 10 minutes into each experimental run (each run generally lasted 30 minutes).

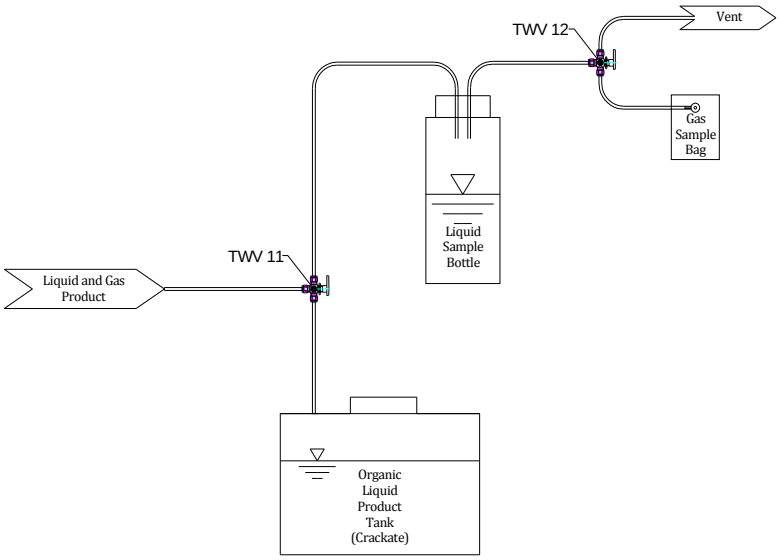

Figure 26. Sample collection system

The liquid sample was collected in a 1 L air tight bottle with screw on lid. The lid was modified with an entry and exit port made with ¼" flexible tubing. Both the gas and liquid product would enter the sample bottle, where separation of the liquid and gas phase product would occur. The 1 L liquid sample was collected and then transferred into a 1 L amber bottle (Chemglass CG-827-15) for cold storage.

The gas sample was collected at the same time the liquid sample was being collected. Tedlar lined, 1 L gas sample bags (SKC model 232-01) were used to store the gas product samples. During normal operation, three way valve 12 was turned to allow the gas vapors to vent. The gas sample collection procedure would begin without a gas sample bag connected to the system. Turn three way valve 12 to divert the gas product from the vent line to the sample line. A few second delay was allowed to permit the sample line to purge. The air sample bag was then connected to the active gas sample

line. The air sample bag valve was then opened, and the bag allowed to fill with product gas, at which time, the sample bag valve was closed, and three way valve 12 was turned to redirect the gas product to the vent. Gas samples were refrigerated prior to analysis to minimize any degradation effects due to heat or light.

Gas Product Analysis

The gas product was analyzed by gas chromatograph (GC) (SRI model 8610C) utilizing a 1.83 meter x 3.175 mm (6'x1/8") column (Alltech HayeSep Q 80/100). Gas components were quantified by two means; flame ionization detector (FID) and thermal conductivity detector (TCD).

FID was used to quantify the gas product mass percentage for carbon based components. The GC was also equipped with a methanizer to allow FID detection of CO and CO_2. A typical FID response graph with the component identification and corresponding elution time in minutes is illustrated in Figure 27. Identified components included carbon monoxide, methane, carbon dioxide, ethylene, propane, propylene, butene, pentane, and hexane. Referring to Figure 27, this work failed to identify a minor peak prior to pentane.

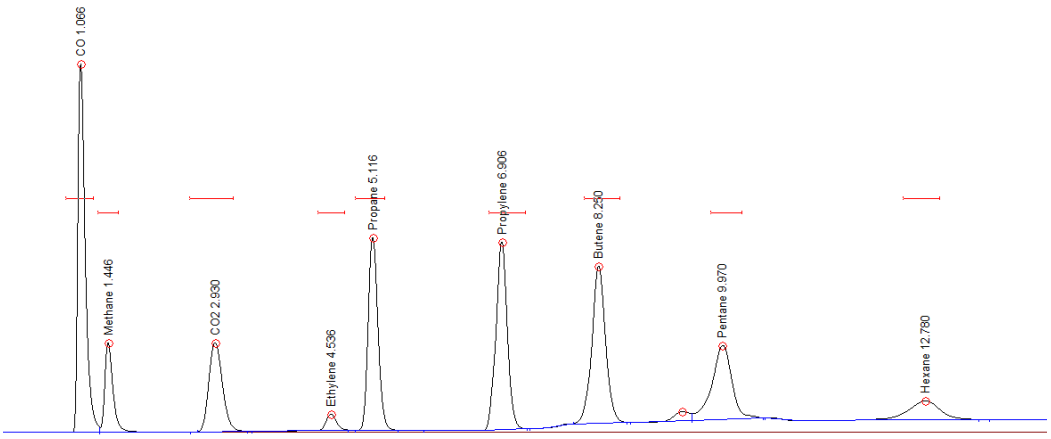

Figure 27. Typical GC-FID chromatogram

Molecular hydrogen was quantified by TCD response. A calibration curve was generated and used to convert the TCD signal to molecular hydrogen mole percentage. Refer to appendix G for more details of GC setup, injection procedures, and sample calculations.

Liquid Product Distillation

A 100 mL liquid product sample from each run was distilled utilizing an ORBIS BV PAM distillation unit. The results were quantified into three distillation cuts, including light ends (<150°C), middle distillate (150 to 250°C), and heavy distillate (>250°C).

Ideally, determination of a middle distillate temperature range from 150 to 300°C was desired, as this range is a better representative of fuel grade liquid products, but proved difficult to achieve with these liquid product samples. At vapor temperature levels above 250°C, the non-vaporized liquid sample appeared to undergo further thermal cracking degradation from the heat being applied to the boiling flask.

Liquid Product Acid Number

An acid number test was performed on the liquid product per ASTM D3242-05, Standard Test Method for Acidity in Aviation Turbine Fuel. Acid number is a measure of fuel reactivity with a caustic solution, and is expressed as milligrams of potassium hydroxide that are neutralized by 1 g of fuel. Even though this test is not intended for intermediate fuel products such as crackate, this test was performed to determine if a relationship exists between acid number measurement and the extent of fatty acid decarboxylation.

CHAPTER V
RESULTS AND DISCUSSION

Experimental Design

A split-plot full factorial experimental design was used in this study. The factors under investigation included pressure, temperature and feed rate.

A split-plot design gets its origins and name from its use in agricultural experiments, where a mixture of hard-to-change (HTC) and easy-to-change (ETC) factors exist in research related to crop test plots. In real world industrial applications, split-plot designs are often used to minimize HTC factor level changes in order to save time and/or the costs of experimental designs.

The HTC factor of concern for these experiments was pressure. During preliminary experiments it was observed that changes in the pressure level caused a major upset to the system, requiring an extensive amount of time for the thermal cracking apparatus to recover and stabilize. Use of the split-plot DOE would require only one pressure level change every 4 runs, or once over a set of 8 runs.

A split-plot design utilizes two randomizations. The HTC factor is randomized into whole-plots, while the ETC factors are randomized within each whole-plot. As a result of this randomization, there are two error terms: one for the HTC factor and one for the ETC factors. Split-plot experiments sacrifice precision on the HTC factors, but gain precision on the ETC factors, and the HTC x ETC interactions.

The factor levels used in this investigation are listed in Table 3.

Table 3. High and low level values for factors studied

Factor	Range of Factor	
	Low Level (-1)	High Level (1)
Pressure	1.38 MPa gauge (200 psig)	2.76 MPa gauge (400 psig)
Temperature	400°C	420°C
Feed Rate	4 L/hr	7 L/hr

Pressure levels were chosen based on the available working pressure design of the new CSTR reactor which is 3.45 MPa gauge (500 psig). The chosen levels will still allow for star point experiments within the 3.45 MPa gauge (500 psig) working pressure design of the CSTR.

Temperature levels were chosen based on prior thermal cracking work by Yan Luo utilizing batch reactors [2]. These levels will also allow for star point experiments within the CSTR design maximum operating temperature of 450°C.

Feed rate level choice was a bit more arbitrary, since we had very limited prior experience with continuous flow reactor experiments. The low level was chosen based upon previous experiments where excessive coking was experienced at feed rates around 2 L/hr. The high level matched closely with the liquid hourly space velocity of the previous PFR reactor design.

The split-plot design used in the study of soybean oil is illustrated in Table 4, and included 8 sets of conditions, with 1 repeat, for a total of 16 runs. A set of 8 runs were carried out per day, and each day of experimenting required 18 hours to complete. Completing 8 runs per day would not have been possible with a completely randomized design (CRD). Overall, the split-plot design allowed completion of design in two days of experimenting, or two weeks total when one considers experiment preparation time and

reactor maintenance and cleaning. A CRD would likely have required an additional two weeks time to complete.

Table 4. Split plot experimental design for soybean oil

Std Order	Run Order	Experiment ID	Run Label	Pressure (psig)	Temperature (°C)	Feed Rate (L/hr)
1	4	BS-2-25-SOC	A	400	400	4
2	2	BS-2-25-SOC	B	400	420	4
3	3	BS-2-25-SOC	C	400	400	7
4	1	BS-2-25-SOC	D	400	420	7
5	6	BS-2-25-SOC	E	200	400	4
6	7	BS-2-25-SOC	F	200	420	4
7	5	BS-2-25-SOC	G	200	400	7
8	8	BS-2-25-SOC	H	200	420	7
9	15	BS-2-26-SOC	AA	400	400	4
10	14	BS-2-26-SOC	BB	400	420	4
11	16	BS-2-26-SOC	CC	400	400	7
12	13	BS-2-26-SOC	DD	400	420	7
13	11	BS-2-26-SOC	EE	200	400	4
14	12	BS-2-26-SOC	FF	200	420	4
15	10	BS-2-26-SOC	GG	200	400	7
16	9	BS-2-26-SOC	HH	200	420	7

The responses being reported in this work are listed in Table 5. Gas components were analyzed by GC-FID and GC-TCD, distillate yields were measured by an ORBIS BV PAM distillation unit, and an acid number test was performed on the liquid product per ASTM D3242-05, Standard Test Method for Acidity in Aviation Turbine Fuel

Table 5. Soybean oil split plot design response measurements

Liquid product distillates (wt% of oil fed)
• <150°C Yield
• 150 to 250°C Yield
• > 250°C Yield
Liquid product (acid number)
Gas Product Yields (wt% of oil fed)
Gas Product Concentration (molar %)

Liquid Product Alkane / Alkene Pressure Effect Results

This section examines the effect of pressure on alkane and alkene yields based upon GC-MS analysis of the liquid product. Two sets of results were compared in performing this assessment of the pressure effect. The DOE was not used in this examination due to a lack of replicate GC-MS qualitative and quantitative data.

The first comparison was conducted between the results of run B, and the duplicate runs of F-FF. Experimental conditions for these runs were 420°C, 4 L/h, with a variable pressure of 2.76 and 1.38 MPa gauge (400 and 200 psig), respectively. Figure 28 shows the alkane and alkene yield results at these different pressure conditions. From these data, there is a reduction in yield of all alkane and alkene products due to an increase in pressure. This was not the expected result based on the initial hypothesis, where it was anticipated that higher pressure would increase the yield of alkanes, while decrease the yield of alkenes.

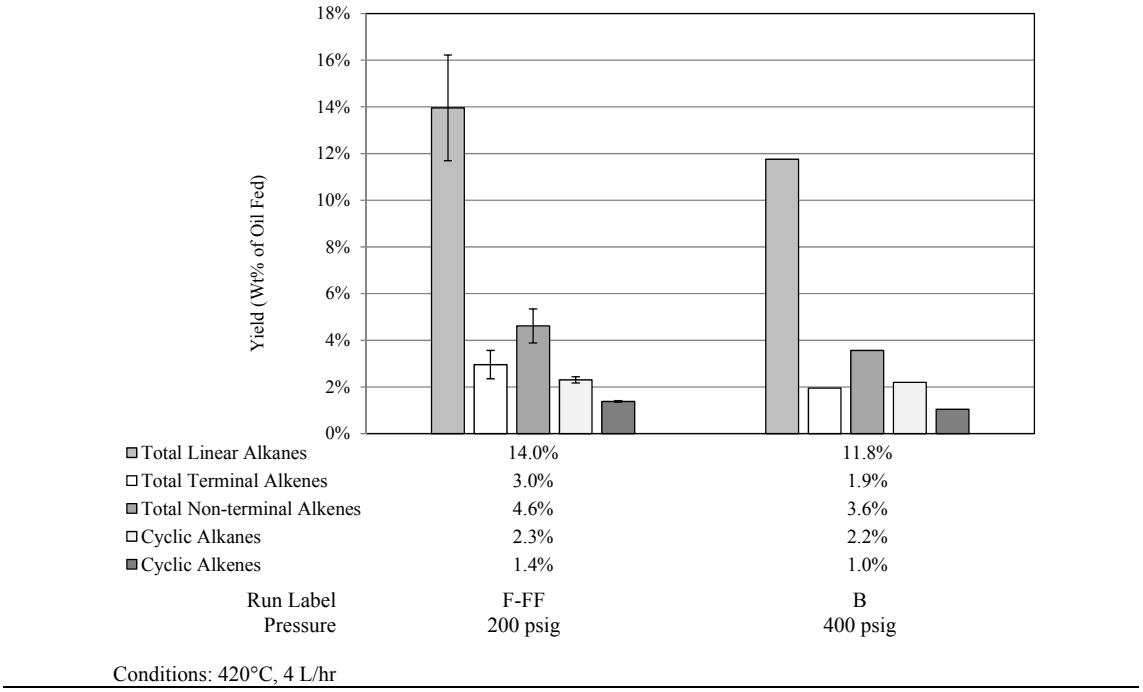

Figure 28. Pressure Effect - alkane and alkene liquid product yields (420°C, 4L/hr)

However, an interesting observation was made after proportioning and comparing the alkane to alkene yield ratios. Figure 29 shows the alkane to alkene yield ratio results at 1.38 and 2.76 MPa gauge (200 and 400 psig). As pressure is increased, alkane products are favored over alkene products, as was hypothesized. A 1.38 MPa (200 psi) increase in pressure from 1.38 to 2.76 MPa gauge (200 to 400 psig) resulted in a 28% increase in linear alkane over terminal alkene yields, a 10% increase in linear alkane over non-terminal alkene yields, and a 24% increase in cyclic alkane over cyclic alkene yields.

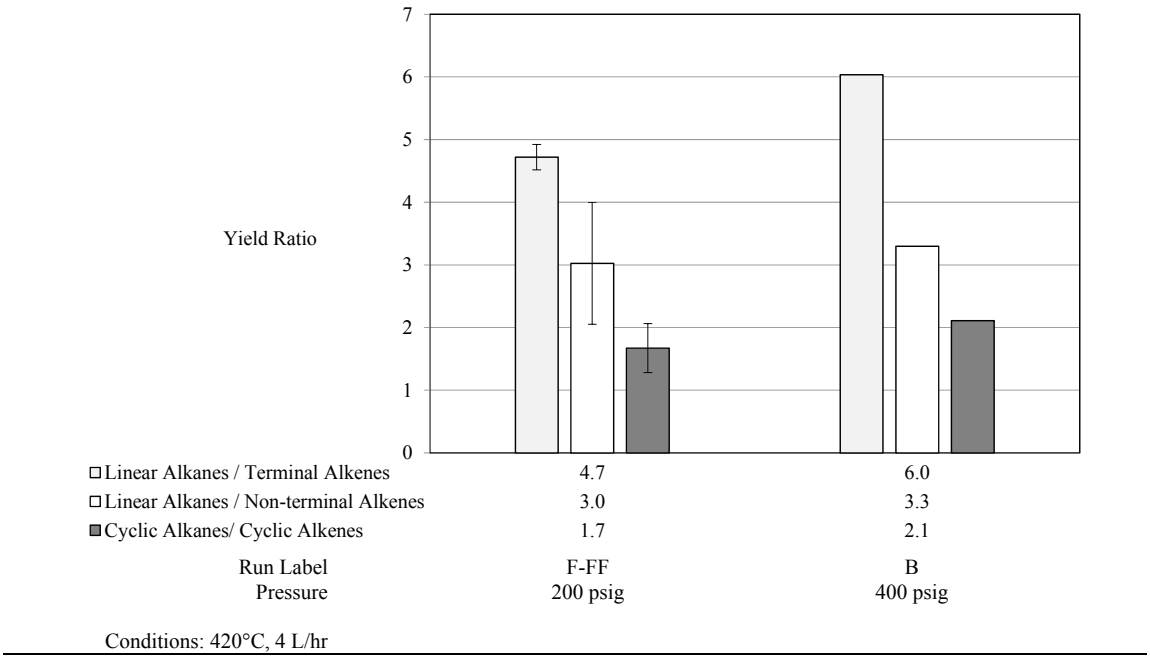

Figure 29. Pressure effect - alkane / alkene liquid product yield ratio (420°C, 4L/hr)

Taking a more detailed look, Figure 30 illustrates the linear alkane and terminal alkene yield ratio data by carbon number. From the chart, alkane favoritism over alkene products at higher pressure was more pronounced at lower carbon number vs higher carbon number products. For example, C7, C8, C9, and C10 alkane / alkene yield

increased by 54%, 56%, 51%, and 48%, respectively, while C11 to C17 alkane yield / alkene yield ratios increased by percentages of less than 25%.

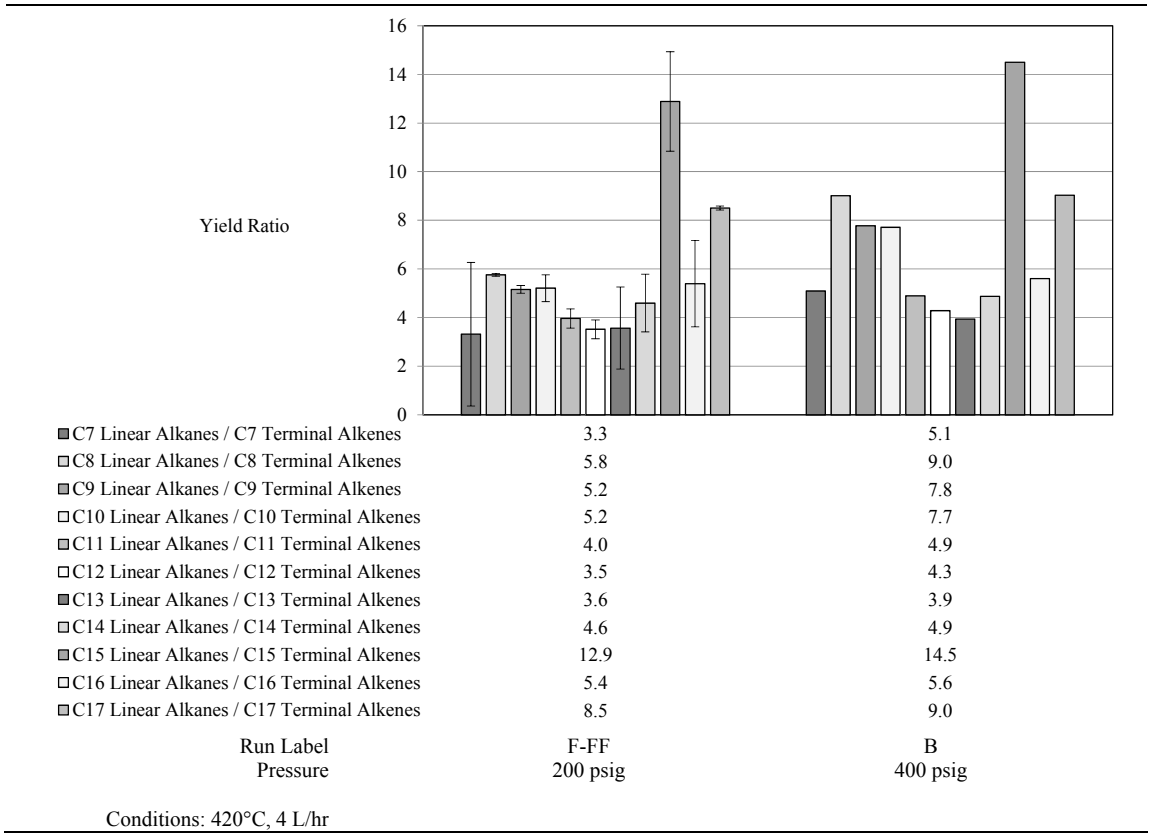

Figure 30. Pressure effect – detailed alkane / alkene liquid product yield ratio (420°C, 4L/hr)

The alkane and alkene yield results for the second comparison are illustrated in Figure 31. Experimental conditions for these runs were 410°C, 5.5 L/h, and a variable pressure of 0.910, 2.07, and 3.23 MPa gauge (132, 300, and 468 psig). The same trend was observed with these data as with the previous condition; with increased pressure, the yield of both the alkane and alkene products trended downward.

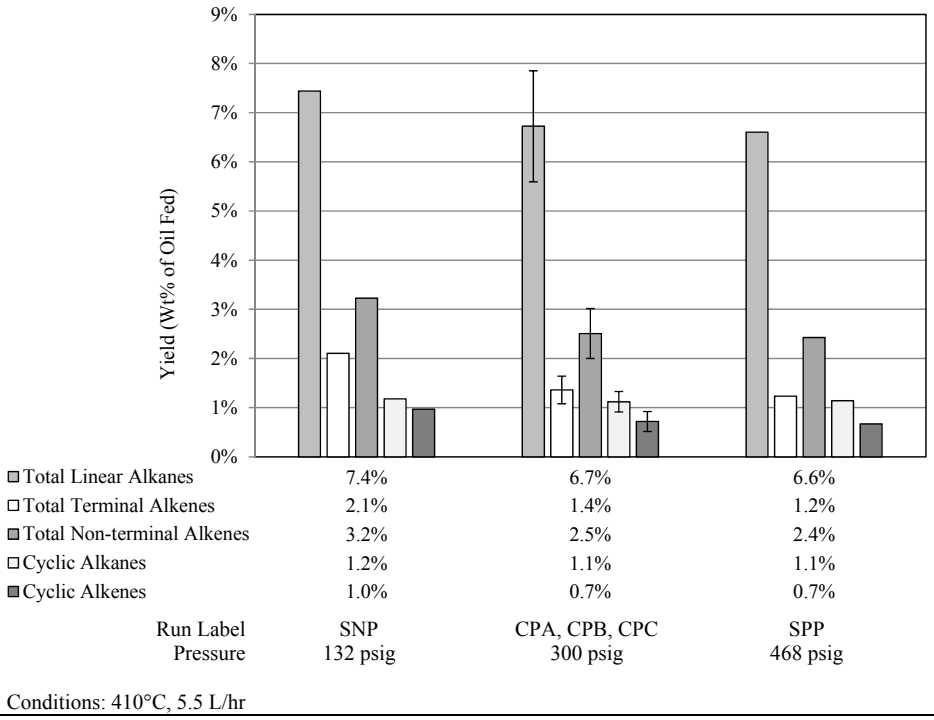

Figure 31. Pressure effect - alkane and alkene liquid product yields (410°C, 5.5 L/hr)

Figure 32 shows how pressure effects the alkane to alkene yield ratios for this second set of conditions. Once again, as pressure is increased, alkane products are favored over alkene products. A 2.32 MPa (336 psi) pressure increase from 0.910 to 3.23 MPa gauge (132 to 468 psig) resulted in a 51% increase in linear alkane over terminal alkene yields, a 28% increase in linear alkane over non-terminal alkene yields, and a 42% increase in cyclic alkane over cyclic alkene yields.

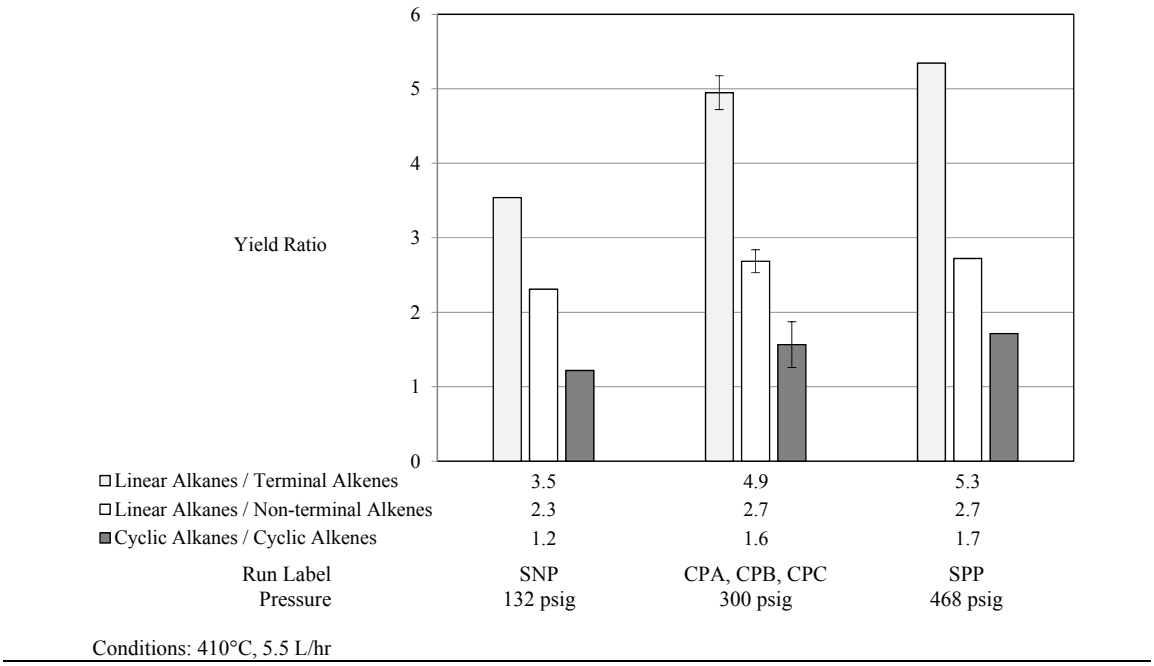

Figure 32. Pressure effect - alkane / alkene liquid product yield ratio (410°C, 5.5 L/hr)

Once more, taking a more detailed look at which alkane / alkene yield ratios are more effected by pressure, Figure 33 illustrates the results broken down by carbon number. From the chart, lower carbon number alkanes again displayed the highest gain over their alkene counterpart. For example, C7, C8, C9, and C10 alkane / alkene yield increased by 113%, 95%, 82%, and 71%, respectively, while C11 to C17 alkane / alkene yield ratios increased by percentages of less than 36%.

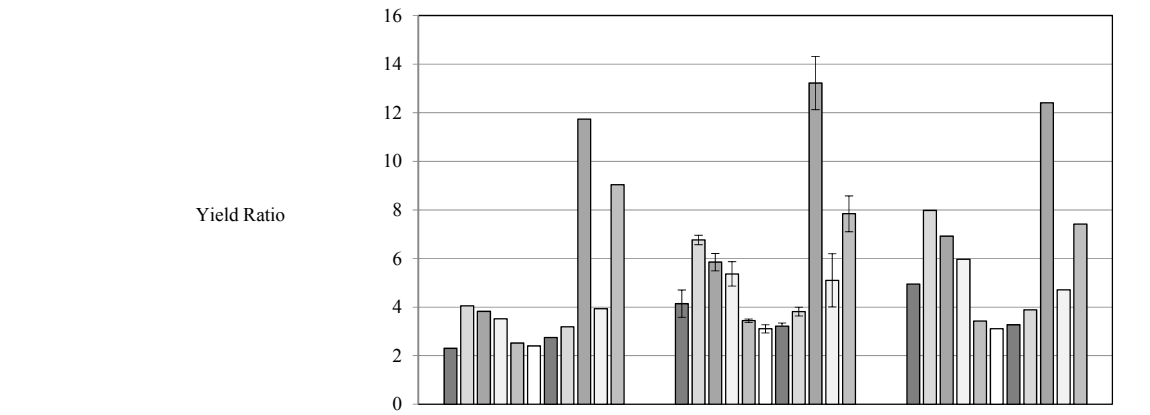

C7 Linear Alkanes / C7 Terminal Alkenes	2.3	4.1	4.9
C8 Linear Alkanes / C8 Terminal Alkenes	4.1	6.8	8.0
C9 Linear Alkanes / C9 Terminal Alkenes	3.8	5.8	6.9
C10 Linear Alkanes / C10 Terminal Alkenes	3.5	5.4	6.0
C11 Linear Alkanes / C11 Terminal Alkenes	2.5	3.4	3.4
C12 Linear Alkanes / C12 Terminal Alkenes	2.4	3.1	3.1
C13 Linear Alkanes / C13 Terminal Alkenes	2.7	3.2	3.3
C14 Linear Alkanes / C14 Terminal Alkenes	3.2	3.8	3.9
C15 Linear Alkanes / C15 Terminal Alkenes	11.7	13.2	12.4
C16 Linear Alkanes / C16 Terminal Alkenes	3.9	5.1	4.7
C17 Linear Alkanes / C17 Terminal Alkenes	9.0	7.8	7.4
Run Label	SNP	CPA, CPB, CPC	SPP
Pressure	132 psig	300 psig	468 psig

Conditions: 410°C, 5.5 L/hr

Figure 33. Pressure effect – detailed alkane/alkene liquid product yield ratio (410°C, 5.5 L/hr)

Based upon these two comparisons, the results suggest that increased pressure has a conflicting effect towards upgrading crop oil into fuel products via the thermal cracking process. Pressure is detrimental to overall middle distillate yield, but beneficial towards favoring alkane products over alkene products.

If higher pressure thermal cracking is utilized as a means to favor alkane over alkene production, the results suggest a loss in single pass conversion efficiency of the reactor unit will be experienced. This may require increased residence times and/or increased recycle stream flow rates to achieve optimum alkane yields.

Three possible explanations for the increased yield of alkanes over alkenes at higher pressure are discussed. The first possible explanation is that higher pressure

favors hydrogenation. Either hydrogenation of alkenes directly to alkanes, or perhaps stabilization of alkane free radicals via hydrogenation before they have the opportunity to cleave unimolecularly, thus preventing generation of a lower molecular weight alkane and alkene product from a parent higher molecular weight alkane (Figure 10).

A second explanation may be that higher pressures lead to increased alkene product loss due to polymerization. It was observed that higher pressure resulted in increased yields of non-GC-elutable products. This observation may suggest that polymerization reactions of alkenyl radicals are favored at higher pressure, as higher pressure would increase the probability of alkenyl free radical contact with higher molecular weight hydrocarbons present in the reactor's liquid phase.

Another explanation that was considered includes an increased loss of alkene yield due to intramolecular cyclization of alkenyl radicals as proposed by Kubatova et al. [14]. This explanation did not appear to be plausible though, as Figure 28 and Figure 31 show that cyclic product yields also decreased with an increase in pressure.

Taking into account the lack of duplicate data and statistical analysis for runs B, SNP, and SPP, the conclusions drawn from these results should be viewed cautiously. However, the observed identical trends between these two comparisons does add some level of credibility to these findings.

Liquid Product Distillation Results

Results from the liquid product distillation are illustrated in Figure 34. Runs F-FF resulted in the highest light distillate (<150) and middle distillate (150-250) yields. It also had the lowest yield for heavy distillate (>250), indicating that the conditions of run F-FF are more favorable for soybean oil conversion. The lowest oil conversion resulted in runs C-CC.

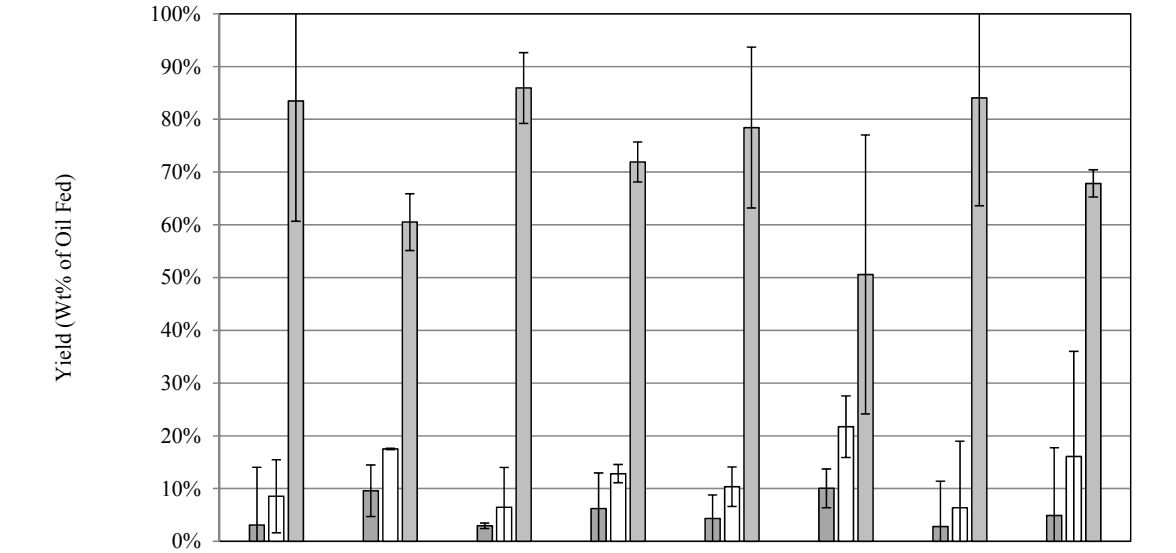

OLP < 150C	3.1%	9.6%	2.9%	6.2%	4.3%	10.1%	2.8%	4.9%
150<OLP<250	8.5%	17.5%	6.5%	12.8%	10.4%	21.7%	6.4%	16.1%
OLP > 250	83.5%	60.5%	85.9%	71.9%	78.4%	50.6%	84.0%	67.8%
Run Label	A-AA	B-BB	C-CC	D-DD	E-EE	F-FF	G-GG	H-HH
Pressure	400	400	400	400	200	200	200	200
Temperature	400	420	400	420	400	420	400	420
Feed Rate	4	4	7	7	4	4	7	7

Figure 34. Liquid product distillation fraction yields

Figure 35 illustrates the significant main effects and interactions for liquid product yield. The effect of reduced yield at higher temperature is the result of increased cracking, pushing the products to lower carbon number gas phase products. The feed rate effect of increasing yield at higher feed rates is likely due to reduced cracking. A

significant interaction effect was also seen, with lower feed rates enhancing the temperature effect.

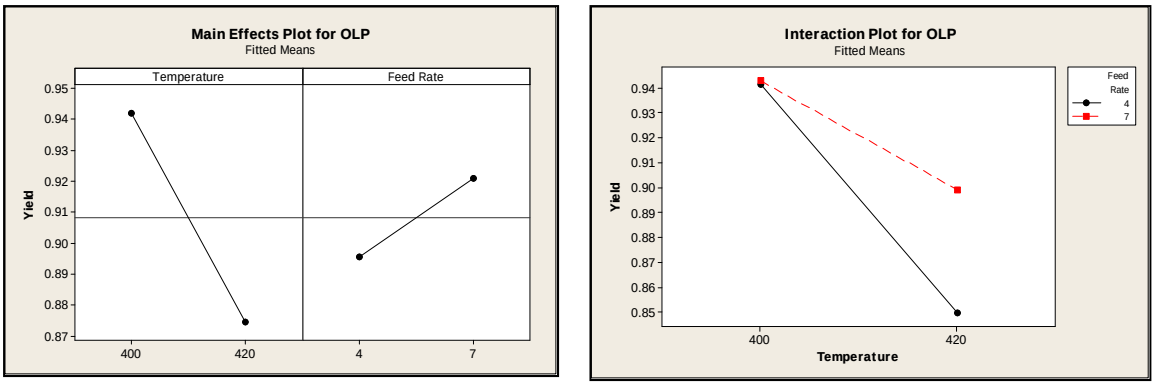

Figure 35. Liquid product yield – DOE main effects and interaction plots

Figure 36 illustrates the significant main effects and interactions for light distillate yield (OLP<150). Light distillate yield is favored at higher temperature and lower feed rate. A two way interaction between temperature and feed rate was also observed. The temperature effect is enhanced at lower feed rates.

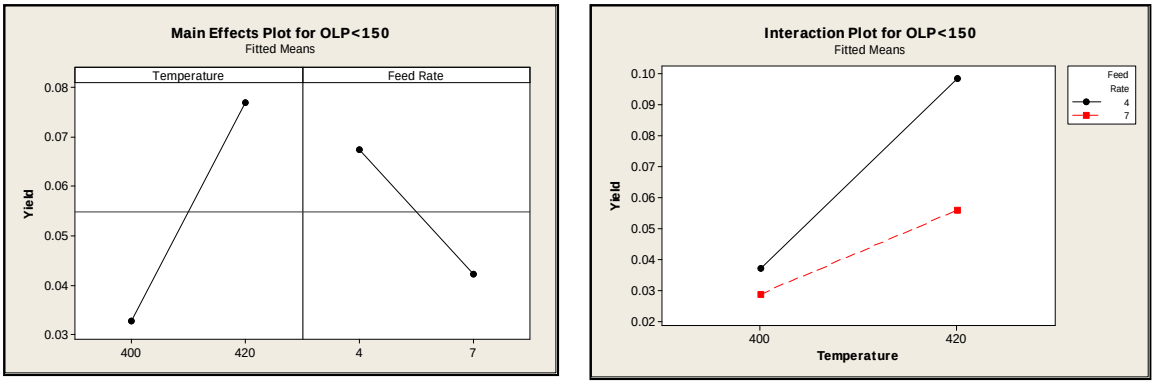

Figure 36. Light distillate (OLP<150) product yield – DOE main effects and interaction plots

The significant main effects and interactions for middle distillate yield (150 to 250) are illustrated in Figure 37. Middle distillate yield is favored at lower pressure,

lower feed rate, and higher temperature. A slight two way interaction was also observed between temperature and feed rate, with an increase in temperature effect at lower feed rate.

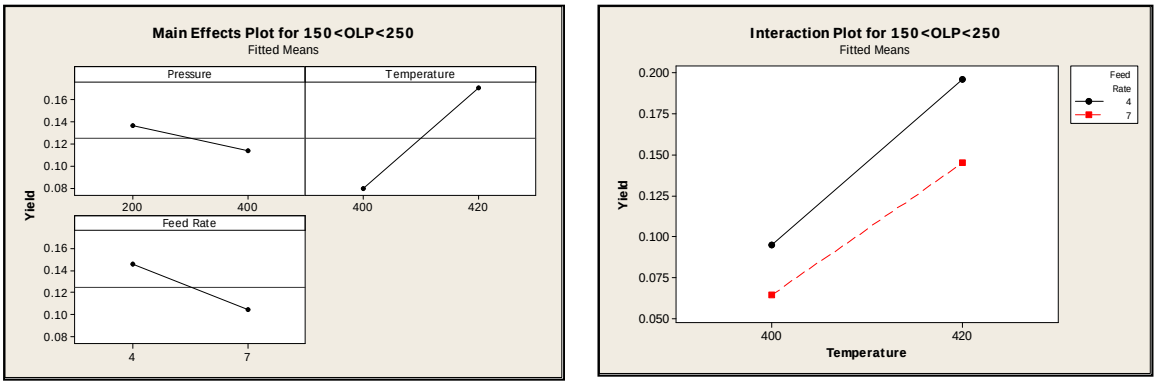

Figure 37. Middle distillate (150-250) product yield – DOE main effects and interaction plots

Figure 38 illustrates the significant main effects and interactions for heavy distillate yield (OLP>250). Heavy distillate yield is reduced at lower pressure, lower feed rate, and higher temperature. There were also two small interactions observed. The positive pressure effect and negative temperature effect were both enhanced at the lower feed rate level.

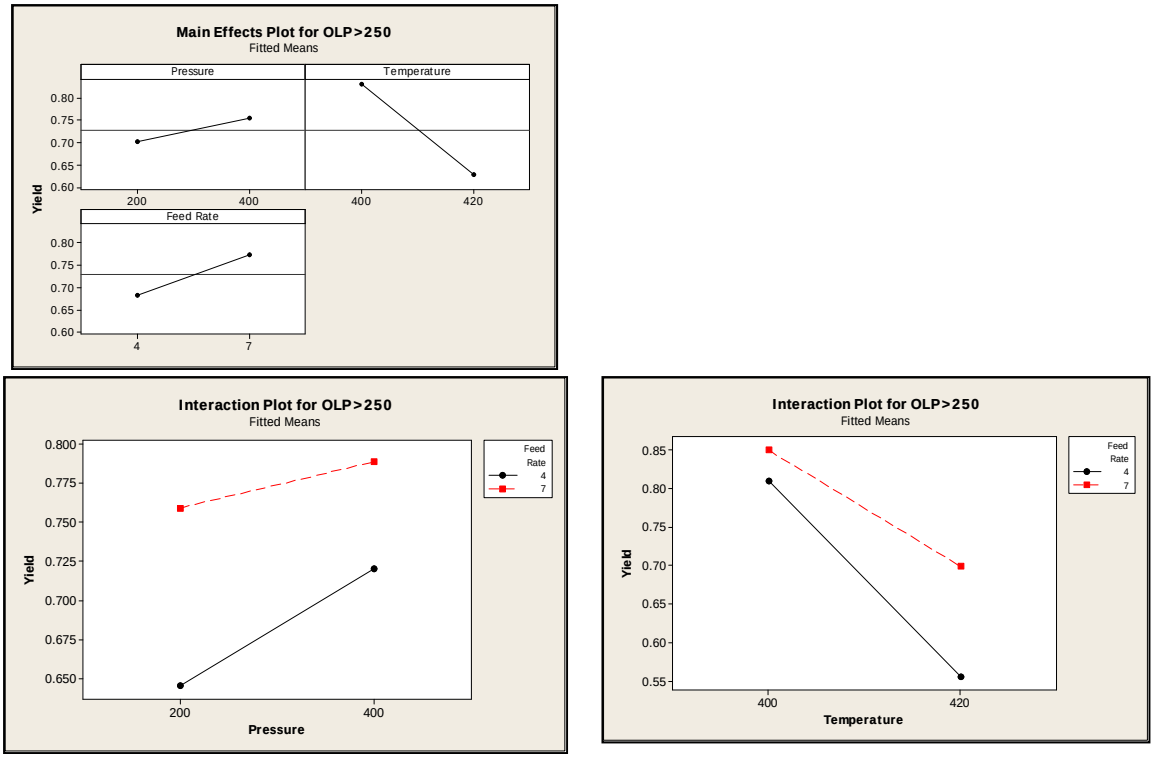

Figure 38. Heavy distillate (>250) product yield – DOE main effects and interaction plots

A comparison of distillate yield among the three different oil feedstocks was conducted. From the bar graph illustrated in Figure 39, it was observed that soybean and canola produced similar liquid product distillate yield results. Jojoba oil however had the lowest conversion among the three oil feedstocks, demonstrated by a heavy distillate (OLP>250) yield of 72.8%. These results indicate that the long chain fatty acids and alcohols (C20:1 and C22:1) of jojoba are less responsive to thermal degradation than the shorter chain fatty acids (C18:1 and C18:2) of soybean and canola oil, suggesting that the optimum cracking temperature for jojoba oil is greater than 420°C.

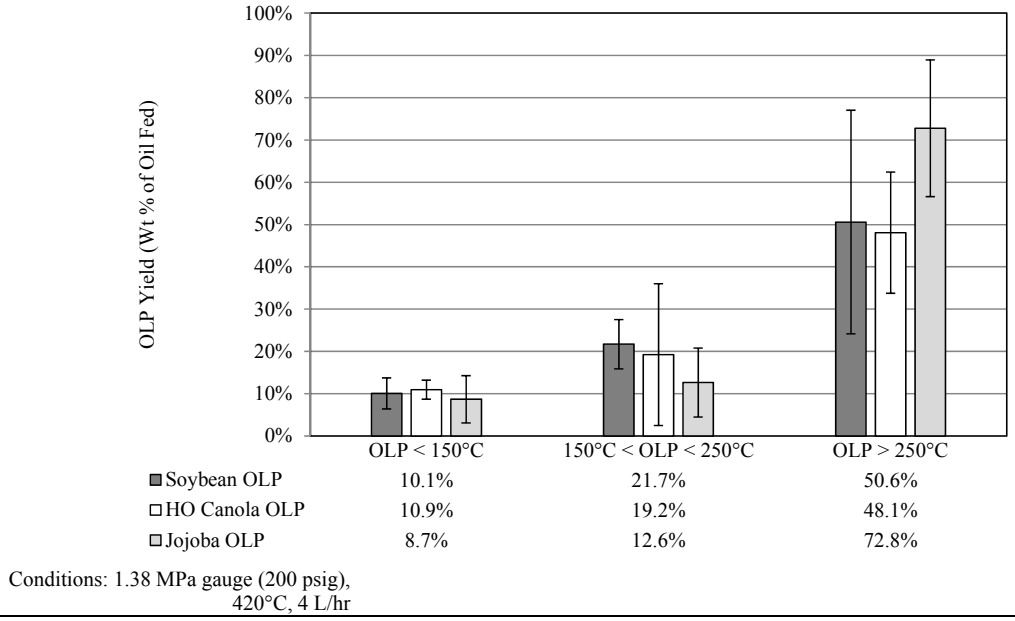

Figure 39. Yield comparison between different liquid products

Liquid Product Acid Number

The acid number results for soybean liquid product are illustrated in Figure 40. Carbon monoxide and carbon dioxide yields are provided for reference. The bar graph shows that there are no major contrasts in the acid numbers among the experimental runs.

It was initially hypothesized that higher CO and CO_2 yields, resulting from carboxylic acid decomposition, would result in lower acid number measurements. However, this initial assumption proved to be incorrect. For example, runs C-CC had an acid number of 105, and had CO and CO_2 yields of 1.6% and 1.0%, respectively. For comparison, runs F-FF had a comparable acid number of 107, yet had CO and CO_2 yields of 6.3% and 2.9%, respectively.

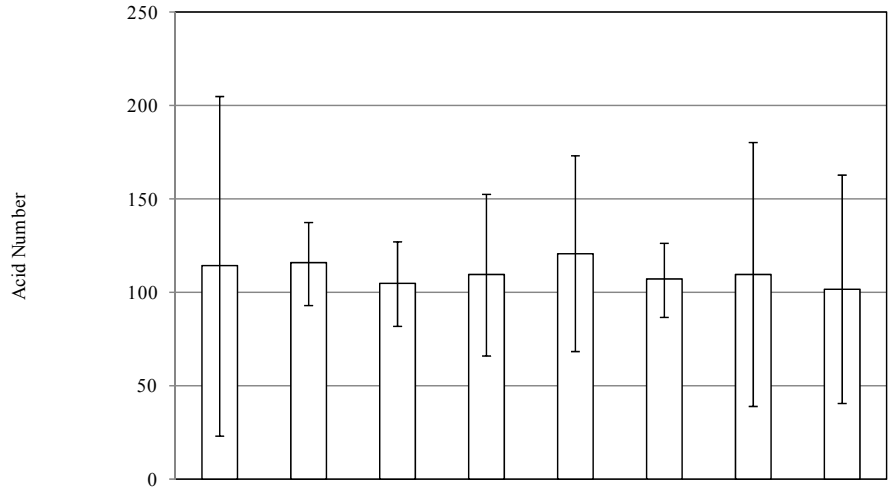

OLP Acid Number	114	116	105	109	121	107	110	102
Run Labels	A-AA	B-BB	C-CC	D-DD	E-EE	F-FF	G-GG	H-HH
Pressure	400	400	400	400	200	200	200	200
Temperature	400	420	400	420	400	420	400	420
Feed Rate	4	4	7	7	4	4	7	7
CO Yield (wt% of oil fed)	1.7%	3.7%	1.6%	2.8%	2.5%	6.3%	2.6%	3.8%
CO2 Yield (wt% of oil fed)	1.1%	2.3%	1.0%	1.7%	1.5%	2.9%	1.5%	1.8%

Figure 40. Acid number of organic liquid product

These results may be due to the differences in the length of the fatty acids in the C-CC and F-FF liquid products. The fatty acids present in the run C-CC liquid samples have likely undergone less degeneration, and are longer (weaker) fatty acids. Conversely, the fatty acids present in the run F-FF liquid samples have undergone more degeneration due to the higher cracking temperature in these runs, resulting in shorter (stronger) fatty acids. This explanation would account for the similarity in acidity and

difference in CO and CO_2 yields between these two sets of runs. Based on this discussion, acid number testing would not be a good measure of the relative level of carboxylic acids in the liquid product.

Figure 41 illustrates the significant main effect of feed rate on the acid number response. Based on the previous discussion, a reduction in acid number at higher feed rates (shorter residence time) can be explained by the level of cracking taking place. Enhanced cracking at the lower feed rate will result in the generation of shorter chain fatty acids (stronger acids); conversely higher feed rates will reduce the level of fatty acid degeneration, resulting in longer chain (weaker) fatty acids.

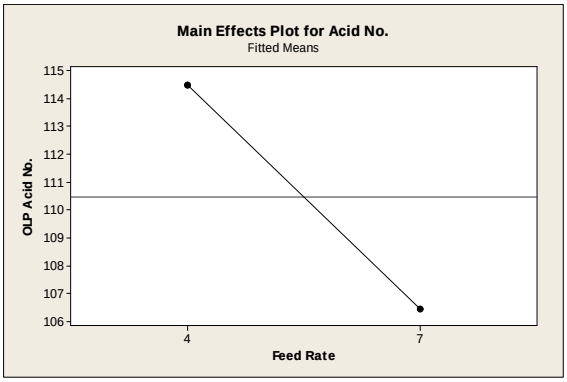

Figure 41. Main effects plot for acid number

Figure 42 compares the acid number results of the three oil feed types. The CO and CO_2 yields are included for reference. High Oleic Canola liquid product yielded the highest acid number, even though the thermal cracking of High Oleic Canola resulted in the highest CO and CO_2 yields among the three feedstock types. The higher acid number for the canola liquid product can be explained by the presence of short chain fatty acids. The low acid number for the jojoba liquid product may be due to a reduced level of cracking. Also, jojoba oil contains ca. 42 carbons per carboxylic acid as compared to ca. 18 carbons per carboxylic acid for canola and soybean oil. In other words, jojoba oil

contains approximately 50% less carboxylic acid, which may play a larger role in this observed result.

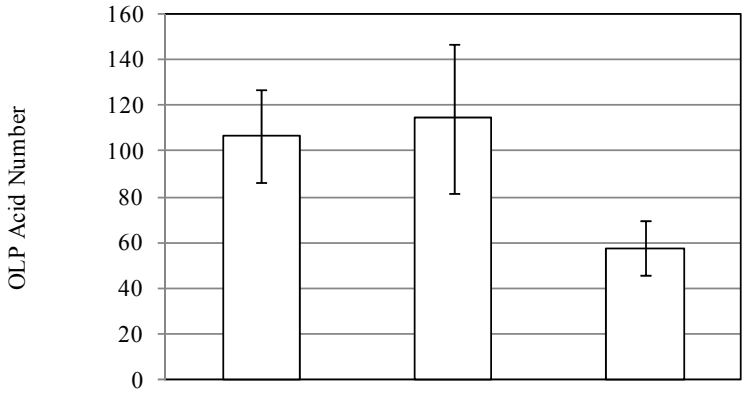

OLP Acid No.	107	114	58
OLP Type	Soybean	High Oleic Canola	Jojoba OLP
CO Yield (wt% of oil fed)	6.53%	6.85%	0.93%
CO2 Yield (wt% of oil fed)	2.95%	5.14%	0.93%

Conditions: 1.38 MPa gauge (200 psig)g, 420°C, 4 L/hr

Figure 42. Acid number comparison between different liquid products

Gas Product Yield

This section examines the results of gas product yield (wt % of oil fed), including the gas phase product as a whole, and the yield of the various gas phase components. Figure 43 provides a summary of the main effects that have been shown to be statistically significant.

	Higher Pressure Level	Higher Temperature Level	Higher Feed Rate Level	Reference
Gas Product		↑ Yield	↓ Yield	Figure 46
H2		↑ Yield	↓ Yield	Figure 49
CO		↑ Yield	↓ Yield	Figure 52
Methane		↑ Yield	↓ Yield	Figure 55
CO_2		↑ Yield	↓ Yield	Figure 57
Ethylene	↓ Yield	↑ Yield	↓ Yield	Figure 60
Propane		↑ Yield	↓ Yield	Figure 63
Propylene		↑ Yield	↓ Yield	Figure 66
Butene		↑ Yield	↓ Yield	Figure 69
Pentane		↑ Yield	↓ Yield	Figure 72
Hexane		↑ Yield		Figure 75

Figure 43. Significant main effects summary on gas product yield response

From Figure 43, ethylene yield is the only component shown to be affected by pressure. Ethylene yield decreased with an increase in pressure level. This may mean either that ethylene formation is being suppressed or ethylene consumption is being enhanced at elevated pressure. According to the reaction scheme proposed by Alencar et al. (Figure 12), ethylene is produced by unimolecular elimination from hydrocarbon radicals during secondary cracking. Increased pressure has been shown to be unfavorable towards unimolecular reactions, and may play a part in this observation. Ethylene may also be consumed by the bimolecular Diels-Alder reaction with a conjugated diene, proposed by Schwab et al. (Figure 13), resulting in the formation of cyclic products. It

has been shown that increased pressure favors bimolecular reactions, however this explanation is less likely since butadiene was not identified as a gas product in this work.

Referring to Figure 43, the yield of all gas phase products increased at elevated temperature levels. This implies that primary reactions such as decarbonylation (formation of CO) and decarboxylation (formation of CO_2) are endothermic reactions. Increased yields of the other hydrocarbon gas products implies that secondary reactions leading to their formation are also endothermic.

Referring again to Figure 43, with the exception of hexane, the yield of all gas phase products decreased as the feed rate was increased (lower residence time). This is typical of cracking reactions and is consistent with the observations of Idem et al [8].

Figure 44 summarizes the statistically significant interactions for the effects on the gas product yield. The figure shows that the majority of components exhibited a two way interaction between feed rate and temperature. Lower feed rate (longer residence time) enhanced the temperature effects.

Gas Product	Significant Interaction	Reference
H2	↓ Feed Rate, ↑ Temperature Effect	Figure 47
CO	↓ Feed Rate, ↑ Temperature Effect	Figure 50
Methane	↓ Feed Rate, ↑ Temperature Effect	Figure 53
CO_2	↓ Feed Rate, ↑ Temperature Effect	Figure 58
Ethylene	↓ Feed Rate, ↑ Temperature Effect	Figure 61
Propane	↓ Feed Rate, ↑ Temperature Effect	Figure 64
Propylene	↓ Feed Rate, ↑ Temperature Effect	Figure 67
Butene	↓ Feed Rate, ↑ Temperature Effect	Figure 70
Pentane	↓ Feed Rate, ↑ Temperature Effect	Figure 73
Hexane		

Figure 44. Significant interactions summary on gas product yield response

Figure 45 through Figure 75 on the following pages illustrate the detailed yield results for the individual gas phase products, and include the main effects and interaction plots from the split-plot DOE analysis. Refer to Appendix J for the DOE statistical analysis results.

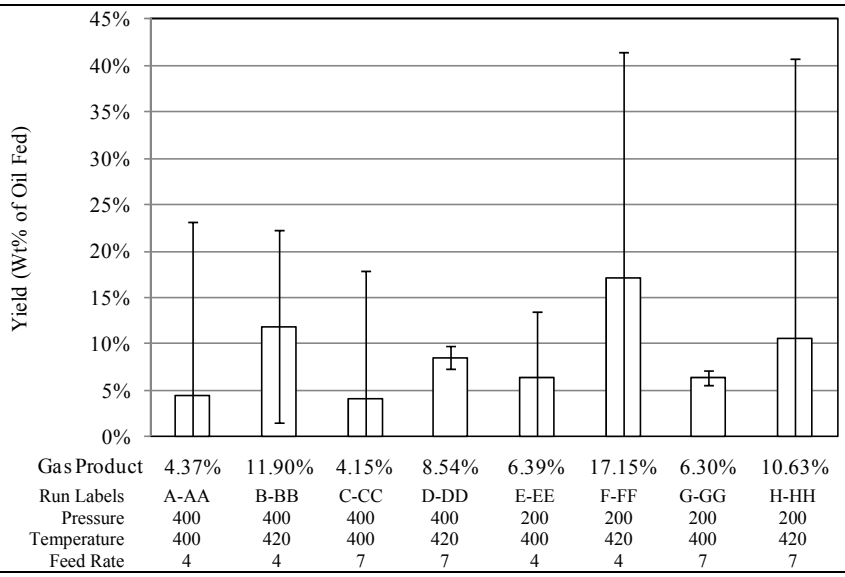

Gas Product	4.37%	11.90%	4.15%	8.54%	6.39%	17.15%	6.30%	10.63%
Run Labels	A-AA	B-BB	C-CC	D-DD	E-EE	F-FF	G-GG	H-HH
Pressure	400	400	400	400	200	200	200	200
Temperature	400	420	400	420	400	420	400	420
Feed Rate	4	4	7	7	4	4	7	7

Figure 45. Gas product yield

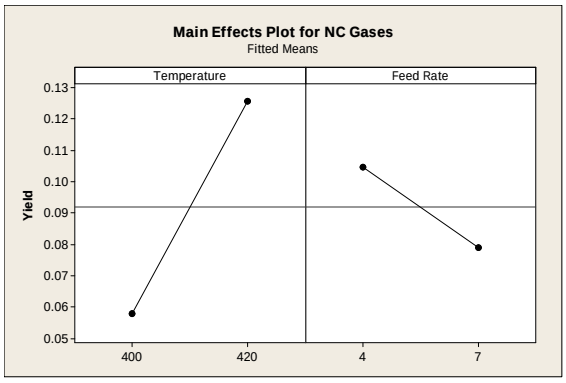

Figure 46. Gas product yield - significant main effects plot

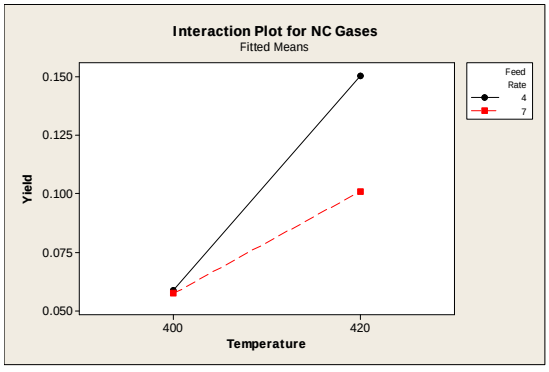

Figure 47. Gas product yield – significant interactions plot

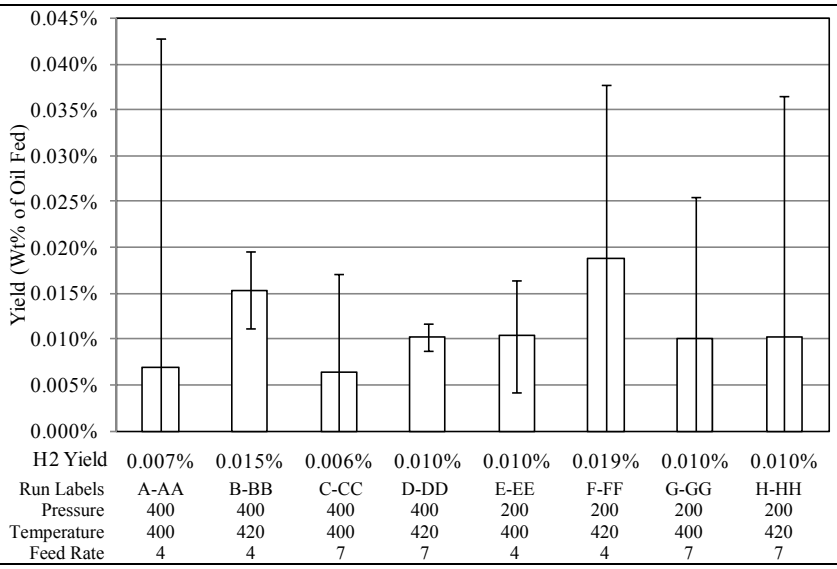

H2 Yield	0.007%	0.015%	0.006%	0.010%	0.010%	0.019%	0.010%	0.010%
Run Labels	A-AA	B-BB	C-CC	D-DD	E-EE	F-FF	G-GG	H-HH
Pressure	400	400	400	400	200	200	200	200
Temperature	400	420	400	420	400	420	400	420
Feed Rate	4	4	7	7	4	4	7	7

Figure 48. Hydrogen product yield

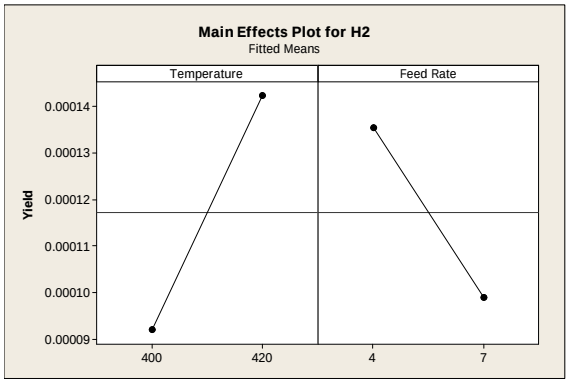

Figure 49. Hydrogen yield – significant main effects plot

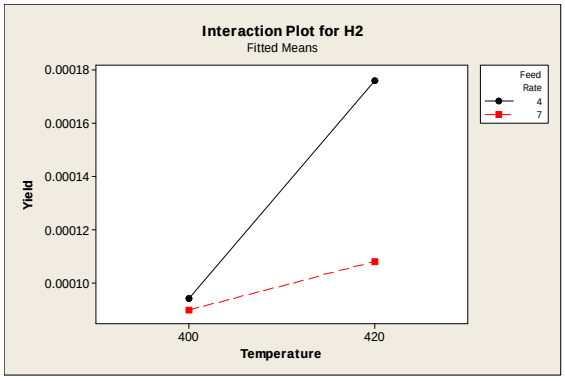

Figure 50. Hydrogen yield – significant main interactions plot

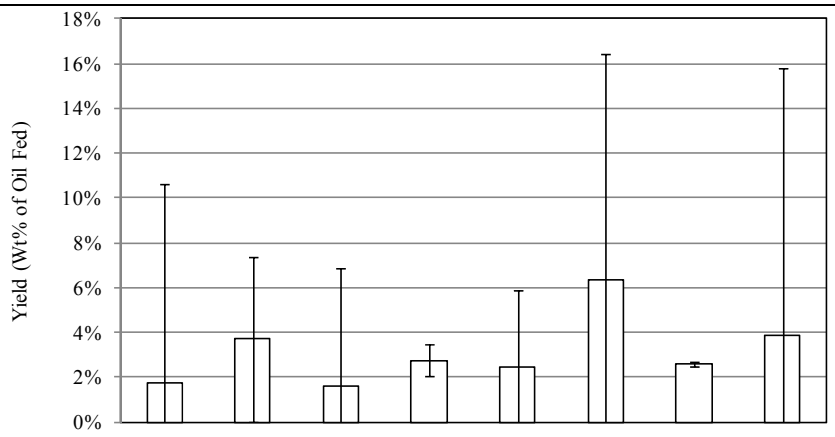

CO Yield	1.72%	3.70%	1.58%	2.76%	2.46%	6.34%	2.60%	3.84%
Run Labels	A-AA	B-BB	C-CC	D-DD	E-EE	F-FF	G-GG	H-HH
Pressure	400	400	400	400	200	200	200	200
Temperature	400	420	400	420	400	420	400	420
Feed Rate	4	4	7	7	4	4	7	7

Figure 51. Carbon monoxide product yield

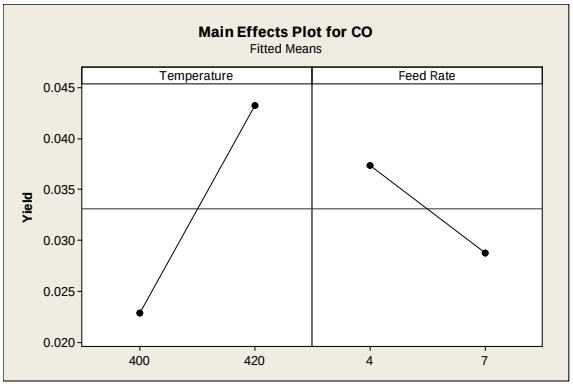

Figure 52. Carbon monoxide yield – significant main effects plot

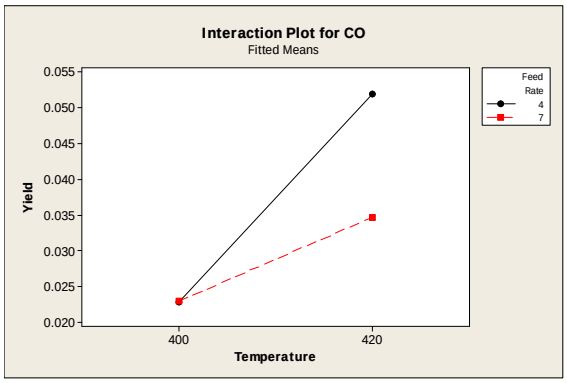

Figure 53. Carbon monoxide yield – significant interactions plot

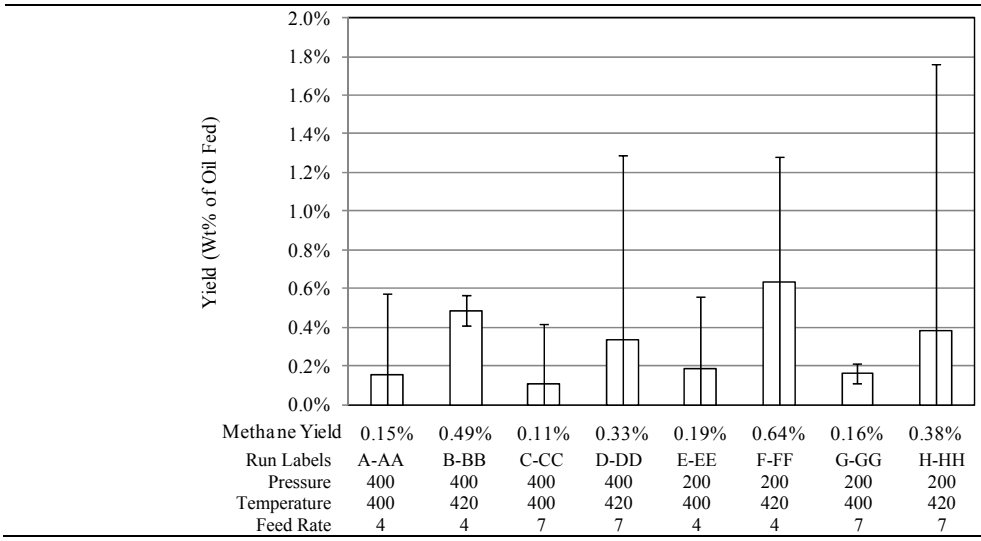

Figure 54. Methane product yield

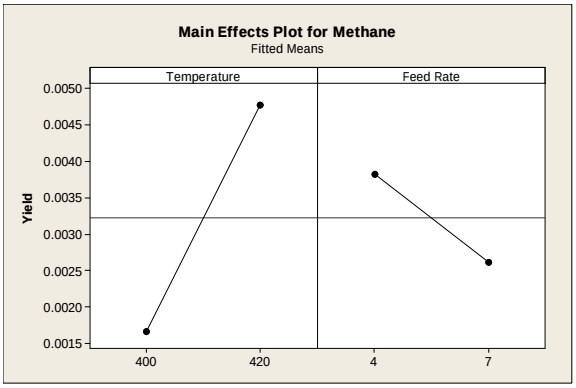

Figure 55. Methane product yield - significant main effects plot

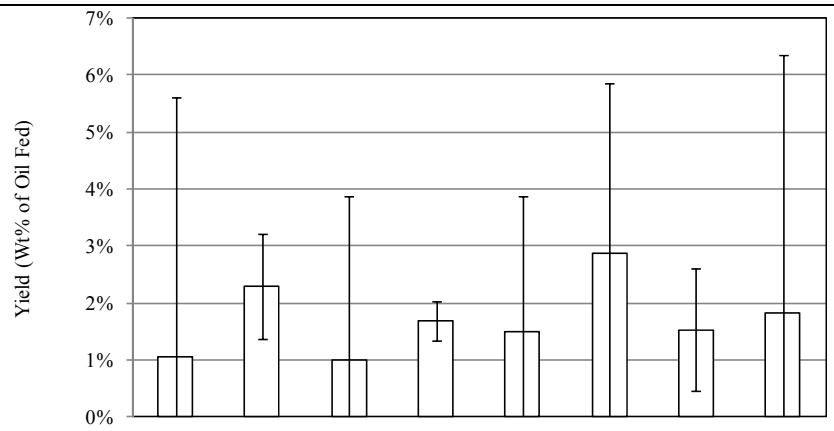

CO2 Yield	1.06%	2.30%	1.01%	1.69%	1.51%	2.87%	1.53%	1.84%
Run Labels	A-AA	B-BB	C-CC	D-DD	E-EE	F-FF	G-GG	H-HH
Pressure	400	400	400	400	200	200	200	200
Temperature	400	420	400	420	400	420	400	420
Feed Rate	4	4	7	7	4	4	7	7

Figure 56. Carbon dioxide product yield

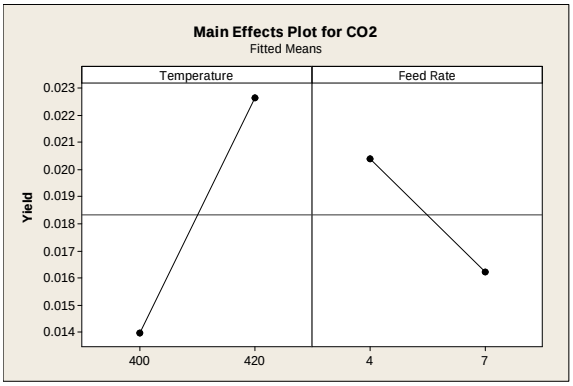

Figure 57. Carbon dioxide product yield - significant main effects plot

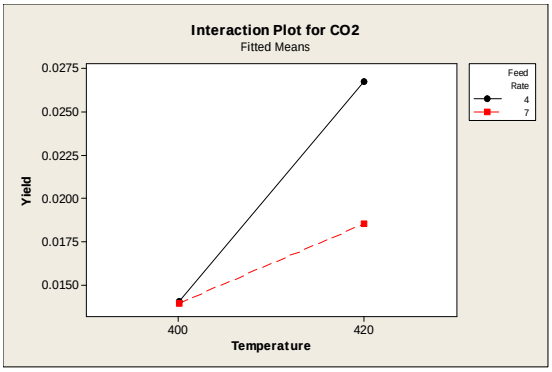

Figure 58. Carbon dioxide product yield – significant interactions plot

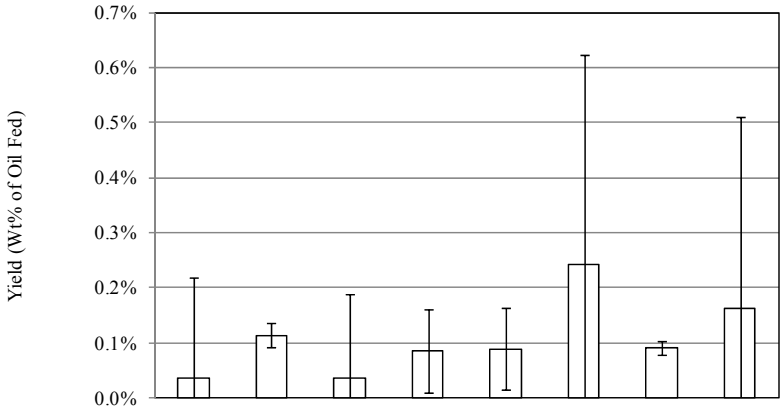

Ethylene Yield	0.03%	0.11%	0.04%	0.09%	0.09%	0.24%	0.09%	0.16%
Run Labels	A-AA	B-BB	C-CC	D-DD	E-EE	F-FF	G-GG	H-HH
Pressure	400	400	400	400	200	200	200	200
Temperature	400	420	400	420	400	420	400	420
Feed Rate	4	4	7	7	4	4	7	7

Figure 59. Ethylene product yield

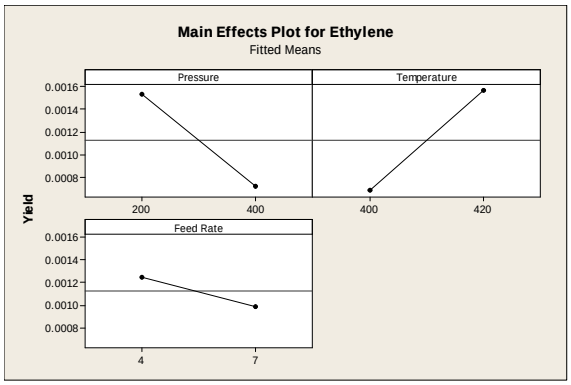

Figure 60. Ethylene product yield - significant main effects plot

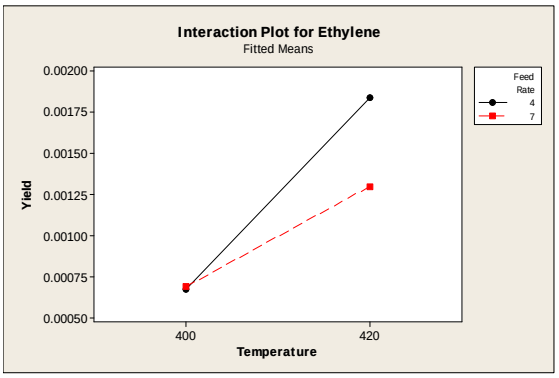

Figure 61. Ethylene product yield – significant interactions plot

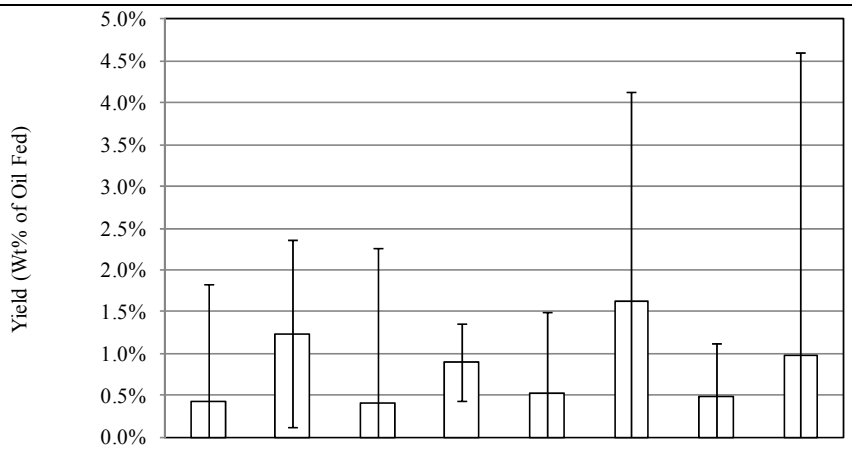

Propane Yield	0.42%	1.24%	0.40%	0.90%	0.53%	1.62%	0.49%	0.98%
Run Labels	A-AA	B-BB	C-CC	D-DD	E-EE	F-FF	G-GG	H-HH
Pressure	400	400	400	400	200	200	200	200
Temperature	400	420	400	420	400	420	400	420
Feed Rate	4	4	7	7	4	4	7	7

Figure 62. Propane product yield

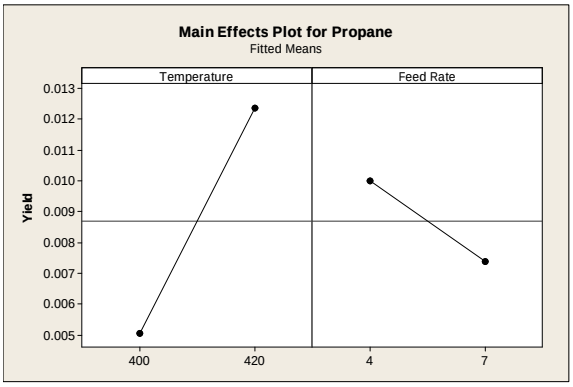

Figure 63. Propane product yield - significant main effects plot

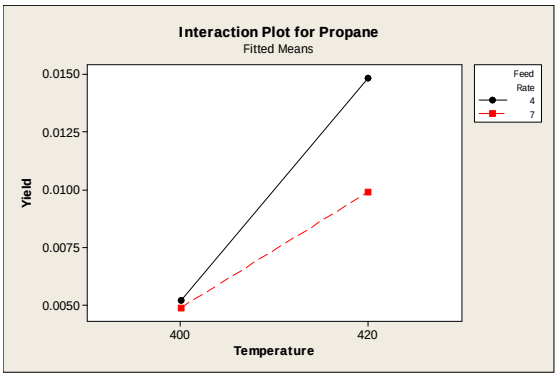

Figure 64. Propane product yield – significant interactions plot

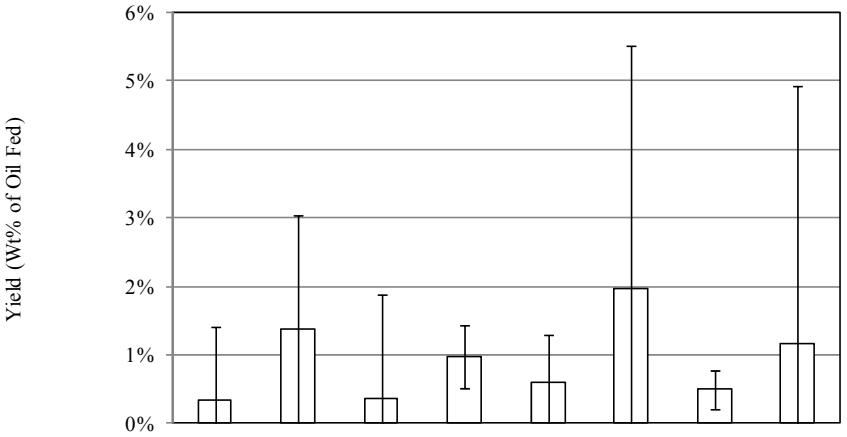

Propylene Yield	0.35%	1.38%	0.36%	0.99%	0.60%	1.96%	0.49%	1.17%
Run Labels	A-AA	B-BB	C-CC	D-DD	E-EE	F-FF	G-GG	H-HH
Pressure	400	400	400	400	200	200	200	200
Temperature	400	420	400	420	400	420	400	420
Feed Rate	4	4	7	7	4	4	7	7

Figure 65. Propylene product yield

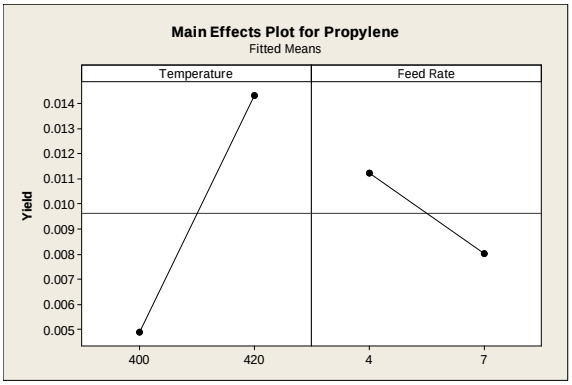

Figure 66. Propylene product yield - significant main effects plot

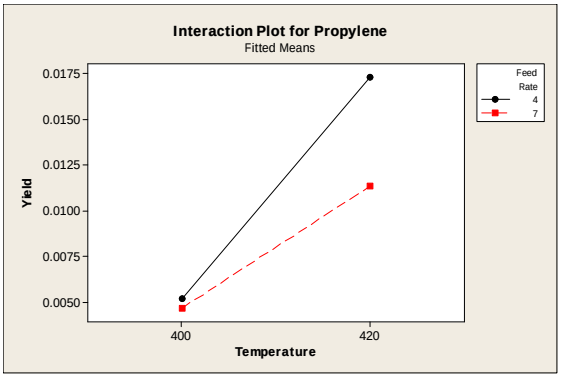

Figure 67. Propylene product yield – significant interactions plot

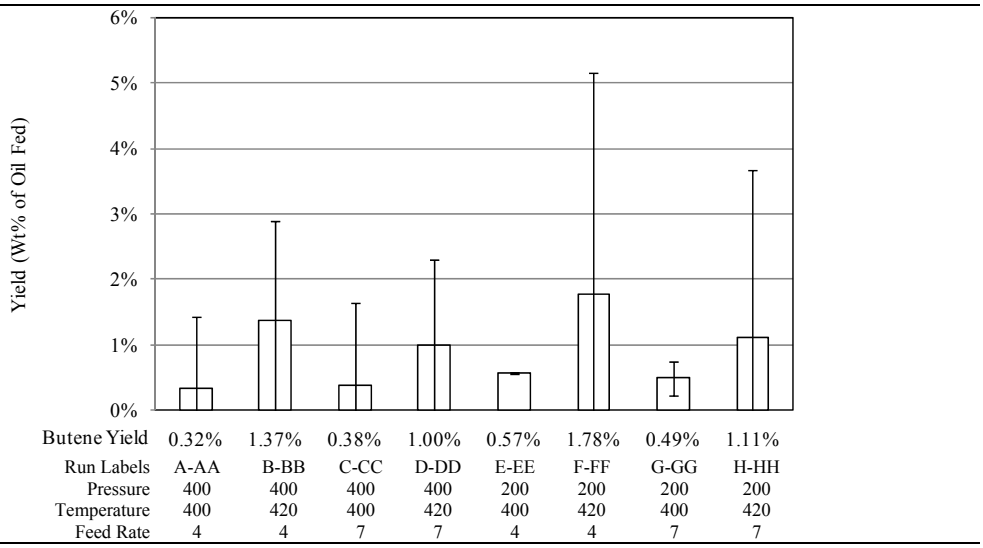

Figure 68. Butene product yield

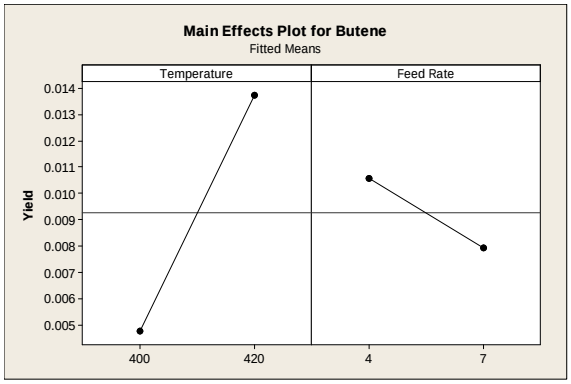

Figure 69. Butene product yield - significant main effects plot

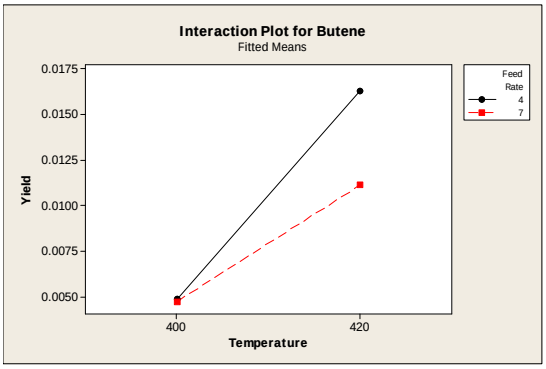

Figure 70. Butene product yield – significant interactions plot

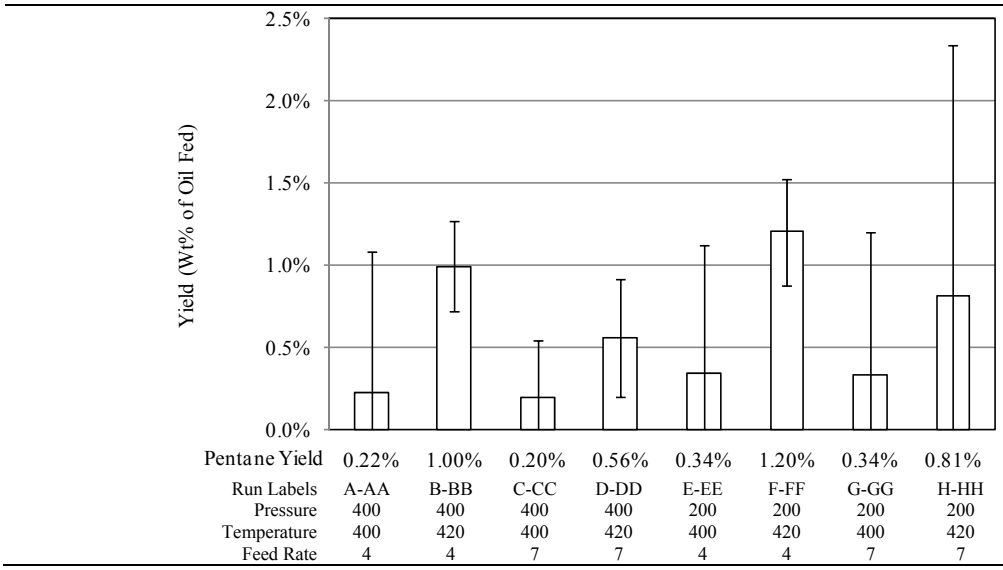

Figure 71. Pentane product yield

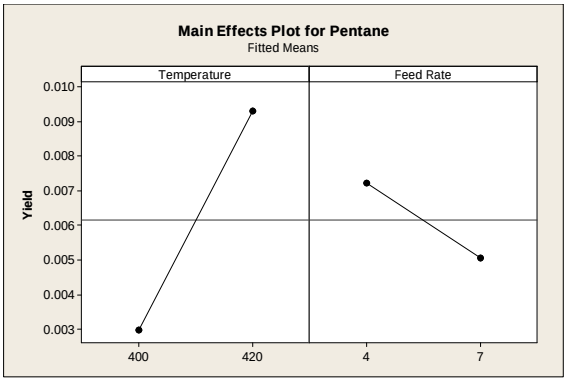

Figure 72. Pentane product yield - significant main effects plot

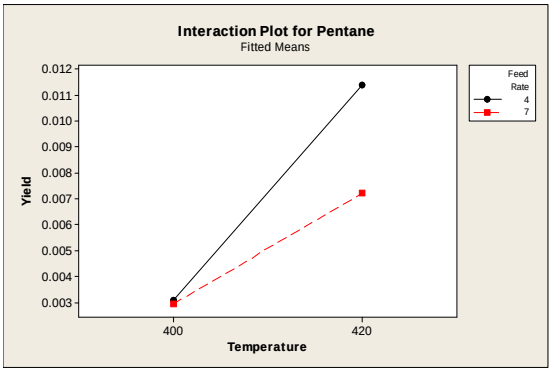

Figure 73. Pentane product yield – significant interactions plot

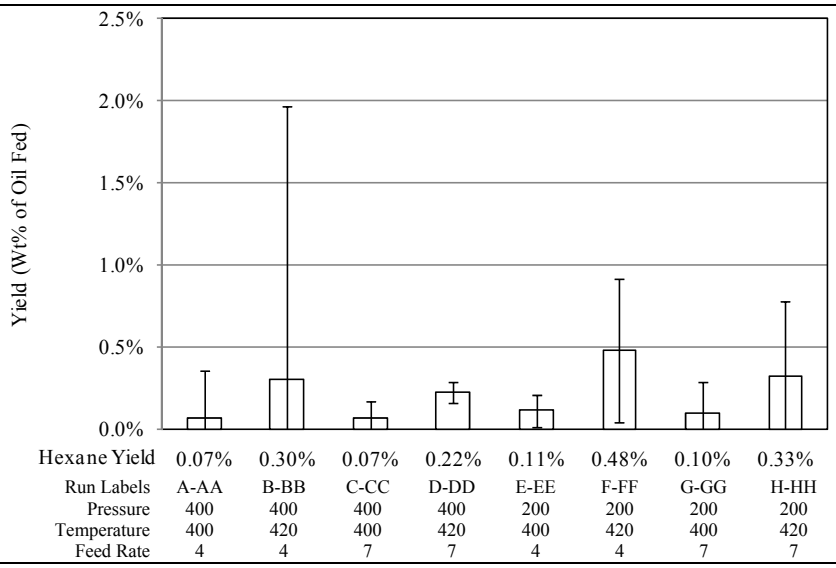

Hexane Yield	0.07%	0.30%	0.07%	0.22%	0.11%	0.48%	0.10%	0.33%
Run Labels	A-AA	B-BB	C-CC	D-DD	E-EE	F-FF	G-GG	H-HH
Pressure	400	400	400	400	200	200	200	200
Temperature	400	420	400	420	400	420	400	420
Feed Rate	4	4	7	7	4	4	7	7

Figure 74. Hexane product yield

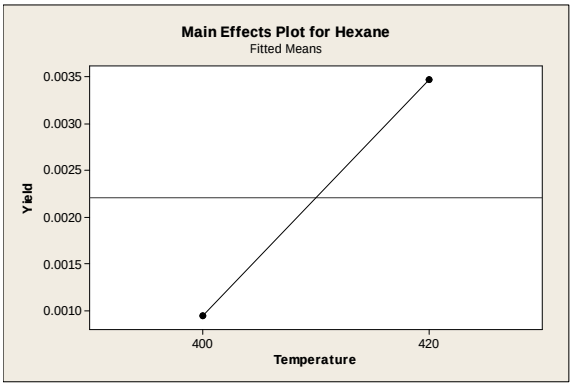

Figure 75. Hexane product yield - significant main effects plot

Gas Product Yield Comparison of Alternative Oil Feedstocks

Three different oil feedstocks (soybean, high oleic canola, and jojoba) were thermally cracked under identical conditions, and the gas product yield results for the three oil feeds are illustrated in Figure 76. The processing conditions were 1.38 MPa gauge (200 psig) pressure, temperature of 420°C, and feed rate of 4 L/hr.

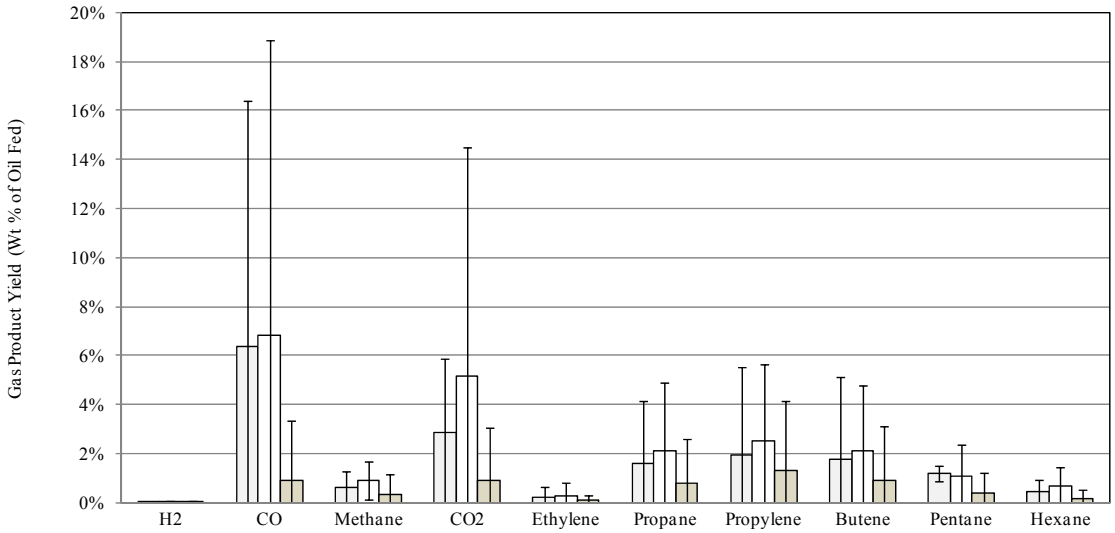

Figure 76. Gas product yield comparison between different oil feedstocks (soybean, high oleic canola, and jojoba)

From Figure 76, the CO_2 yield for high oleic canola and soybean was 5.14% and 2.87%, respectively. The canola feedstock composed of 75% oleic acid (C18:1) underwent a higher level of decarboxylation than the soybean feedstock comprised of 54% linoleic acid (C18:2). This result suggests that the quantity of fatty acid unsaturated sites has an influence on decarboxylation reaction mechanism, with a monounsaturated

fatty acid favoring decarboxylation over a polyunsaturated fatty acid. Carbon monoxide yields of these two feedstocks are similar (6.85% for canola and 6.34% for soybean). This result implies that decarbonylation reaction mechanism is not affected by the level of triglyceride fatty acid unsaturation.

From Figure 76, the CO_2 yield for high oleic canola and jojoba was 5.14% and 0.93%, respectively. The canola feedstock composed of 75% oleic acid (C18:1) underwent a higher level of decarboxylation than the jojoba feedstock comprised mainly of a C_{42} ester structure. This result appears to suggest that canola oil cracking was more prevalent under these conditions, and the fact that the carbon to carboxylic acid ratio for jojoba oil is roughly double that of the triglyceride oils may play a part in this observation as well. Carbon monoxide yields of these two feedstocks favored canola oil also at 6.85%, compared to jojoba oil at 0.93%.

Overall, jojoba oil thermal cracking resulted in lower gas phase product yields when compared with soybean and canola. Soybean oil however displayed similar gas product yields as canola, with the exception of CO_2 yield.

Gas Product Concentration

This section addresses the concentration (mole %) of the gas product components. Beyond the gas product yield results in the previous section, the gas product concentration can be used to better understand the reaction scheme of the gas phase products. Figure 77 provides a summary of the statically significant main effects.

	Higher Pressure Level	Higher Temperature Level	Higher Feed Rate Level	Reference
H2		↓ Mole %		Figure 80
CO		↓ Mole %		Figure 82
Methane		↑ Mole %		Figure 85
CO_2		↓ Mole %	↑ Mole %	Figure 87
Ethylene	↓ Mole %	↑ Mole %		Figure 90
Propane	↑ Mole %	↑ Mole %		Figure 92
Propylene		↑ Mole %		Figure 94
Butene		↑ Mole %		Figure 96
Pentane		↑ Mole %		Figure 98
Hexane		↑ Mole %		Figure 100

Figure 77. Summary of Gas Product Concentration - Significant Main Effects.

From Figure 77, ethylene concentration decreased with an increase in pressure level. This may mean either that ethylene formation is being suppressed or ethylene consumption is being enhanced at elevated pressure. According to the reaction scheme proposed by Alencar et al. from Figure 12, ethylene may be formed by its unimolecular elimination from hydrocarbon radicals during secondary cracking. Increased pressure has been shown to be unfavorable towards unimolecular reactions, and may play a part in this observation. Ethylene may also be consumed by the bimolecular Diels-Alder reaction with a conjugated diene, proposed by Schwab et al. from Figure 13, resulting in the formation of cyclic products. It is known that increased pressure favors bimolecular

reactions, however this explanation is maybe less likely since butadiene was not identified as a gas product.

Referring to Figure 77, propane concentration increased with an increase in pressure level. Bimolecular reactions are favored at elevated pressure, and this observation may be the result of an enhanced bimolecular pathway leading to propane product generation.

Elevated temperatures had a varied effect on the molar distribution of gas phase products. Elevated temperatures reduced the concentration of CO and CO_2. This may be explained by literature accounts that decarbonylation and decarboxylation are primary reactions. However at elevated temperatures, it appears that the rate of secondary cracking reactions in the production of methane, ethylene, propane, propylene, butene, pentane, and hexane are dominant.

Elevated temperatures also reduced the concentration of molecular hydrogen. Hydrogen generation is favored at elevated temperatures [15], yet the results show a reduction of hydrogen concentration in the gas product. Hydrogen is generated by proton extraction in the formation of cycloolefins, aromatics, coke formation, and polymerization of olefins and aromatics, and hydrogen is consumed by hydrocarbon radical stabilization [8]. Since higher temperatures favor hydrogen generation, one is left to assume that the observed reduction in hydrogen concentration at elevated temperature is the result of increased hydrogen consumption due to the stabilization of hydrocarbon radicals.

Figure 78 summarizes the statistically significant interactions for the effects on the gas product concentration. The figure shows that a CO and CO_2 exhibited a two way

interaction between pressure and temperature. The higher pressure level enhanced the temperature effect on CO concentration, and diminishes the temperature effect on CO_2 concentration.

	Significant Interaction	Reference
H2		
CO	↑ Pressure, ↑ Temperature Effect	Figure 83
Methane		
CO_2	↑ Pressure, ↓ Temperature Effect	Figure 88
Ethylene		
Propane		
Propylene		
Butene		
Pentane		
Hexane		

Figure 78. Summary of Gas Product Concentration – Significant Interactions

Figure 79 through Figure 100 on the following pages illustrates the concentration results for the gas phase products, and includes the main effects and interaction plots from the split-plot DOE analysis. Refer to Appendix K for the DOE statistical analysis results.

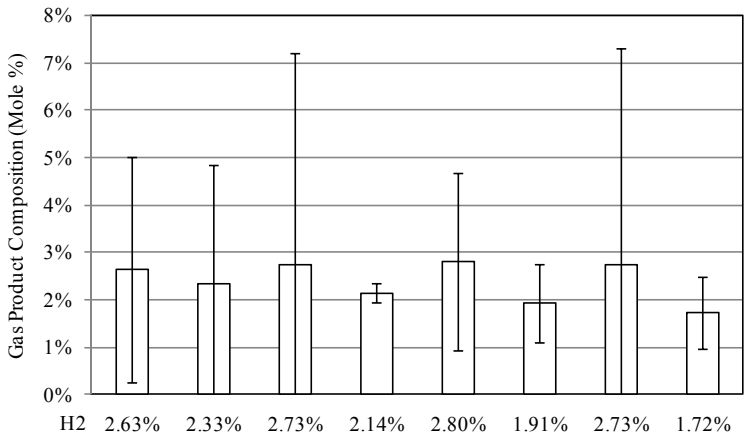

H2	2.63%	2.33%	2.73%	2.14%	2.80%	1.91%	2.73%	1.72%
Run Labels	A-AA	B-BB	C-CC	D-DD	E-EE	F-FF	G-GG	H-HH
Pressure	400	400	400	400	200	200	200	200
Temperature	400	420	400	420	400	420	400	420
Feed Rate	4	4	7	7	4	4	7	7

Figure 79. Hydrogen - Gas Product Molar Composition

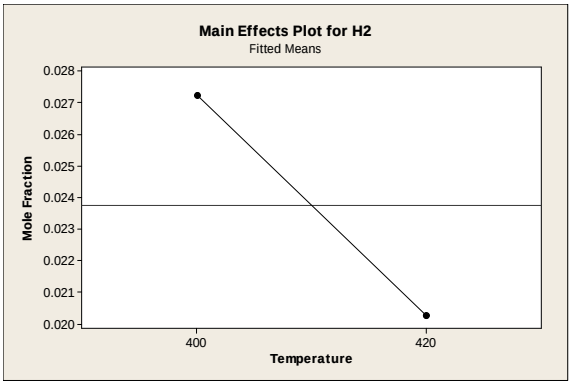

Figure 80. Hydrogen Gas Molar Composition – Significant Main Effects

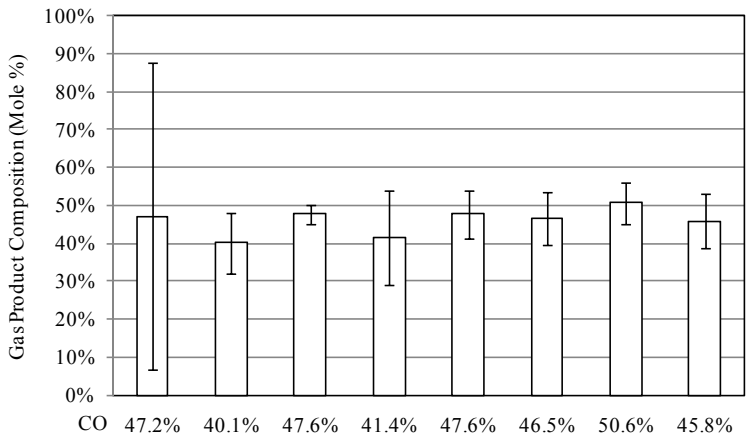

CO	47.2%	40.1%	47.6%	41.4%	47.6%	46.5%	50.6%	45.8%
Run Labels	A-AA	B-BB	C-CC	D-DD	E-EE	F-FF	G-GG	H-HH
Pressure	400	400	400	400	200	200	200	200
Temperature	400	420	400	420	400	420	400	420
Feed Rate	4	4	7	7	4	4	7	7

Figure 81. Carbon Monoxide - Gas Product Molar Composition

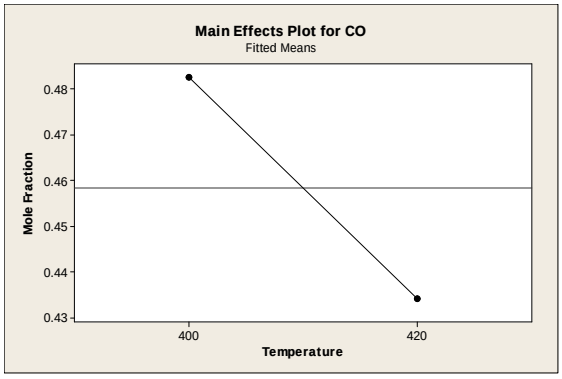

Figure 82. Carbon Monoxide Gas Molar Composition – Significant Main Effects

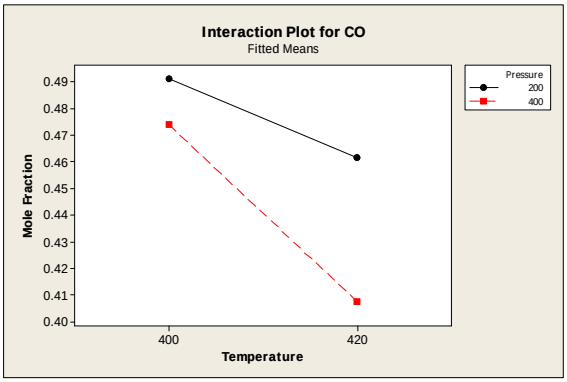

Figure 83. Carbon Monoxide Gas Molar Composition – Significant Interactions

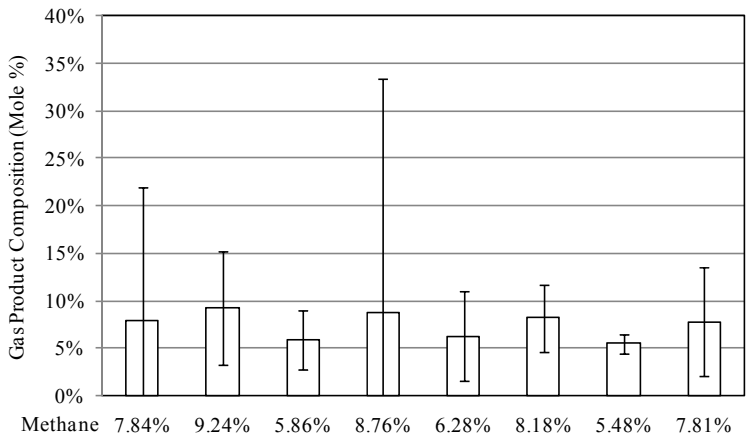

Methane	7.84%	9.24%	5.86%	8.76%	6.28%	8.18%	5.48%	7.81%
Run Labels	A-AA	B-BB	C-CC	D-DD	E-EE	F-FF	G-GG	H-HH
Pressure	400	400	400	400	200	200	200	200
Temperature	400	420	400	420	400	420	400	420
Feed Rate	4	4	7	7	4	4	7	7

Figure 84. Methane - Gas Product Molar Composition

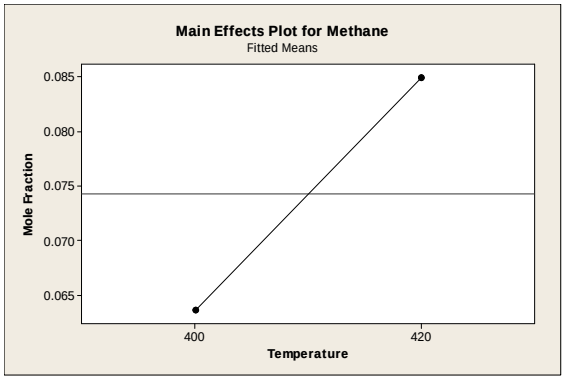

Figure 85. Methane Gas Molar Composition – Significant Main Effects

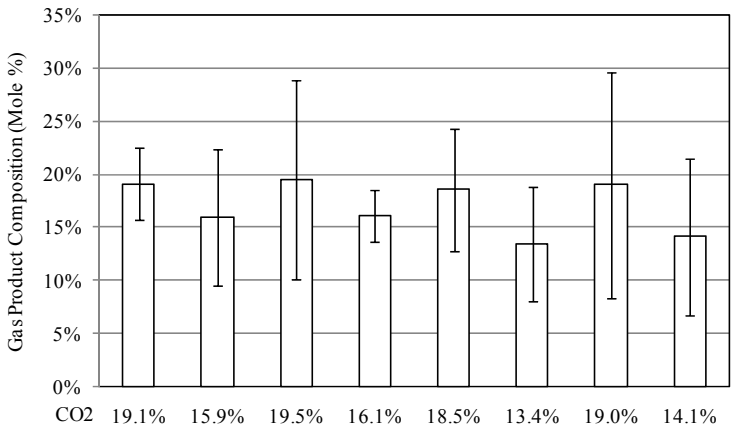

Figure 86. Carbon Dioxide - Gas Product Molar Composition

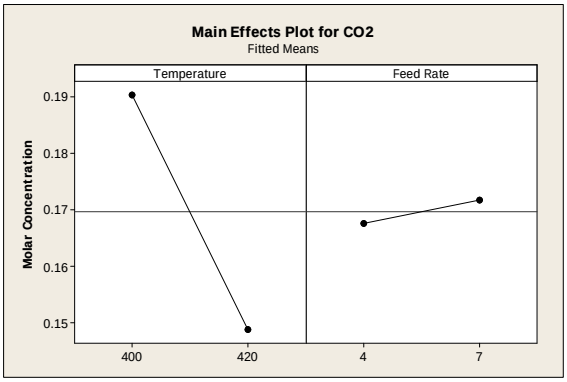

Figure 87. Carbon Dioxide Gas Molar Composition – Significant Main Effects

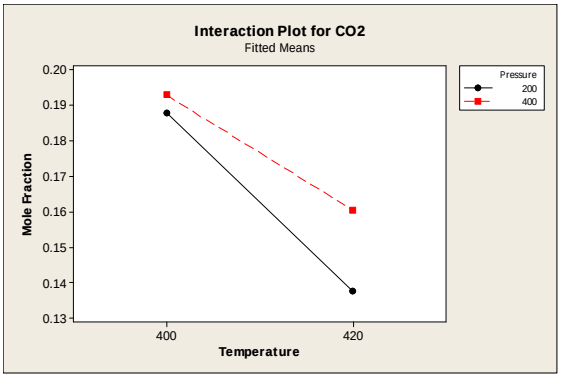

Figure 88. Carbon Dioxide Gas Molar Composition – Significant Interactions

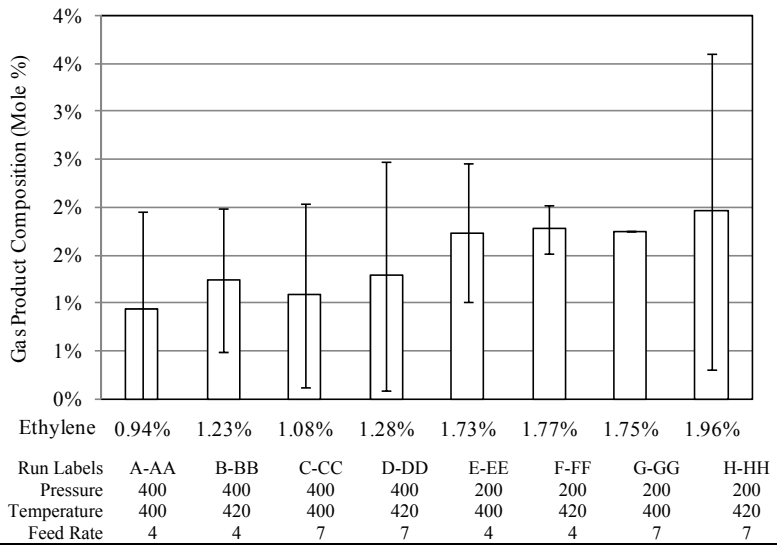

Ethylene	0.94%	1.23%	1.08%	1.28%	1.73%	1.77%	1.75%	1.96%
Run Labels	A-AA	B-BB	C-CC	D-DD	E-EE	F-FF	G-GG	H-HH
Pressure	400	400	400	400	200	200	200	200
Temperature	400	420	400	420	400	420	400	420
Feed Rate	4	4	7	7	4	4	7	7

Figure 89. Ethylene - Gas Product Molar Composition

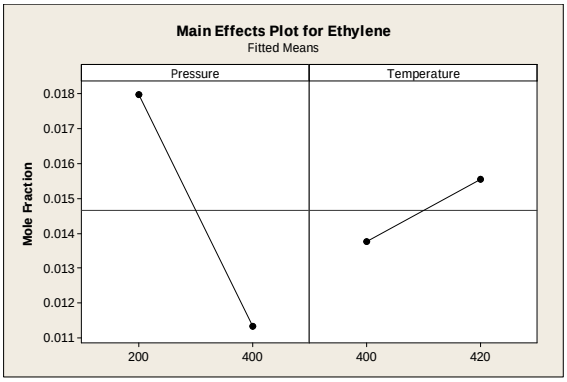

Figure 90. Ethylene Gas Molar Composition – Significant Main Effects

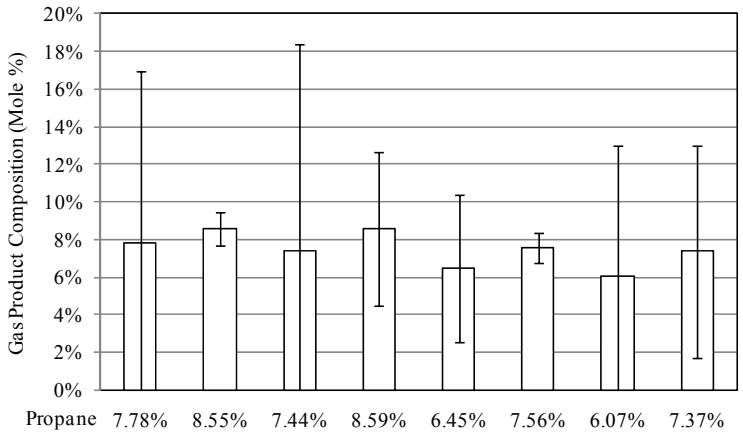

Propane	7.78%	8.55%	7.44%	8.59%	6.45%	7.56%	6.07%	7.37%
Run Labels	A-AA	B-BB	C-CC	D-DD	E-EE	F-FF	G-GG	H-HH
Pressure	400	400	400	400	200	200	200	200
Temperature	400	420	400	420	400	420	400	420
Feed Rate	4	4	7	7	4	4	7	7

Figure 91. Propane - Gas Product Molar Composition

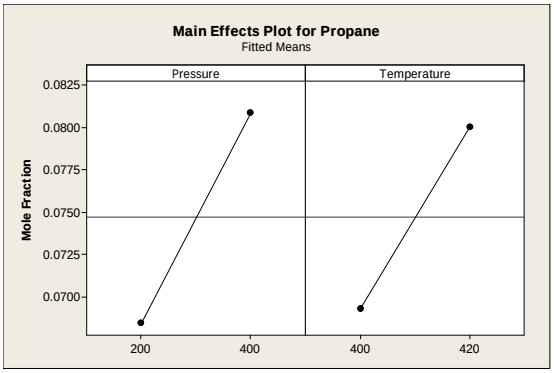

Figure 92. Propane Gas Molar Composition – Significant Main Effects

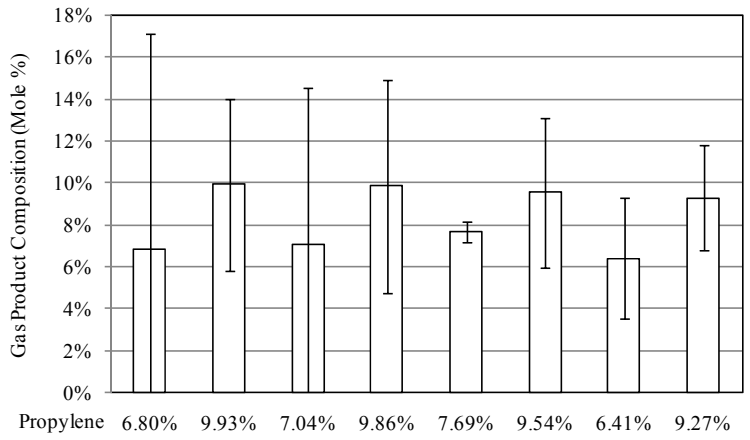

Propylene	6.80%	9.93%	7.04%	9.86%	7.69%	9.54%	6.41%	9.27%
Run Labels	A-AA	B-BB	C-CC	D-DD	E-EE	F-FF	G-GG	H-HH
Pressure	400	400	400	400	200	200	200	200
Temperature	400	420	400	420	400	420	400	420
Feed Rate	4	4	7	7	4	4	7	7

Figure 93. Propylene - Gas Product Molar Composition

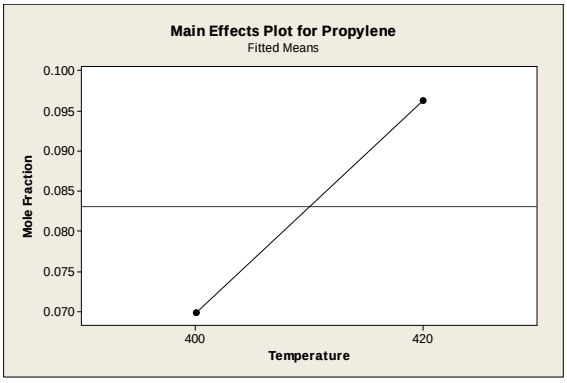

Figure 94. Propylene Gas Molar Composition – Significant Main Effects

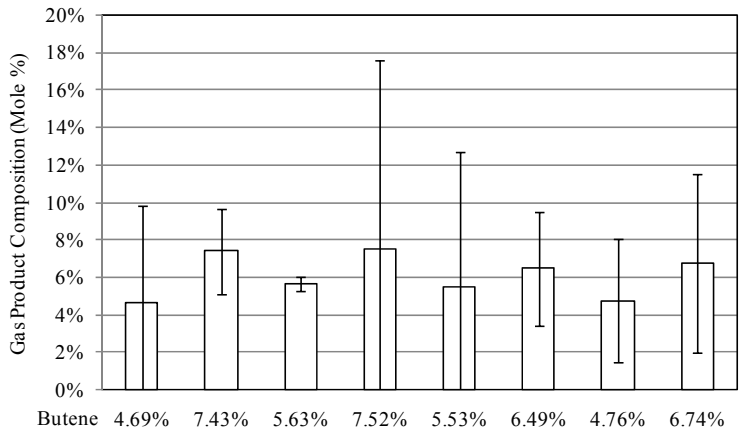

Butene	4.69%	7.43%	5.63%	7.52%	5.53%	6.49%	4.76%	6.74%
Run Labels	A-AA	B-BB	C-CC	D-DD	E-EE	F-FF	G-GG	H-HH
Pressure	400	400	400	400	200	200	200	200
Temperature	400	420	400	420	400	420	400	420
Feed Rate	4	4	7	7	4	4	7	7

Figure 95. Butene - Gas Product Molar Composition

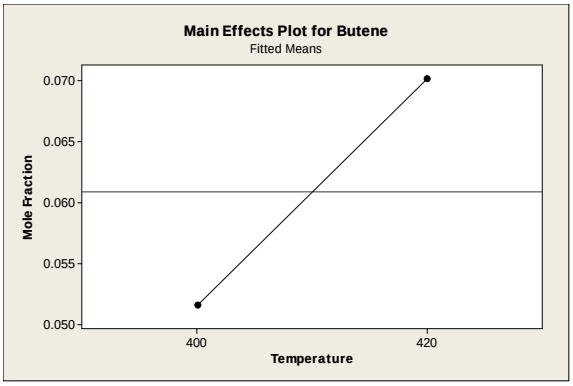

Figure 96. Butene Gas Molar Composition – Significant Main Effects

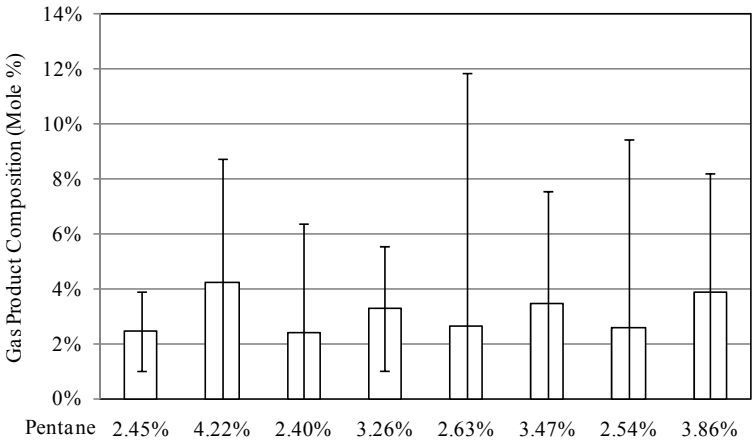

Pentane	2.45%	4.22%	2.40%	3.26%	2.63%	3.47%	2.54%	3.86%
Run Labels	A-AA	B-BB	C-CC	D-DD	E-EE	F-FF	G-GG	H-HH
Pressure	400	400	400	400	200	200	200	200
Temperature	400	420	400	420	400	420	400	420
Feed Rate	4	4	7	7	4	4	7	7

Figure 97. Pentane - Gas Product Molar Composition

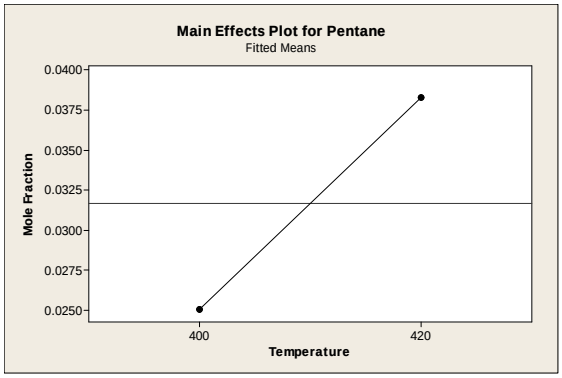

Figure 98. Pentane Gas Molar Composition – Significant Main Effects

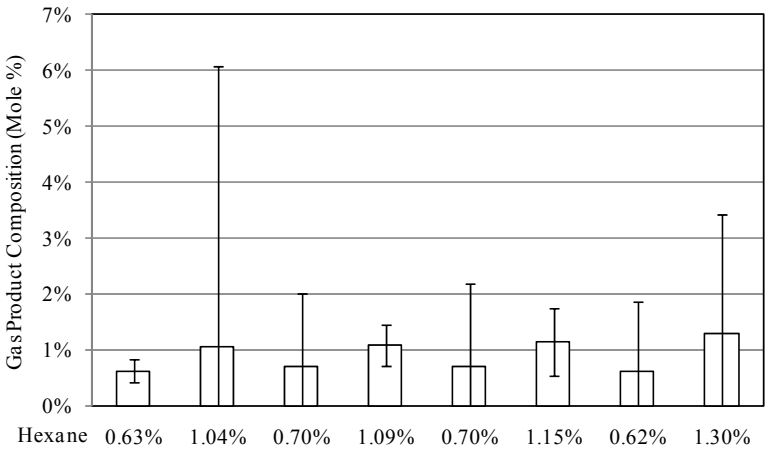

Hexane	0.63%	1.04%	0.70%	1.09%	0.70%	1.15%	0.62%	1.30%
Run Labels	A-AA	B-BB	C-CC	D-DD	E-EE	F-FF	G-GG	H-HH
Pressure	400	400	400	400	200	200	200	200
Temperature	400	420	400	420	400	420	400	420
Feed Rate	4	4	7	7	4	4	7	7

Figure 99. Hexane - Gas Product Molar Composition

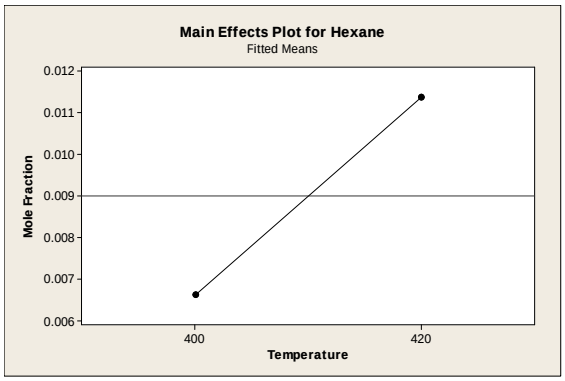

Figure 100. Hexane Gas Molar Composition – Significant Main Effects

Gas Product Concentration Comparison of Alternative Oil Feedstocks

Three different oil feedstocks (soybean, high oleic canola, and jojoba) were thermally cracked under identical conditions. The processing conditions were a pressure of 1.38 MPa gauge (200 psig), temperature of 420°C, and feed rate of 4 L/hr. The gas product molar percentage results for the three oil feeds are illustrated in Figure 101. Figure 16 may be referenced for the fatty acid compositions of the three oil feedstocks.

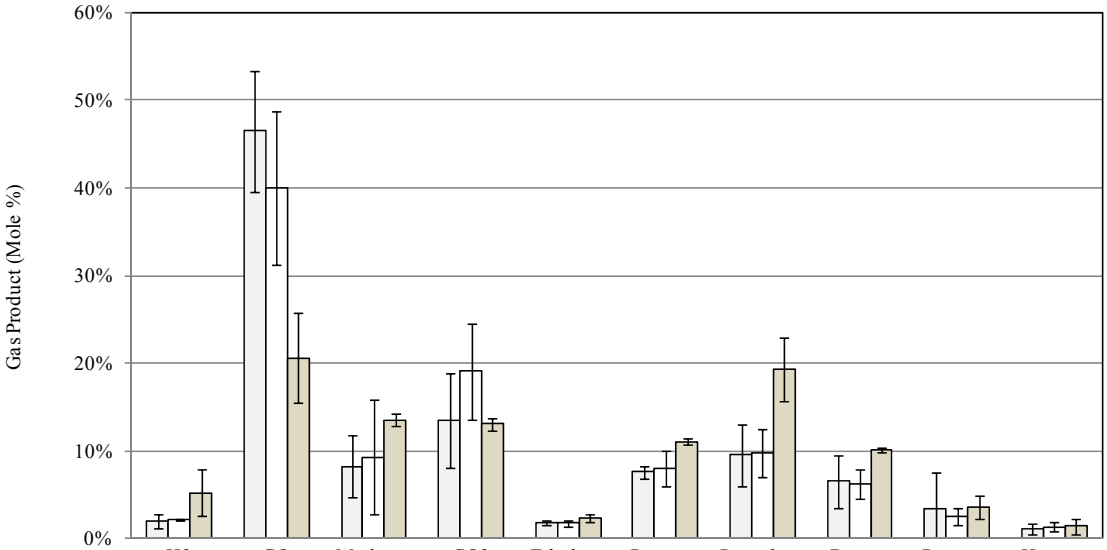

	H2	CO	Methane	CO2	Ethylene	Propane	Propylene	Butene	Pentane	Hexane
Soybean	1.9%	46.5%	8.2%	13.4%	1.8%	7.6%	9.5%	6.5%	3.5%	1.1%
HO Canola	2.1%	40.0%	9.3%	19.1%	1.8%	8.0%	9.8%	6.2%	2.5%	1.3%
Jojoba	5.2%	20.6%	13.5%	13.1%	2.3%	11.0%	19.2%	10.1%	3.5%	1.4%

Conditions: 1.38 MPa gauge (200 psig)g, 420°C, 4 L/hr

Figure 101. Gas Product Molar Composition of Alternative Oil Feedstocks (Soybean, High Oleic Canola, and Jojoba)

From Figure 101, the gas product from canola oil feedstock favored carbon dioxide gas phase products over the two other feedstocks. This observation suggests crop oils with monounsaturated fatty acids such as high oleic canola favor the decarboxylation reaction pathway more than polyunsaturated crop oils such as soybean. Also,

monounsaturated fatty acids of shorter carbon length favor decarboxylation over monounsaturated fatty acids of longer carbon length.

Again referring to Figure 101, the gas product from soybean oil feedstock favored carbon monoxide gas phase products over the two other feedstocks. Carbon monoxide may be generated from decarbonylation of oxygenated hydrocarbons such as ketones, aldehydes, fatty acids and esters, or by hydrogenation of carbon dioxide. This observation suggests that polyunsaturated fatty acids either favor the formation of ketones and aldehydes intermediate products leading to the production of CO by decarbonylation, or an increase in the hydrogenation reaction pathway from CO_2 to CO.

CHAPTER VI
CONCLUSIONS AND RECOMMENDATIONS

The goal of this work was to explore the thermal cracking effects of pressure, temperature, and feed rate on the characterization of the liquid and gas products generated from crop oil feed stocks.

This work was initiated to try and address problems with olefin product generation in the previous UND bench scale plug flow reactor (PFR). The PFR reactor was only capable of being operated at pressures of around 0.34 MPa gauge (50 psig), and it was postulated that olefins generated during liquid phase cracking in the PFR lacked sufficient gas phase residence time under these low pressure conditions to further react to alkanes and aromatics, which are more desirable liquid fuel compounds. Preliminary experimentation with the new pressurized CSTR reactor supported this theory.

One noted success of this work was overcoming previous UND bench scale PFR reactor design deficiencies of poor feed rate control, poor temperature control, leakage issues, coking, and maintenance shortcomings that hindered experimental efforts. This reactor design was capable of long term continuous operation at steady state conditions which made it possible to carry out these experiments.

Some important aspects of this work that contributed to this area of study include the continuous flow and bench scale design, as published research into the thermal cracking of crop oils has focused on utilization of lab scale batch reactors. This work is

an important step towards any future commercialization and scale up of the crop oil thermal cracking process.

A second important aspect of this work was incorporating the ability to examine the effects of pressure. The thermal cracking apparatus was designed and constructed to operate under pressurized, high temperature conditions, with a working pressure of 3.45 MPa gauge (500 psig). Research into the effects of pressure on the thermal cracking products from crop oils is an area of study void of published research.

A summary of significant findings are listed as follows.

- Pressure can be used to favor alkane over alkene products. At thermal cracking conditions of 420°C and 4 L/h, a 1.38 MPa (200 psi) increase in pressure from 1.38 to 2.76 MPa gauge (200 to 400 psig) resulted in in a 28% increase in linear alkane over terminal alkene yields, a 10% increase in linear alkane over non-terminal alkene yields, and a 24% increase in cyclic alkane over cyclic alkene yields. At thermal cracking conditions of 410°C and 5.5 L/h, a 2.32 MPa (336 psi) pressure increase from 0.910 to 3.23 MPa gauge (132 to 468 psig) resulted in a 51% increase in linear alkane over terminal alkene yields, a 28% increase in linear alkane over non-terminal alkene yields, and a 42% increase in cyclic alkane over cyclic alkene yields.
- Soybean oil middle distillate (150 to 250°C) product yield was favored at lower pressure (1.38 MPa gauge (200 psig)), higher temperature (420°C), and lower feed rate (4L/hr). All three variables were significant factors per the DOE.
- Acid number testing does not correlate with the level of liquid product decarboxylation. For example, runs F-FF showed the highest level of

decarboxylation with a CO_2 yield of 2.9%, and an acid number of 107. Comparing that to runs C-CC which had the lowest decarboxylation at a CO_2 yield of 1.0%, and an acid number of 105. This finding suggest that acid number testing in not a good measure of the relative level of carboxylic acids in the liquid product.

- Ethylene was the only gas product yield identified with pressure as a significant factor per the DOE. Ethylene yield decreased with an increase in pressure level. This finding suggests either that ethylene formation is being suppressed or ethylene consumption is being enhanced at elevated pressure. Increased pressure has been shown to be unfavorable towards unimolecular reactions, and may play a part in this observation by limiting secondary cracking reaction pathways toward ethylene products.
- Under identical thermal cracking conditions of 1.38 MPa gauge (200 psig), 420°C, and 4 L/hr, the predominant C_{42} wax esters of jojoba oil proved much less responsive to thermal degradation than the predominant C18:2 polyunsaturated fatty acids of soybean oil and C18:1 mono unsaturated fatty acids of canola oil. The middle distillate (150 to 250°C) product yields for jojoba, soybean, and canola were 12.6, 21.7, and 19.2%, respectively. This finding suggests that the wax esters of jojoba will require higher processing temperatures and/or longer residence times to achieve equivalent middle distillate results.

Future study recommendations to continue this research are listed as follows.

- Complete the qualitative and quantitative data processing of the liquid product GC-MS results, and analyze these results within the experimental DOE for the purpose of measuring the effects of pressure, temperature, and feed rate on the liquid chemical products.

APPENDICES

APPENDIX A
REACTOR DESIGN

Reactor design was a two part process. The first step included selecting a reactor volume and diameter. The second step involved the choice of wall thickness and flange classification to withstand the operating conditions.

Reactor Volume and Diameter

Reactor volume was sized based on a previous reactor setup at UND. The previous reactor had a volume of 5.5 liters, diameter of 3", Length/Diameter ratio of 16, and could be described as a plug flow reactor (PFR). A PFR is suited for gas phase reactions. It was the objective of this work however to explore liquid phase thermal cracking, so a continuous stirred tank reactor (CSTR) design was desired.

Figure 102. UND PFR reactor.

The volume of the new CSTR was based upon the previous UND PFR reactor. It was an objective to maintain a comparable throughput and conversion efficiency between the old and new design. It was assumed that the new CSTR would be 100% less efficient at conversion than the old PFR reactor, since CSTR's have less reaction stages, so the

CSTR was sized by roughly doubling the PFR volume of 5.5 liters. The final CSTR volume was established as 9.7 liters.

There were several competing factors that were used in selecting a diameter of the new CSTR. The reactor had to be of sufficient diameter to lower the L/D ratio. The reactor diameter also had to be sufficiently large enough to accept a mixer, numerous thermocouples, and allow for easy maintenance and cleaning.

Reactor vessel diameter was however limited by the exterior heaters. The reactor was to be heated by exterior ceramic heaters wrapped around the outside of the reactor. An increase of the reactor diameter would decrease the wall surface area available for exterior heating, thus increasing the heat flux requirement and temperature of the reactor walls. Coking was a problem with the previous PFR reactor, so it was desired to minimize the probability of coking by limiting the temperature of the reactor walls. A secondary constraint on a large diameter was space limitations in the laboratory.

To balance these competing objectives, a 6 inch diameter vessel was chosen, resulting in a reactor with a length/diameter ratio of 4.

Reactor Wall Thickness and Flange Classification

Reactor wall thickness and flange classification requirements were designed around the pressure and temperature of the reactor.

The first step in calculating the reactor wall thickness requirement was to select a design pressure. It was the objective to operate the new CSTR reactor at 500 psig. EQ 7 and EQ 8 were used to apply two factors of safety to the working pressure of 500 psig. The design pressure used for calculation purposes was 580 psig.

$$\begin{aligned} P_{maximum} &= 25 \text{ psi} + P_{working} \\ &= 25 \text{ psi} + 500 \text{ psig} \\ &= 525 \text{ psig} \end{aligned} \qquad \text{EQ 7 [17]}$$

$$P_{design} = 1.10 * P_{maximum}$$
$$= 1.10 * 525 \text{ psig} \qquad \text{EQ 8 [17]}$$
$$= 578 \text{ psig} \ldots \text{ use } 580 \text{ psig}$$

EQ 9 was used to calculate the minimum reactor wall thickness required.

$$t_{minimum} = \frac{P_{design} \cdot D_0}{2(S*E+P*y)} + C \qquad \text{EQ 9 [18]}$$

$$t_{minimum} = 0.333 \; inchs$$

Where:

P = Design Pressure (580 psig)
D_0 = Outside Diameter (6.625 inch)
S = allowable tensile stress (5820 psi @ 700°C for 304/304L stainless steel)
E = weld joint efficiency factor for seam-welded pipe (1)
y =dimensionless factor which varies with temperature (0.5)
C = corrosion, erosion, thread depth (0.02 inch)

The wall thickness was also adjusted to account for manufacturing tolerances of seamless rolled pipe. Manufacturers are allowed to produce pipe that is +0 to -12.5 percent from the stated nominal thickness, therefore EQ 10 adjusts $t_{minimum}$ for this potential reduction in thickness.

$$t_{\substack{minimum \\ nominal}} = \frac{t_{minimum}}{0.875} \qquad \text{EQ 10 [18]}$$

$$t_{\substack{minimum \\ nominal}} = 0.381 \; inchs$$

The thickness for 6 inch schedule 40 and 80 pipe are 0.280 and 0.432 inches respectively. Schedule 40 falls below the required thickness of 0.381 inches, therefore schedule 80 pipe was used for the CSTR reactor.

$t_{sch\ 40} = 0.280$ in >? $t_{minimum} = 0.381$ in; No

$t_{sch\ 80} = 0.432$ in >? $t_{minimum} = 0.381$ in; Yes

Reactor flanges were chosen from pressure-temperature rating for various flange classifications from Table 6. Unlike the reactor walls, the flanges would not be used as a means to transfer heat into the reactor. Therefore, it was assumed that the flange temperature would not exceed the processing temperature of 450°C.

Table 6. Pressure –Temperature Ratings for Type 304 Stainless Steel Flanges [19]

Temperature	Flange Class Working Pressure	
	400 Class	**600 Class**
800°F (427°C)	540 psig	810 psig
850°F (454°C)	**530 psig**	**790 psig**
900°F (482°C)	520 psig	780 psig
950°F (510°C)	510 psig	765 psig
1000°F (538°C)	470 psig	710 psig

From Table 6, a 400 Class flange is sufficient for this design. At 450°C, the working pressure of approximately 530 psig provided by a 400 Class flange meets the design objective of 500 psig. However, to error on the side of safety, a 600 Class flange was chosen for this application. The 600 Class flange will withstand a working pressure of about 790 psig @ 450°C, providing a 1.58 factor of safety.

The new CSTR reactor designed for these thermal cracking experiments, and used to replace the previous PFR reactor, is illustrated in Figure 103.

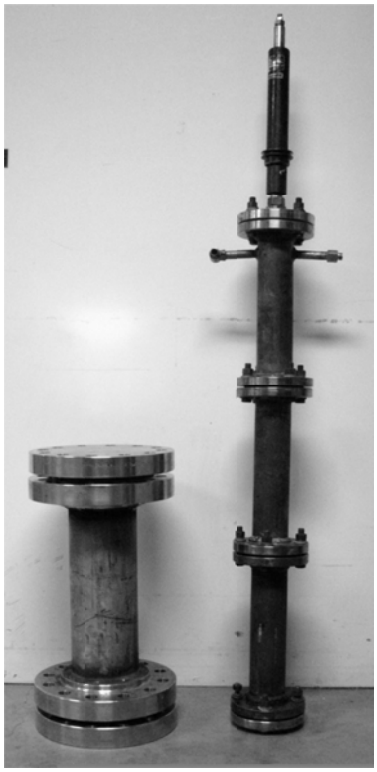

Figure 103. New CSTR vs. old PFR visual comparison.

APPENDIX B

REACTOR HEATER DESIGN

Heater design included an estimation of the heat rate required for a crop oil feed rate of 4L/hr, and a temperature increase from 25°C to 450°C. The heat rate estimation was divided into a three part assumption.

Assumption 1 included the heating of liquid oil from 25°C to 375°C. Heat rate requirements through this temperature range would treat the liquid stream as vegetable oil, and utilize specific heat capacity data for vegetable oil.

Part 2 assumed liquid vaporization at 375°C, and accounted for the heat of vaporization. For simplicity, stearic acid ($C_{18}H_{36}O_2$) was taken as the sole vaporized component.

Part 3 assumed heating of vapor crackate from 375°C to 450°C. The specific heat of crackate vapor was estimated by a thermodynamic software package.

From EQ 11, determine the oil feed mass rate ($\dot{m}_{Oil\ Feed}$)

$$\dot{m}_{\text{Oil Feed}} = \rho_{\text{Oil}} \dot{V}_{\text{Oil Feed}} \qquad \text{EQ 11}$$

Where:

$\rho_{\text{Oil}} = \text{oil density } (0.92\ \text{kg/L})$
$\dot{V}_{\text{Oil Feed}} = \text{oil volumetric feed rate } (4\ \text{L/hr})$

$$\dot{m}_{\text{Oil Feed}} = 0.92 \frac{\text{kg}}{\text{L}} \cdot 4\ \frac{\text{L}}{\text{Hr}} = 3.68 \frac{\text{kg}}{\text{Hr}}$$

Part 1

Assume: Liquid Vegetable Oil and ΔT of 350°C (25°C to 375°C)

From EQ 12, determine the specific heat capacity (C_p)of vegetable oil at 375°C.

$$C_p(t) = \left[\frac{A}{\sqrt{d}} + B(t-15)\right] * \frac{1}{0.239} \qquad \text{EQ 12 [19]}^{\text{Table 2-177}}$$

Where:

$C_p(t)$ = Oil Specific Heat Capacity as a function of temperature (J/(g·°C))
d = Oil density (g/cm^3)
t = oil temperature (°C)
A = 0.45 [19] Table 2-177
B = 0.0007 [19] Table 2-177

$$C_p(375°C) = \left[\frac{0.45}{\sqrt{0.92}} + 0.0007(375-15)\right] \cdot \frac{1}{0.239} = 3.02\ \frac{J}{g \cdot °C}$$

From EQ 13, determine the energy rate requirement

$$\dot{Q}_{liquid} = \dot{m}_{Oil\ Feed} C_p \Delta T \qquad \text{EQ 13}$$

$$\dot{Q}_{liquid} = 3.68 \frac{kg}{Hr} \cdot 3.02 \frac{J}{g \cdot °C} \cdot 350°C \cdot \frac{1000g}{kg} \cdot \frac{Hr}{3600\ sec} \cdot \frac{Watt}{J/sec} = 1080\ Watts$$

Part 2

Assume: Vaporization of Stearic Acid and $\Delta H°_{vap}$ = 588 J / g [19] Table 2-150

From EQ 14, determine the energy rate requirement

$$\dot{Q}_{vaporization} = \dot{m}_{Oil\ Feed} \Delta H°_{vap} \qquad \text{EQ 14}$$

$$\dot{Q}_{vaporization} = 3.68\frac{kg}{Hr} \cdot 588\frac{J}{g} \cdot \frac{1000g}{kg} \cdot \frac{Hr}{3600\ sec} \cdot \frac{Watt}{J/sec} = 600\ Watts$$

Part 3

Assume

ΔT of 75°C (375°C to 450°C)

$C_p = 3.44\ \frac{J}{g \cdot ℃}$ ChemCad Simulation of Crackate Components

From EQ 15, determine the energy requirement

$$\dot{Q}_{vapor} = \dot{m}_{Oil\ Feed} C_p \Delta T \qquad \text{EQ 15}$$

$$\dot{Q}_{vapor} = 3.68\frac{kg}{Hr} \cdot 3.44\frac{J}{g \cdot ℃} \cdot 75℃ \cdot \frac{1000g}{kg} \cdot \frac{Hr}{3600\ sec} \cdot \frac{Watt}{J/sec} = 270\ Watts$$

$$\dot{Q}_{total\ required} = \dot{Q}_{liquid} + \dot{Q}_{vaporization} + \dot{Q}_{vapor}$$

$$\dot{Q}_{total\ required} = 1080\ Watts + 600\ Watts + 270\ Watts = 1950\ Watts$$

From Appendix A, the size of the reactor has been established, and the surface area available for heating on the exterior reactor wall is 437 in2. Based upon the heat rate requirement of 1950 Watts, the heat rate flux requirement for the reactor is

$$Heat\ rate\ flux_{required} = \frac{1950\ Watt}{437\ in^2} = 4.5\frac{Watt}{in^2}$$

A common output for ceramic heaters is 25 Watt/in2. Based upon this comparison, ceramic heaters in the range of 28 watt/in2 were chosen for this application.

The extra capacity of over 500% will allow for cycling of the heaters, and also address unknown heat requirements not accounted for in the calculation such as heat loss, heat transfer efficiency, and endothermic reaction heat requirements.

APPENDIX C

REACTOR PARTS LIST

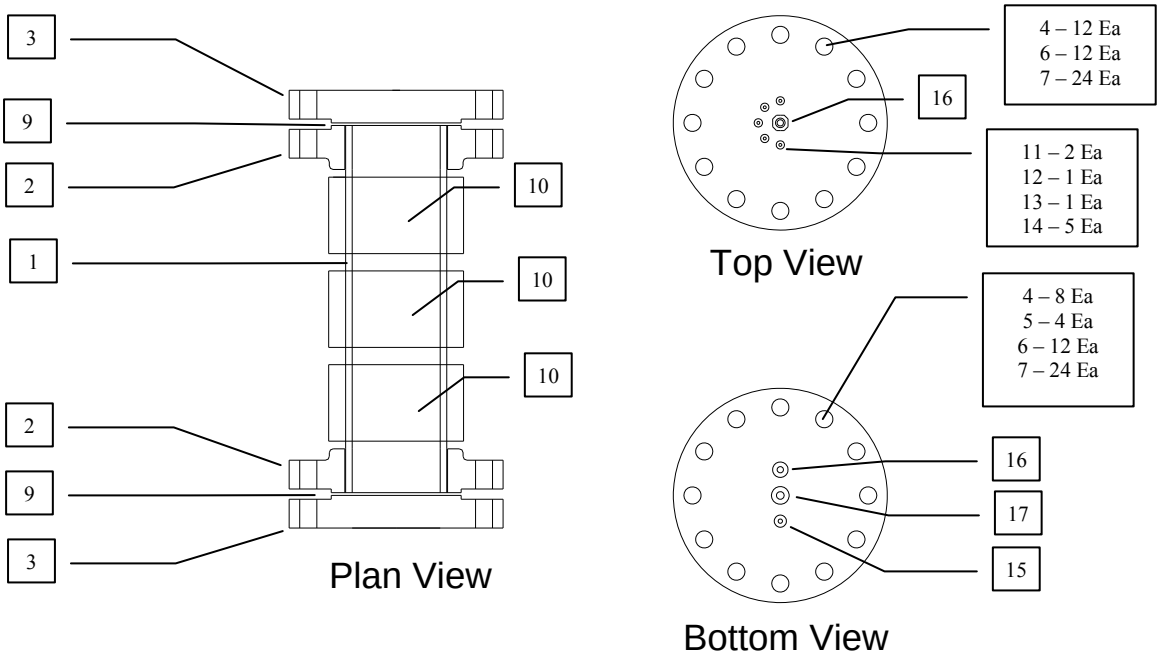

Item	Description	Part No	Supplier
1	6" Schedule 80, 304/304L SS Pipe		World Wide Pipe
2	6" Class 600 304/304L SS Slip On Flange		World Wide Pipe
3	6" Class 600 304/304L SS Blind Flange		World Wide Pipe
4	1" x 6" Hardened Bolts	HCS 1-14 x 6 P8 - 18475	Fastenal
5	1" x 7" Hardened Bolts	HCS 1-14 x 7 P8 - 18477	Fastenal
6	1" Hardened Nuts	1" - 14 FHN P8- 36469	Fastenal
7	Lock Washers	L/W P1 - 33635	Fastenal
8	1" Hardened Flat Washers	SAE Thru-Hard 1" P - 33805	Fastenal
9	Gasket, Spiral Wound, 6" Pipe, 600 lb, 304 SS,CG-F, WR-L, Graphite,	GSKT 6 600 CG 304 w/Flexicarb	Challenger Industries, Inc
10	Ceramic Heater, 6-1/2" ID x 5" W 3500W, 240V	C06J005-CEVN-JC-76671	Omega Heater
11	Thermal Couple	KQSS-14(u)-12	Omega
12	Thermal Couple	KQSS-14(u)-18	Omega
13	Thermal Couple	KQSS-14(u)-24	Omega
14	Male Pipe Weld (1/4" - 1/4")	SS-400-1-4W	Swagelok
15	Male Pipe Weld (3/8" - 3/8")	SS-600-1-6W	Swagelok
16	Male Pipe Weld (1/2" - 1/2")	SS-810-1-8W	Swagelok
17	5/8" tube to 1/2" pipeweld	SS-1010-1-8W	Swagelok

APPENDIX D

PREHEATER DESIGN

Problem:

Determine how many watts ($\dot{Q}$) are required to heat a liquid triglyceride (vegetable oil) stream from 20°C to 300°C (ΔT = 280°C) flowing at 4 L/hr ($\dot{V}$).

Solution:

From EQ 16, determine the specific heat capacity (C_p)of vegetable oil at 300°C.

$$C_p(t) = \frac{A}{\sqrt{d}} + B(t - 15) \qquad \text{EQ 16 [19]}^{\text{Table 2-177}}$$

Where:

$C_p(t)$ = Oil Specific Heat Capacity as a function of temperature(cal/(g·°C))
d = Oil density (g/cm^3)
t = oil temperature (°C)
A = 0.45 [19] Table 2-177
B = 0.0007 [19] Table 2-177

$$\mathbf{C_p}(300°C) = \frac{0.45}{\sqrt{0.92}} + 0.0007(300 - 15) = \mathbf{0.67}\ \frac{\mathbf{cal}}{\mathbf{g} \cdot °C}$$

From EQ 8, determine the oil feed mass rate ($\dot{m}_{Oil\ Feed}$)

$$\dot{m}_{Oil\ Feed} = \rho_{Oil}\dot{V}_{Oil\ Feed} \qquad \text{EQ 17}$$

Where:

ρ_{Oil} = oil density (0.92 kg/L)
$\dot{V}_{Oil\ Feed}$ = oil volumetric feed rate (4 L/hr)

$$\dot{\boldsymbol{m}}_{\boldsymbol{Oil\ Feed}} = 0.92\frac{kg}{L} \cdot 4\ \frac{L}{Hr} = \mathbf{3.68}\frac{\boldsymbol{kg}}{\boldsymbol{Hr}}$$

From EQ 9, determine the energy requirement

$$\dot{Q} = \dot{m}_{\text{Oil Feed}} C_p \Delta T \qquad \text{EQ 18}$$

$$\dot{Q} = 3.68 \frac{kg}{Hr} \cdot 0.67 \frac{\text{cal}}{\text{g} \cdot ℃} \cdot 280℃ \cdot \frac{1000\text{g}}{\text{kg}} \cdot \frac{\text{J}}{0.239\ \text{cal}} \cdot \frac{\text{Hr}}{3600\ \text{sec}} \cdot \frac{Watt}{J/sec} = 800\ Watts$$

Preheater Notes:

From the calculations, 800 Watts are required to increase a crop oil liquid feed stream by 280°C from 20°C to 300°C, assuming 100 percent heat transfer. The largest heater available for the preheater was 1000 Watts, which is what was used for the preheater apparatus. The 1000 Watt preheater performed well, and was able to heat a 4 L/hr soybean oil feed stream from 20 to 350°C during preliminary runs.

APPENDIX E

PREHEATER PARTS LIST

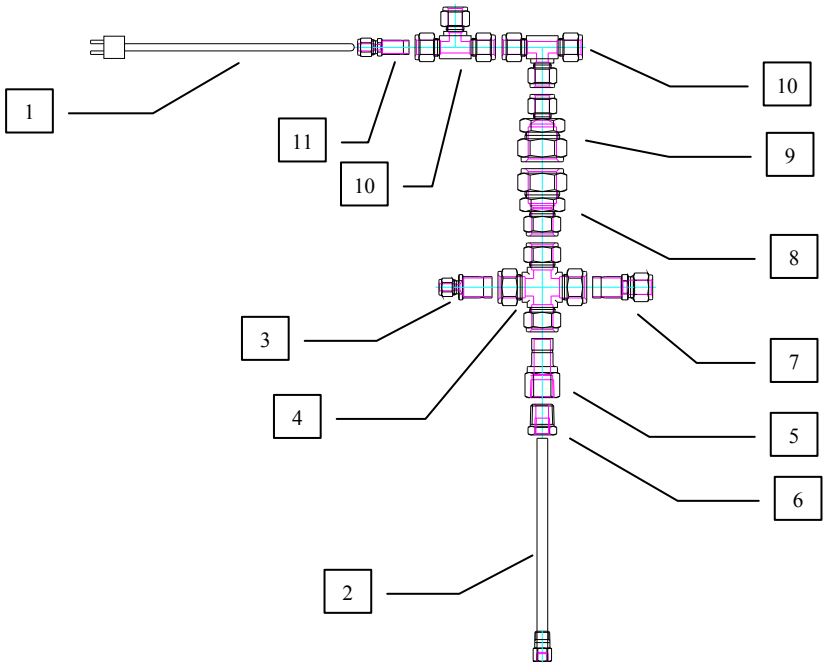

Item	Description	Part No.	Supplier
1	Thermocouple - Type K, 1/4" x 12"	KQSS-14(U)-12	Omega
2	Cartridge Heater - 3/8" OD x 12"L, 1000W, 240V	U00G012-AKVN-HXU-76670	Omega Heater
3	Reducer (1/4" to 3/4")	SS-400-R-12	Swagelok
4	Cross Union (3/4")	SS-1210-4	Swagelok
5	3/4" tube to 1/2" NPT	SS-12-TA-7-8	Swagelok
6	1/2" male NPT to 1/4" female NPT reducing bushing	SS-8-RB-4	Swagelok
7	Reducer (1/2" to 3/4")	SS-810-R-12	Swagelok
8	Union (3/4" to 1")	SS-1610-6-12	Swagelok
9	Union (1/2" to 1")	SS-1610-6-8	Swagelok
10	Tee (1/2")	SS-810-3	Swagelok
11	Reducer	SS-400-R-8	Swagelok

APPENDIX F

REACTOR TEAR DOWN

There are two levels of reactor tear down. The first level includes removal of the top flange. This level allows for inspection and cleaning of the reactor in place. This is the quickest and simplest method of cleaning the reactor, and will be the most common method for maintaining the reactor. The second level of tear down is removal of the reactor in one piece. This level of tear down is required if cleaning the reactor from the bottom is required, or if shop maintenance is required.

The procedures for the level 2 tear down follows:

1. Remove hose clamps and insulation wrapping around the reactor.

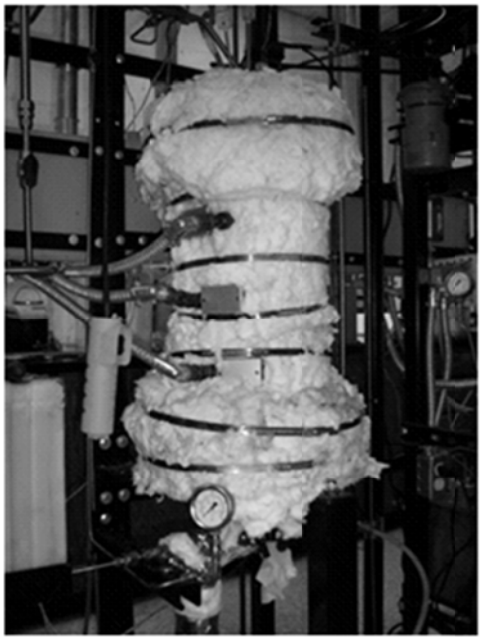

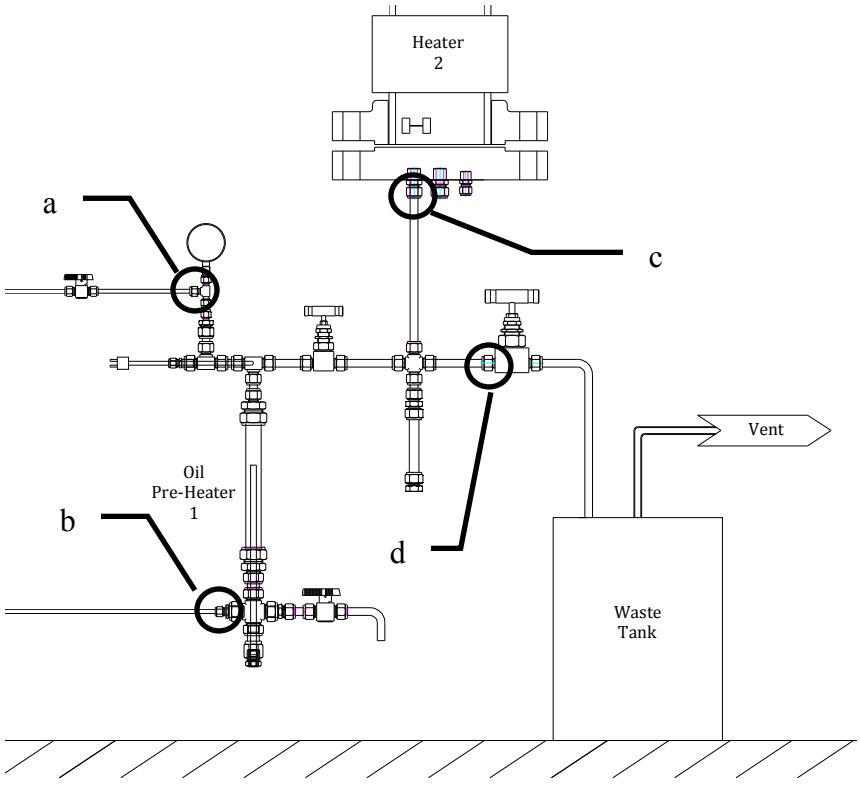

2. Remove and set aside pre-heater assembly by disconnect N2 supply line (a), oil feed line (b), reactor feed line (c), and waste line (d).

4. Remove heater hose clamps. Note: Heaters are not interchangeable. Each heater is wired to a specific thermocouple and controller. For this reason, label each heater (top, middle, and bottom) prior to removal to ensure proper placement during reassembly.

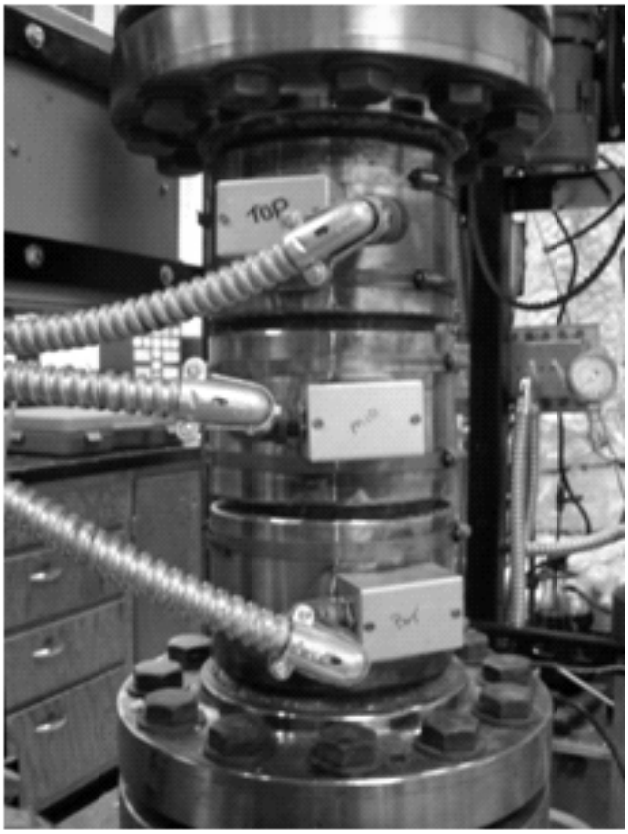

5. Remove and secure ceramic heaters with zip ties.

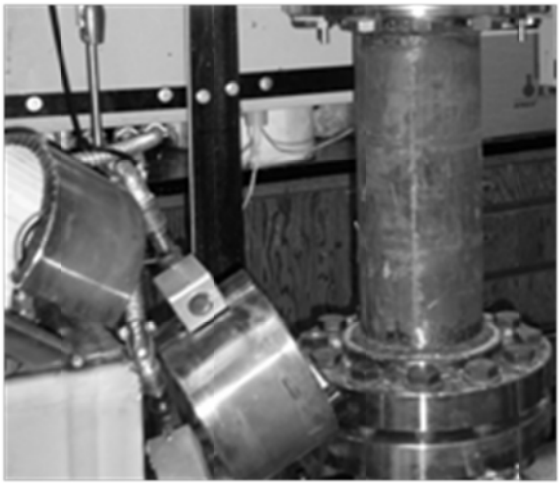

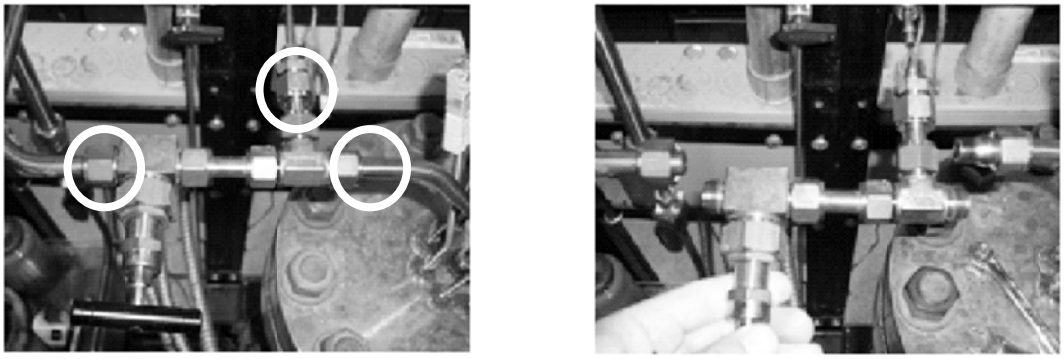

6. Disconnect and remove outlet valve assembly

7. Disconnect and remove pressure gauge assembly

.

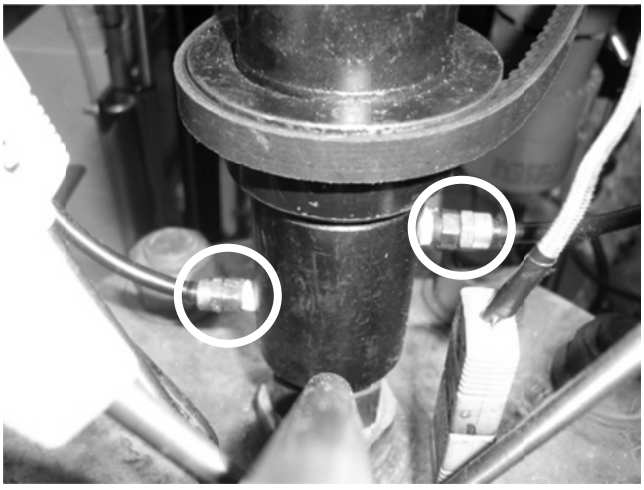

8. Disconnect water lines and remove the drive belt from the magnetic stirrer

9. To prevent cross threading of the nuts and bolts, lubricate prior to removal.

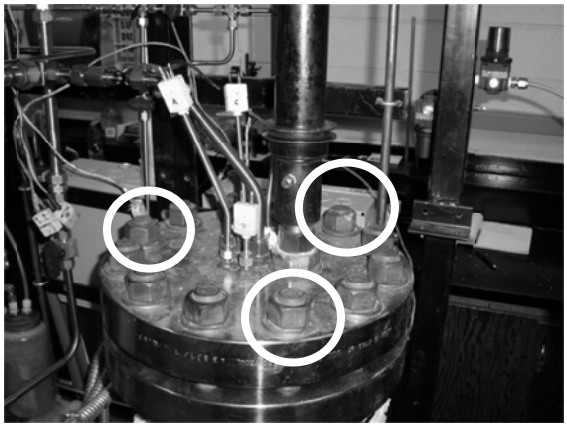

10. Remove bolts at 1, 5, and 9 o'clock locations to allow for installation of the lifting ring assembly. Loosen nuts utilizing ¾" drive set as shown.

11. Install lifting ring assembly eye bolts at the 1, 5, and 9 o'clock locations. Secure eye bolts to the bottom side flange with the flat metal washer and 5/8" bolt. Attach lifting ring to hoist.

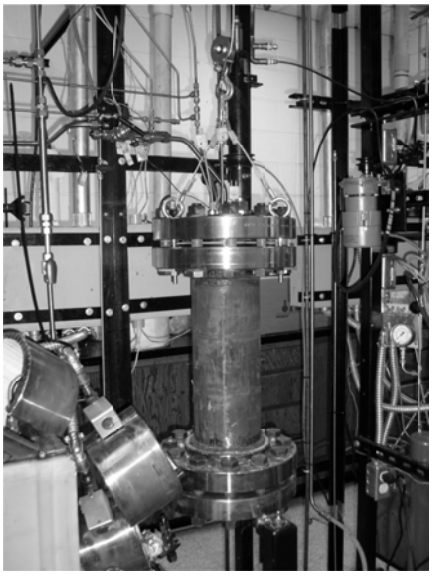

12. Operate hoist lift until hoist cable is slightly taught. This will allow for removal of the bottom support system.

Lubricate and remove the front leg bolt (1 ea) and rear back bolts (3 ea)

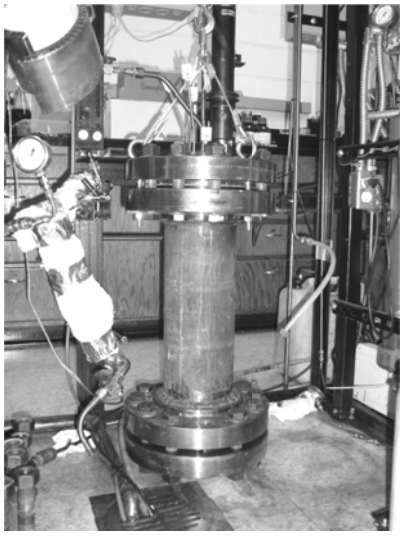

15. Lower reactor to the ground and cart reactor to the shop for cleaning. Complete removal of the top and bottom flange in the shop area.

16. Clean interior walls of reactor with 6" wheel brush and drill.

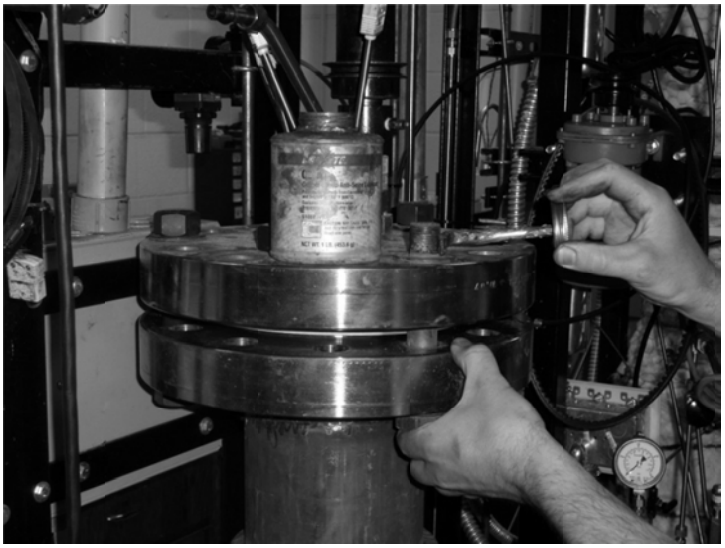

Reassembly special notes:

Lubricate bolts with copper based anti seize paste during reassembly.

Bolt tighten:
Tighten all bolts hand tight.
Tighten bolts with torque wrench in an alternating pattern to 75 ft-lbs torque. Repeat alternating pattern

APPENDIX G

GAS PRODUCT - GC SETUP, ANALYSIS PROCEDURE, & CALCULATIONS

General GC information:

- GC: SRI model 8610-C with methanizer
- Detectors: Flame Ionization Detector (FID) and Thermal Conductivity Detector (TCD)
- Column: Alltech HayeSep 80/100 matrix, Porapak Q, stainless steel, 6'x1/8"

Analysis of CO, CO_2, and C1 to C6 alkanes and alkenes using Flame Ionization Detector (FID):

GC Setup

- FID Temperature: 375°C
- FID Collector Gain – High Amplified
- FID Hydrogen Gas Pressure: 22 psi
- Carrier Gas : Helium (12 psi)
- Column Oven Temperature Program

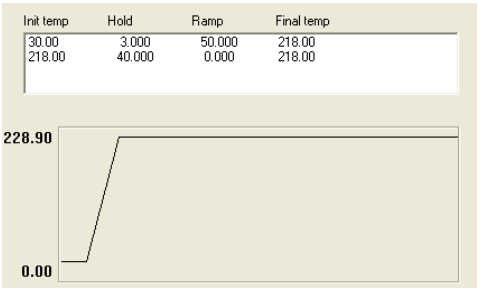

Gas Sample Injection Procedure

- Purge syringe (1 mL Hamilton model 1001 Gastight syringe) once with helium prior to each run.
- Draw a 0.1mL syringe sample from the gas sample bag
- Dilute the syringe sample by drawing another 0.9mL of helium, for a total sample volume of 1.0 mL.
- Eject 0.8 mL of the diluted sample leaving a remaining volume of 0.2 mL.
- Inject the 0.2 mL diluted sample into the GC slowly and at a steady pace.
- Integrate response areas using Peaksimple version 3.72 software, utilizing the rubber band integration tool to manually adjust the baseline

Sample Result Calculations

GC-FID Results and Calculations									
Component	Retention	FID Area Response	Carbons	MW	Response Factor (Methane Basis)	Factored Response	Mass %	Moles	Mole %
		[1]	[2]	[3]	[4]	[5]	[6]	[7]	[8]
CO	1.053	36609	1	28.01	1.75	63929	43.1%	0.015381	53.3%
methane	1.493	4976	1	16.04	1.00	4976	3.4%	0.002091	7.2%
CO2	3.186	13088	1	44.01	2.74	35910	24.2%	0.005499	19.1%
ethylene	4.7	1256	2	28.05	0.87	1098	0.7%	0.000264	0.9%
propane	5.256	13910	3	44.09	0.92	12745	8.6%	0.001948	6.8%
propylene	6.983	11456	3	42.08	0.87	10018	6.8%	0.001604	5.6%
butene	8.316	10496	4	56.1	0.87	9177	6.2%	0.001102	3.8%
pentane	10.05	9440	5	72.15	0.90	8492	5.7%	0.000793	2.8%
hexane	12.89	2279	6	86.17	0.90	2041	1.4%	0.00016	0.6%
Sumtotal						148386	100.0%	0.028842	100.0%

Spreadsheet Calculations

[1] = GC FID area response

[2] = number of carbon atoms per molecule

[3] = molecular mass

[4] = [3] / ([2]*16.04)

[5] = [1] * [4]

[6] = [5] / [$5_{sumtotal}$]

[7] = [6] / [3]

[8] = [7] / [$7_{sumtotal}$]

Analysis of molecular hydrogen using Thermal Conductivity Detector (TCD):

GC Setup

- Carrier Gas : Nitrogen (10 psi)

GC Molecular Hydrogen Calibration Curve

- Four different volumes of pure hydrogen were used for the calibration (0.5, 0.250, 0.1 and 0.05 mL). Each volume was injected six times.
- Peak simple software was used to integrate the area response.
- Plot resulting area responses against the moles molecular hydrogen injected (calculated from the injection volume using the ideal gas law).

Run	H2 volume injection (µL) [1]	H2 (Moles) [2]	GC-TCD Response Area
1	500	2.06126E-05	4768.397
2	500	2.06126E-05	5192.229
3	500	2.06126E-05	4751.356
4	500	2.06126E-05	5048.03
5	500	2.06126E-05	4815.184
6	500	2.06126E-05	4709.927
7	250	1.03063E-05	2727.352
8	250	1.03063E-05	2688.882
9	250	1.03063E-05	2798.618
10	250	1.03063E-05	2674.034
11	250	1.03063E-05	2752.901
12	100	4.12251E-06	1128.93
13	100	4.12251E-06	1211.194
14	100	4.12251E-06	1172.714
15	100	4.12251E-06	1106.942
16	100	4.12251E-06	1180.269
17	100	4.12251E-06	1081.022
18	50	2.06126E-06	595.1022
19	50	2.06126E-06	467.1244
20	50	2.06126E-06	568.8254
21	50	2.06126E-06	610.1276
22	50	2.06126E-06	633.8602
23	50	2.06126E-06	485.3378
24	50	2.06126E-06	650.5758
25	50	2.06126E-06	603.3724

$$[2] = \frac{PV}{RT} = \frac{1\ atm * [1]\mu L}{82507 \frac{\mu L * atm}{K * mol} * (21 + 273)K}$$

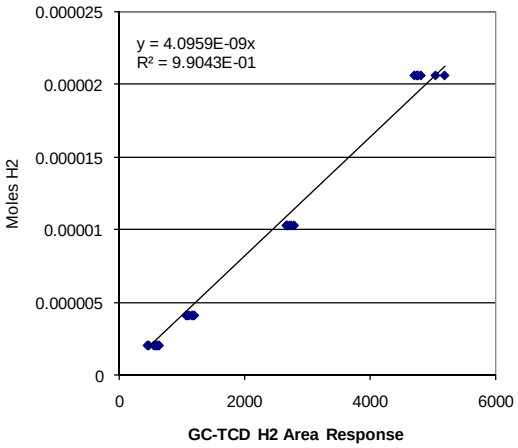

Gas Product Sample Analysis Procedure

- Purge syringe (1.0 mL Hamilton model 1001 Gastight syringe) once with helium prior to each run.
- Draw a 1.0 mL syringe sample from the gas sample bag
- Inject the sample into the GC slowly and at a steady pace.
- Integrate the area response using Peaksimple version 3.72 software

Calculations

- Calculate moles molecular hydrogen in the gas sample by multiplying the area response by the calibration curve slope ($4.0959*10^{-09}$ moles H2/area response).
- Calculate total gas sample moles injected in the 1.0 mL sample size by using the ideal gas law ($4.1225*10^{-5}$ total moles injected at 21°C and 1 atm)
- Calculate hydrogen molar percentage by dividing moles molecular hydrogen detected by the total gas product moles injected

APPENDIX H

OIL FEED PUMP CALIBRATION CURVE

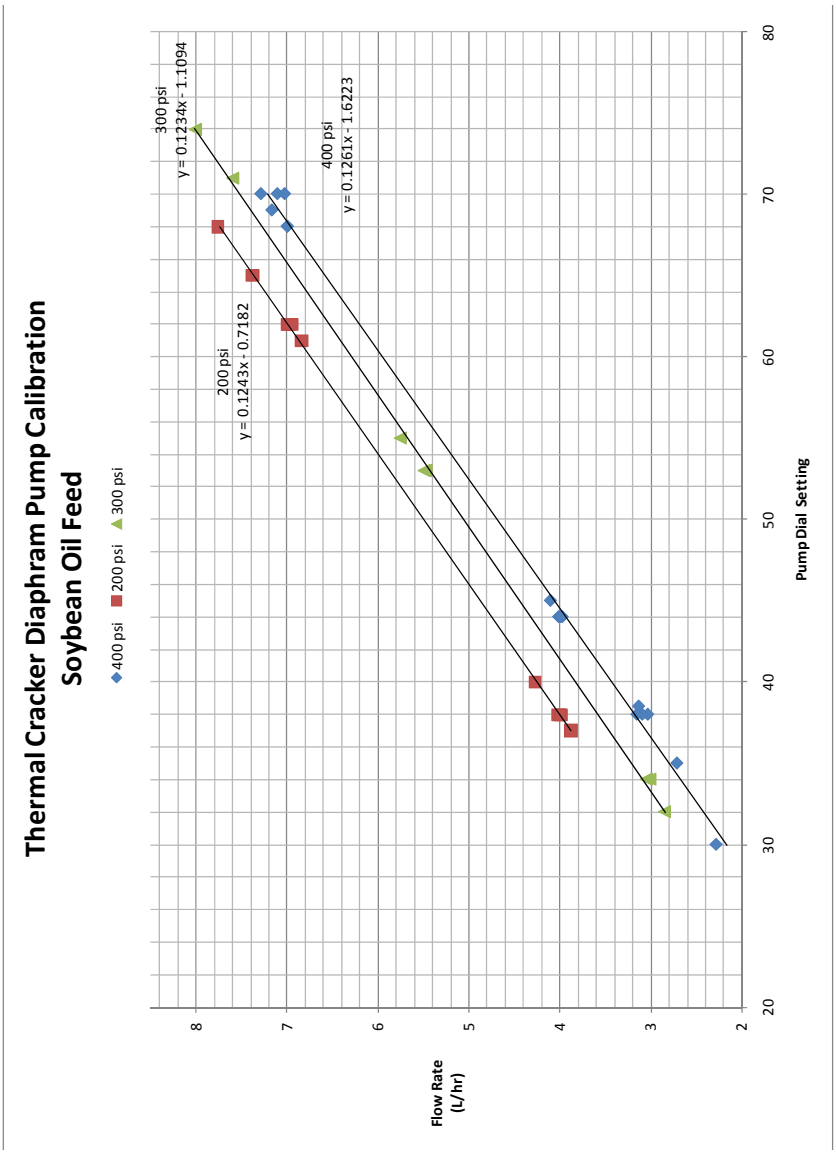

APPENDIX I

CONTROLLER PID SETTINGS

CAL 9400 Controller PID Settings at 4 L/hr Oil Feed Rate

	Proportional Band (BAND)	Integral Time (INT.T)	Derivative Time (DER.T)	Derivative Approach Control (DAC)	Proportional Cycle Time (CYC.T)
Preheater Controller	70	4.5	16	1.5	20
Bottom Heater Controller	60	12	200	1.5	81
Mid Heater Controller	18	14	61	1.5	56
Top Heater Controller	57	11	46	1.5	41

CAL 9400 Controller PID Settings at 7 L/hr Oil Feed Rate

	Proportional Band (BAND)	Integral Time (INT.T)	Derivative Time (DER.T)	Derivative Approach Control (DAC)	Proportional Cycle Time (CYC.T)
Preheater Controller	38	3.5	14	1.5	13
Bottom Heater Controller	57	27	119	1.5	81
Mid Heater Controller	16	24	117	1.5	30
Top Heater Controller	23	24	117	1.5	40

APPENDIX J

SPLIT-PLOT DOE - GAS PRODUCT YIELD STATISICAL ANALYSIS

Soybean Oil Split Plot DOE Gas Yield Data																		
Std	Run	Center	Rep	Pressure	Temperature	Feed Rate	Experiment	Yield (Wt % of Oil Fed)										
Order	Order	Pt		(psig)	(C)	(L/hr)	ID	NC Gases	H2	CO	Methane	CO2	Ethylene	Propane	Propylene	Butene	Pentane	Hexane
1	4	1	1	400	400	4	A	6.34%	0.0106%	2.63%	0.201%	1.54%	0.053%	0.580%	0.470%	0.448%	0.314%	0.098%
2	2	1	1	400	420	4	B	13.22%	0.0156%	4.14%	0.511%	2.47%	0.120%	1.382%	1.567%	1.550%	1.013%	0.451%
3	3	1	1	400	400	7	C	5.73%	0.0078%	2.19%	0.147%	1.35%	0.053%	0.600%	0.526%	0.520%	0.247%	0.084%
4	1	1	1	400	420	7	D	9.13%	0.0107%	2.97%	0.274%	1.76%	0.097%	0.913%	1.081%	1.168%	0.621%	0.241%
5	6	1	2	200	400	4	E	6.34%	0.0107%	2.38%	0.171%	1.44%	0.091%	0.488%	0.586%	0.616%	0.436%	0.128%
6	7	1	2	200	420	4	F	19.56%	0.0207%	7.32%	0.704%	3.19%	0.279%	1.868%	2.298%	2.097%	1.261%	0.526%
7	5	1	2	200	400	7	G	6.74%	0.0122%	2.80%	0.170%	1.57%	0.096%	0.476%	0.510%	0.552%	0.436%	0.122%
8	8	1	2	200	420	7	H	13.51%	0.0128%	4.97%	0.506%	2.28%	0.196%	1.316%	1.523%	1.364%	0.970%	0.374%
9	15	1	3	400	400	4	AA	3.39%	0.0048%	1.20%	0.140%	0.83%	0.024%	0.366%	0.312%	0.278%	0.180%	0.054%
10	14	1	3	400	420	4	BB	11.58%	0.0164%	3.56%	0.501%	2.33%	0.117%	1.204%	1.302%	1.309%	1.063%	0.180%
11	16	1	3	400	400	7	CC	3.57%	0.0063%	1.36%	0.100%	0.91%	0.029%	0.296%	0.277%	0.321%	0.200%	0.071%
12	13	1	3	400	420	7	DD	8.95%	0.0110%	2.86%	0.434%	1.81%	0.084%	0.992%	1.005%	0.953%	0.562%	0.230%
13	11	1	4	200	400	4	EE	7.44%	0.0116%	2.93%	0.232%	1.81%	0.102%	0.646%	0.699%	0.605%	0.298%	0.110%
14	12	1	4	200	420	4	FF	15.74%	0.0178%	5.73%	0.604%	2.72%	0.219%	1.473%	1.736%	1.561%	1.217%	0.459%
15	10	1	4	200	400	7	GG	6.87%	0.0096%	2.81%	0.178%	1.75%	0.098%	0.583%	0.559%	0.505%	0.288%	0.090%
16	9	1	4	200	420	7	HH	8.76%	0.0087%	3.08%	0.286%	1.57%	0.142%	0.741%	0.926%	0.967%	0.736%	0.307%

NC Gases

Factor	Type	Levels	Values
Pressure	fixed	2	200, 400
Rep(Pressure)	random	4	2, 4, 1, 3
Temperature	fixed	2	400, 420
Feed Rate	fixed	2	4, 7

Analysis of Variance for NC Gases, using Adjusted SS for Tests

Source	DF	Seq SS	Adj SS	Adj MS	F	P
Pressure	1	0.0033171	0.0033171	0.0033171	5.20	0.150
Rep(Pressure)	2	0.0012757	0.0012757	0.0006378	2.60	0.143
Temperature	1	0.0182487	0.0182487	0.0182487	74.27	**0.000**
Feed Rate	1	0.0025952	0.0025952	0.0025952	10.56	**0.014**
Pressure*Temperature	1	0.0002492	0.0002492	0.0002492	1.01	0.347
Pressure*Feed Rate	1	0.0002287	0.0002287	0.0002287	0.93	0.367
Temperature*Feed Rate	1	0.0022930	0.0022930	0.0022930	9.33	**0.018**
Error	7	0.0017199	0.0017199	0.0002457		
Total	15	0.0299276				

S = 0.0156750 R-Sq = 94.25% R-Sq(adj) = 87.68%

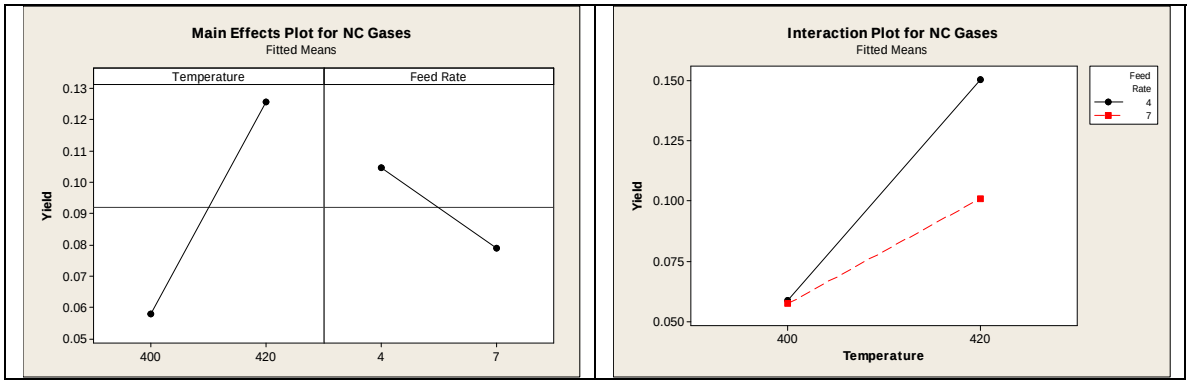

H2

Factor	Type	Levels	Values
Pressure	fixed	2	200, 400
Rep(Pressure)	random	4	2, 4, 1, 3
Temperature	fixed	2	400, 420
Feed Rate	fixed	2	4, 7

Analysis of Variance for H2, using Adjusted SS for Tests

Source	DF	Seq SS	Adj SS	Adj MS	F	P
Pressure	1	0.0000000	0.0000000	0.0000000	3.74	0.193
Rep(Pressure)	2	0.0000000	0.0000000	0.0000000	2.15	0.187
Temperature	1	0.0000000	0.0000000	0.0000000	29.75	**0.001**
Feed Rate	1	0.0000000	0.0000000	0.0000000	15.55	**0.006**
Pressure*Temperature	1	0.0000000	0.0000000	0.0000000	1.28	0.295
Pressure*Feed Rate	1	0.0000000	0.0000000	0.0000000	0.68	0.437
Temperature*Feed Rate	1	0.0000000	0.0000000	0.0000000	12.04	**0.010**
Error	7	0.0000000	0.0000000	0.0000000		
Total	15	0.0000000				

S = 0.0000183807 R-Sq = 91.10% R-Sq(adj) = 80.92%

Unusual Observations for H2

Obs	H2	Fit	SE Fit	Residual	St Resid
1	0.000106	0.000080	0.000014	0.000026	2.11 R

R denotes an observation with a large standardized residual.

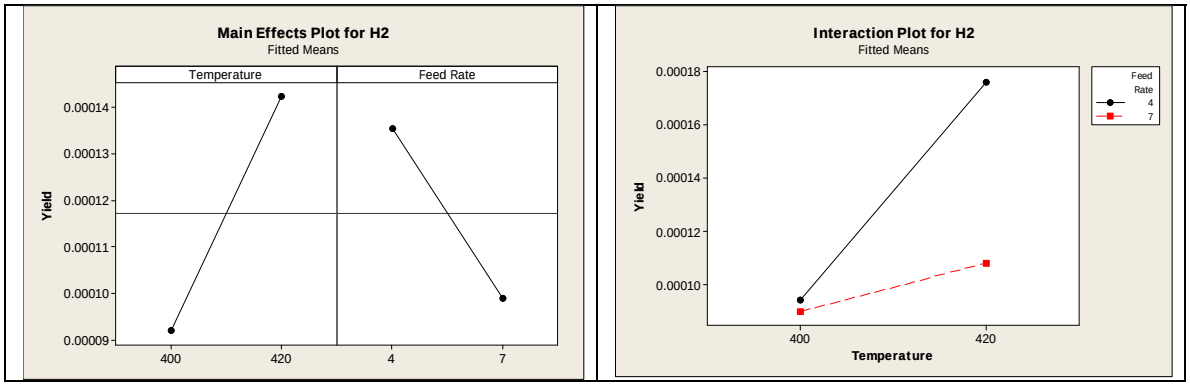

CO

Factor	Type	Levels	Values
Pressure	fixed	2	200, 400
Rep(Pressure)	random	4	2, 4, 1, 3
Temperature	fixed	2	400, 420
Feed Rate	fixed	2	4, 7

Analysis of Variance for CO, using Adjusted SS for Tests

Source	DF	Seq SS	Adj SS	Adj MS	F	P
Pressure	1	0.0007691	0.0007691	0.0007691	7.12	0.116
Rep(Pressure)	2	0.0002161	0.0002161	0.0001080	2.19	0.182
Temperature	1	0.0016689	0.0016689	0.0016689	33.87	**0.001**
Feed Rate	1	0.0002935	0.0002935	0.0002935	5.96	**0.045**
Pressure*Temperature	1	0.0001011	0.0001011	0.0001011	2.05	0.195
Pressure*Feed Rate	1	0.0000409	0.0000409	0.0000409	0.83	0.393
Temperature*Feed Rate	1	0.0002987	0.0002987	0.0002987	6.06	**0.043**
Error	7	0.0003449	0.0003449	0.0000493		
Total	15	0.0037334				

S = 0.00701944 R-Sq = 90.76% R-Sq(adj) = 80.20%

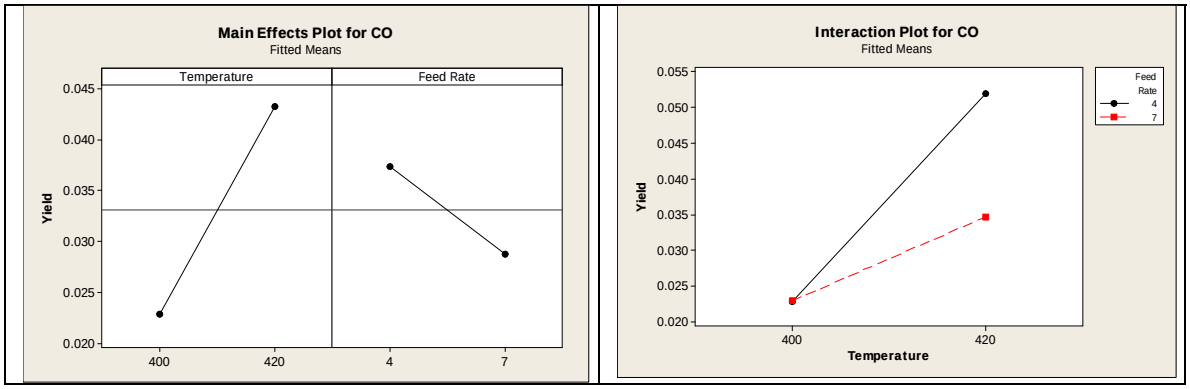

Methane

Factor	Type	Levels	Values
Pressure	fixed	2	200, 400
Rep(Pressure)	random	4	2, 4, 1, 3
Temperature	fixed	2	400, 420
Feed Rate	fixed	2	4, 7

Analysis of Variance for Methane, using Adjusted SS for Tests

Source	DF	Seq SS	Adj SS	Adj MS	F	P
Pressure	1	0.0000018	0.0000018	0.0000018	4.54	0.167
Rep(Pressure)	2	0.0000008	0.0000008	0.0000004	0.66	0.545
Temperature	1	0.0000385	0.0000385	0.0000385	62.89	**0.000**
Feed Rate	1	0.0000059	0.0000059	0.0000059	9.60	**0.017**
Pressure*Temperature	1	0.0000003	0.0000003	0.0000003	0.49	0.507
Pressure*Feed Rate	1	0.0000002	0.0000002	0.0000002	0.30	0.600
Temperature*Feed Rate	1	0.0000028	0.0000028	0.0000028	4.63	0.068
Error	7	0.0000043	0.0000043	0.0000006		
Total	15	0.0000547				

S = 0.000782588 R-Sq = 92.16% R-Sq(adj) = 83.19%

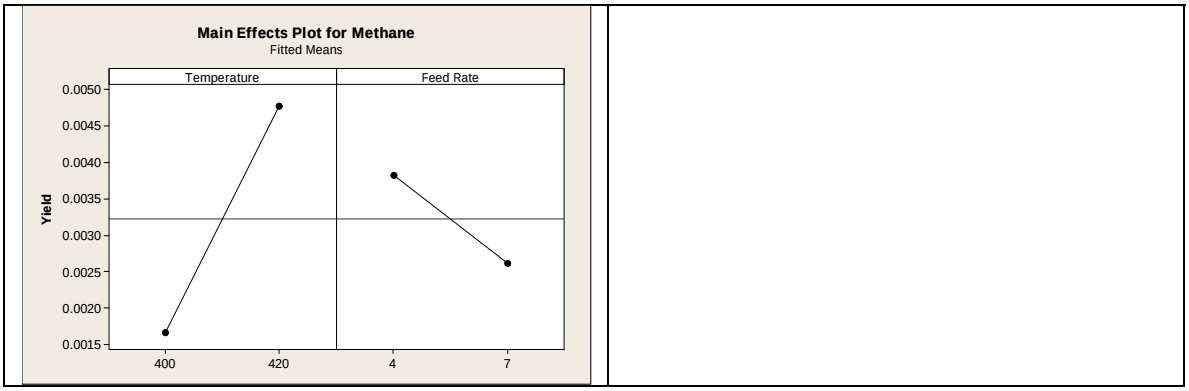

CO2

Factor	Type	Levels	Values
Pressure	fixed	2	200, 400
Rep(Pressure)	random	4	2, 4, 1, 3
Temperature	fixed	2	400, 420
Feed Rate	fixed	2	4, 7

Analysis of Variance for CO2, using Adjusted SS for Tests

Source	DF	Seq SS	Adj SS	Adj MS	F	P
Pressure	1	0.0000684	0.0000684	0.0000684	5.77	0.138
Rep(Pressure)	2	0.0000237	0.0000237	0.0000119	1.31	0.329
Temperature	1	0.0003001	0.0003001	0.0003001	33.11	**0.001**
Feed Rate	1	0.0000698	0.0000698	0.0000698	7.70	**0.027**
Pressure*Temperature	1	0.0000019	0.0000019	0.0000019	0.21	0.662
Pressure*Feed Rate	1	0.0000027	0.0000027	0.0000027	0.30	0.604
Temperature*Feed Rate	1	0.0000657	0.0000657	0.0000657	7.25	**0.031**
Error	7	0.0000635	0.0000635	0.0000091		
Total	15	0.0005958				

S = 0.00301093 R-Sq = 89.35% R-Sq(adj) = 77.18%

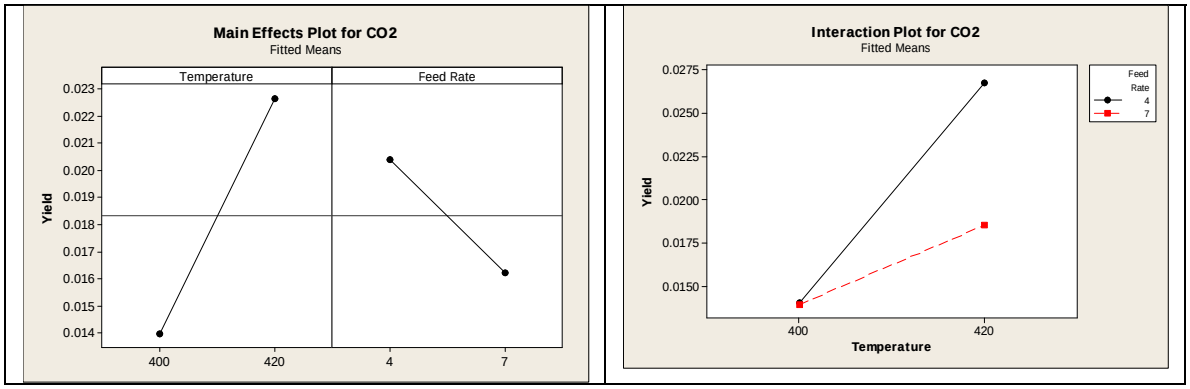

Ethylene

Factor	Type	Levels	Values
Pressure	fixed	2	200, 400
Rep(Pressure)	random	4	2, 4, 1, 3
Temperature	fixed	2	400, 420
Feed Rate	fixed	2	4, 7

Analysis of Variance for Ethylene, using Adjusted SS for Tests

Source	DF	Seq SS	Adj SS	Adj MS	F	P
Pressure	1	0.0000026	0.0000026	0.0000026	27.92	**0.034**
Rep(Pressure)	2	0.0000002	0.0000002	0.0000001	2.25	0.176
Temperature	1	0.0000031	0.0000031	0.0000031	75.11	**0.000**
Feed Rate	1	0.0000003	0.0000003	0.0000003	6.46	**0.039**
Pressure*Temperature	1	0.0000002	0.0000002	0.0000002	5.46	0.052
Pressure*Feed Rate	1	0.0000001	0.0000001	0.0000001	1.70	0.233
Temperature*Feed Rate	1	0.0000003	0.0000003	0.0000003	7.35	**0.030**
Error	7	0.0000003	0.0000003	0.0000000		
Total	15	0.0000071				

S = 0.000204241 R-Sq = 95.89% R-Sq(adj) = 91.20%

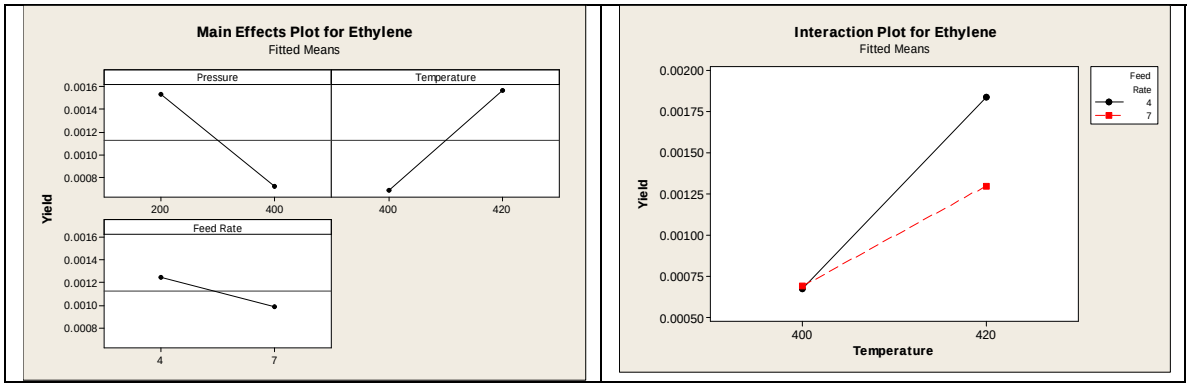

Propane

Factor	Type	Levels	Values
Pressure	fixed	2	200, 400
Rep(Pressure)	random	4	2, 4, 1, 3
Temperature	fixed	2	400, 420
Feed Rate	fixed	2	4, 7

Analysis of Variance for Propane, using Adjusted SS for Tests

Source	DF	Seq SS	Adj SS	Adj MS	F	P
Pressure	1	0.0000099	0.0000099	0.0000099	1.81	0.311
Rep(Pressure)	2	0.0000110	0.0000110	0.0000055	1.47	0.293
Temperature	1	0.0002141	0.0002141	0.0002141	57.44	**0.000**
Feed Rate	1	0.0000273	0.0000273	0.0000273	7.32	**0.030**
Pressure*Temperature	1	0.0000019	0.0000019	0.0000019	0.51	0.496
Pressure*Feed Rate	1	0.0000025	0.0000025	0.0000025	0.66	0.442
Temperature*Feed Rate	1	0.0000212	0.0000212	0.0000212	5.69	**0.049**
Error	7	0.0000261	0.0000261	0.0000037		
Total	15	0.0003139				

S = 0.00193058 R-Sq = 91.69% R-Sq(adj) = 82.19%

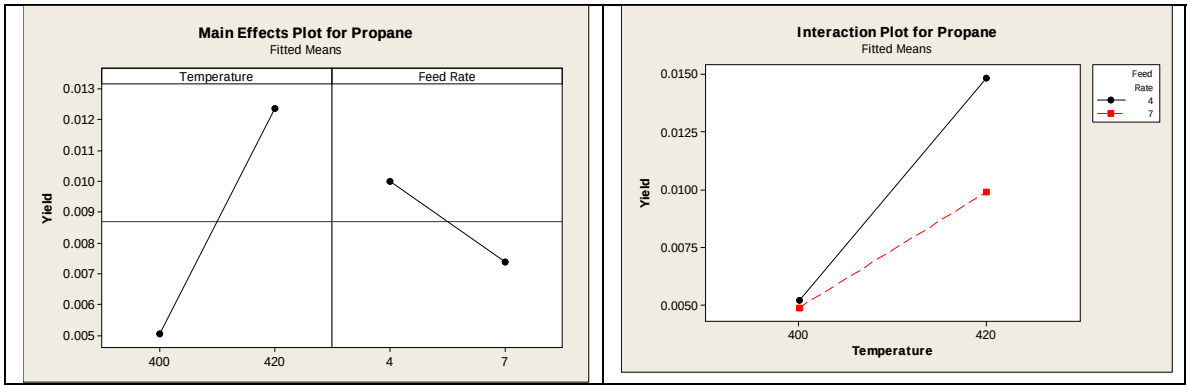

Propylene

Factor	Type	Levels	Values
Pressure	fixed	2	200, 400
Rep(Pressure)	random	4	2, 4, 1, 3
Temperature	fixed	2	400, 420
Feed Rate	fixed	2	4, 7

Analysis of Variance for Propylene, using Adjusted SS for Tests

Source	DF	Seq SS	Adj SS	Adj MS	F	P
Pressure	1	0.0000330	0.0000330	0.0000330	3.40	0.207
Rep(Pressure)	2	0.0000194	0.0000194	0.0000097	2.71	0.135
Temperature	1	0.0003516	0.0003516	0.0003516	98.14	**0.000**
Feed Rate	1	0.0000411	0.0000411	0.0000411	11.46	**0.012**
Pressure*Temperature	1	0.0000036	0.0000036	0.0000036	1.00	0.350
Pressure*Feed Rate	1	0.0000068	0.0000068	0.0000068	1.89	0.212
Temperature*Feed Rate	1	0.0000295	0.0000295	0.0000295	8.23	**0.024**
Error	7	0.0000251	0.0000251	0.0000036		
Total	15	0.0005100				

S = 0.00189292 R-Sq = 95.08% R-Sq(adj) = 89.46%

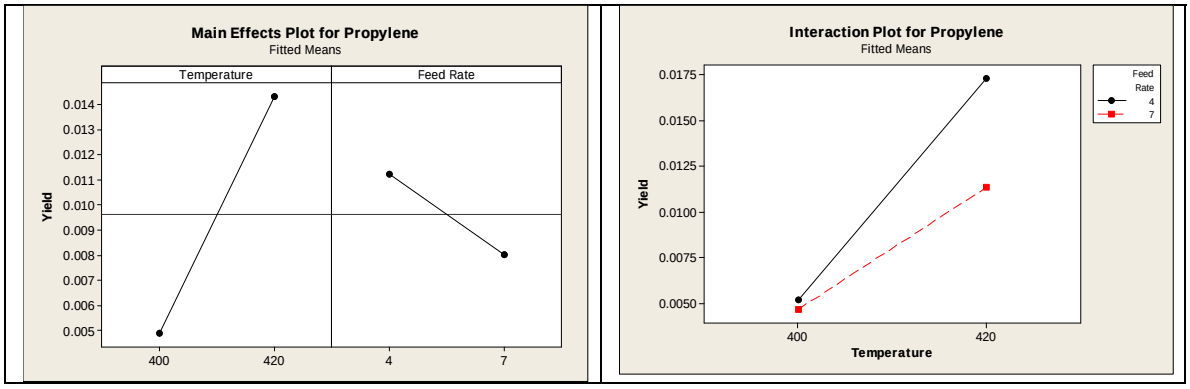

Butene

Factor	Type	Levels	Values
Pressure	fixed	2	200, 400
Rep(Pressure)	random	4	2, 4, 1, 3
Temperature	fixed	2	400, 420
Feed Rate	fixed	2	4, 7

Analysis of Variance for Butene, using Adjusted SS for Tests

Source	DF	Seq SS	Adj SS	Adj MS	F	P
Pressure	1	0.0000185	0.0000185	0.0000185	1.78	0.314
Rep(Pressure)	2	0.0000208	0.0000208	0.0000104	6.70	0.024
Temperature	1	0.0003172	0.0003172	0.0003172	204.80	**0.000**
Feed Rate	1	0.0000279	0.0000279	0.0000279	18.03	**0.004**
Pressure*Temperature	1	0.0000006	0.0000006	0.0000006	0.36	0.568
Pressure*Feed Rate	1	0.0000047	0.0000047	0.0000047	3.03	0.125
Temperature*Feed Rate	1	0.0000254	0.0000254	0.0000254	16.40	**0.005**
Error	7	0.0000108	0.0000108	0.0000015		
Total	15	0.0004258				

S = 0.00124450 R-Sq = 97.45% R-Sq(adj) = 94.54%

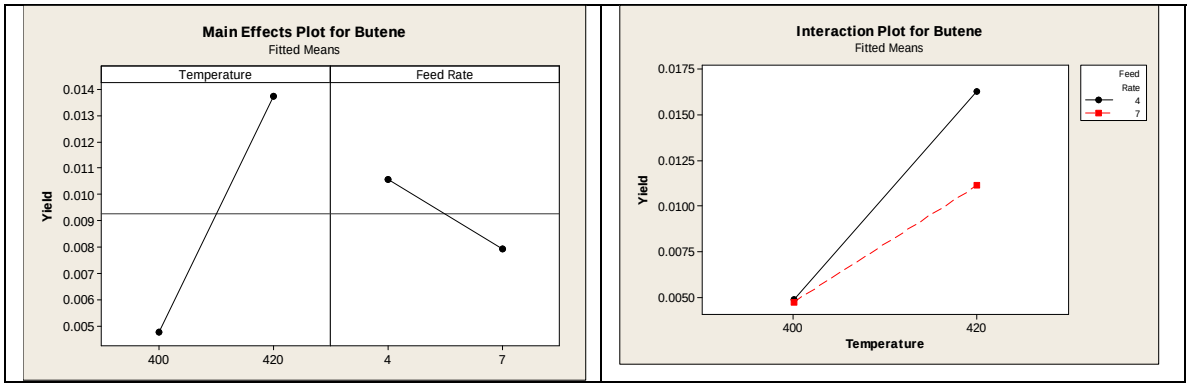

Pentane

Factor	Type	Levels	Values
Pressure	fixed	2	200, 400
Rep(Pressure)	random	4	2, 4, 1, 3
Temperature	fixed	2	400, 420
Feed Rate	fixed	2	4, 7

Analysis of Variance for Pentane, using Adjusted SS for Tests

Source	DF	Seq SS	Adj SS	Adj MS	F	P
Pressure	1	0.0000130	0.0000130	0.0000130	5.87	0.136
Rep(Pressure)	2	0.0000044	0.0000044	0.0000022	8.58	0.013
Temperature	1	0.0001589	0.0001589	0.0001589	615.04	**0.000**
Feed Rate	1	0.0000185	0.0000185	0.0000185	71.70	**0.000**
Pressure*Temperature	1	0.0000010	0.0000010	0.0000010	4.02	0.085
Pressure*Feed Rate	1	0.0000002	0.0000002	0.0000002	0.58	0.470
Temperature*Feed Rate	1	0.0000162	0.0000162	0.0000162	62.59	**0.000**
Error	7	0.0000018	0.0000018	0.0000003		
Total	15	0.0002141				

S = 0.000508360 R-Sq = 99.16% R-Sq(adj) = 98.19%

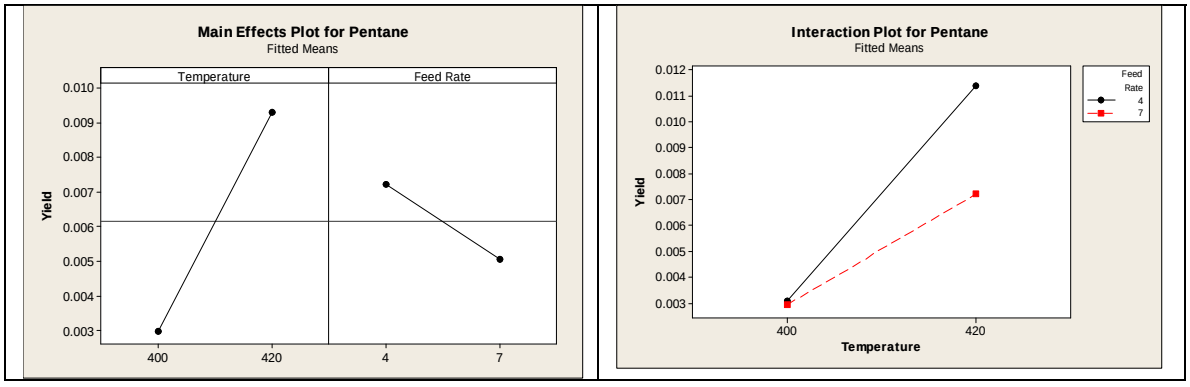

Hexane

Factor	Type	Levels	Values
Pressure	fixed	2	200, 400
Rep(Pressure)	random	4	2, 4, 1, 3
Temperature	fixed	2	400, 420
Feed Rate	fixed	2	4, 7

Analysis of Variance for Hexane, using Adjusted SS for Tests

Source	DF	Seq SS	Adj SS	Adj MS	F	P
Pressure	1	0.0000031	0.0000031	0.0000031	3.35	0.209
Rep(Pressure)	2	0.0000019	0.0000019	0.0000009	2.57	0.145
Temperature	1	0.0000253	0.0000253	0.0000253	69.79	**0.000**
Feed Rate	1	0.0000015	0.0000015	0.0000015	4.08	0.083
Pressure*Temperature	1	0.0000011	0.0000011	0.0000011	3.06	0.123
Pressure*Feed Rate	1	0.0000002	0.0000002	0.0000002	0.50	0.501
Temperature*Feed Rate	1	0.0000012	0.0000012	0.0000012	3.33	0.111
Error	7	0.0000025	0.0000025	0.0000004		
Total	15	0.0000369				

S = 0.000602450 R-Sq = 93.11% R-Sq(adj) = 85.23%

Unusual Observations for Hexane

Obs	Hexane	Fit	SE Fit	Residual	St Resid
2	0.004514	0.003654	0.000452	0.000860	2.16 R
10	0.001797	0.002804	0.000452	-0.001007	-2.53 R

R denotes an observation with a large standardized residual.

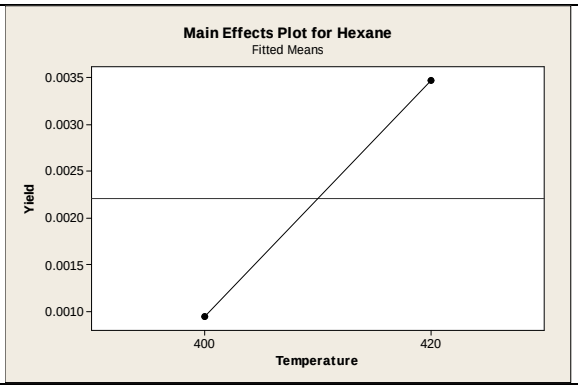

APPENDIX K

SPLIT-PLOT DOE - GAS PRODUCT MOLE PERCENTAGE STATISICAL ANALYSIS

Soybean Oil Split-Plot DOE Gas Molar Percentage Data																	
Std	Run	Center	Rep	Pressure	Temperature	Feed Rate	Experiment	Molar Percentage									
Order	Order	Pt		(psig)	(°C)	(L/hr)	ID	H2	CO	Methane	CO2	Ethylene	Propane	Propylene	Butene	Pentane	Hexane
1	4	1	1	400	400	4	A	2.81%	50.34%	6.73%	18.81%	1.02%	7.06%	5.99%	4.29%	2.33%	0.61%
2	2	1	1	400	420	4	B	2.13%	40.71%	8.77%	15.44%	1.17%	8.62%	10.25%	7.60%	3.86%	1.44%
3	3	1	1	400	400	7	C	2.37%	47.82%	5.61%	18.75%	1.16%	8.31%	7.63%	5.66%	2.09%	0.59%
4	1	1	1	400	420	7	D	2.13%	42.37%	6.81%	15.93%	1.38%	8.27%	10.26%	8.31%	3.44%	1.12%
5	6	1	2	200	400	4	E	2.95%	47.11%	5.90%	18.10%	1.79%	6.14%	7.73%	6.09%	3.35%	0.82%
6	7	1	2	200	420	4	F	1.85%	47.03%	7.90%	13.02%	1.79%	7.62%	9.82%	6.72%	3.14%	1.10%
7	5	1	2	200	400	7	G	3.09%	51.05%	5.40%	18.17%	1.75%	5.52%	6.18%	5.02%	3.08%	0.72%
8	8	1	2	200	420	7	H	1.66%	46.40%	8.26%	13.54%	1.83%	7.81%	9.47%	6.36%	3.52%	1.14%
9	15	1	3	400	400	4	AA	2.44%	43.99%	8.95%	19.35%	0.86%	8.51%	7.61%	5.09%	2.56%	0.65%
10	14	1	3	400	420	4	BB	2.53%	39.47%	9.71%	16.45%	1.29%	8.48%	9.60%	7.25%	4.57%	0.65%
11	16	1	3	400	400	7	CC	3.08%	47.45%	6.10%	20.22%	1.01%	6.58%	6.44%	5.60%	2.71%	0.80%
12	13	1	3	400	420	7	DD	2.16%	40.41%	10.70%	16.31%	1.19%	8.91%	9.46%	6.72%	3.08%	1.06%
13	11	1	4	200	400	4	EE	2.66%	48.14%	6.66%	19.00%	1.68%	6.76%	7.65%	4.97%	1.90%	0.59%
14	12	1	4	200	420	4	FF	1.98%	45.94%	8.46%	13.88%	1.75%	7.50%	9.26%	6.25%	3.79%	1.20%
15	10	1	4	200	400	7	GG	2.37%	50.19%	5.56%	19.84%	1.75%	6.61%	6.64%	4.51%	2.00%	0.53%
16	9	1	4	200	420	7	HH	1.78%	45.29%	7.35%	14.70%	2.09%	6.93%	9.08%	7.11%	4.20%	1.47%

Factor	Type	Levels	Values
Pressure	fixed	2	200, 400
Rep(Pressure)	random	4	2, 4, 1, 3
Temperature	fixed	2	400, 420
Feed Rate	fixed	2	4, 7

Analysis of Variance for H2, using Adjusted SS for Tests

Source	DF	Seq SS	Adj SS	Adj MS	F	P
Pressure	1	0.0000106	0.0000106	0.0000106	1.45	0.351
Rep(Pressure)	2	0.0000146	0.0000146	0.0000073	0.89	0.453
Temperature	1	0.0001938	0.0001938	0.0001938	23.57	**0.002**
Feed Rate	1	0.0000030	0.0000030	0.0000030	0.37	0.564
Pressure*Temperature	1	0.0000260	0.0000260	0.0000260	3.16	0.119
Pressure*Feed Rate	1	0.0000008	0.0000008	0.0000008	0.09	0.771
Temperature*Feed Rate	1	0.0000042	0.0000042	0.0000042	0.51	0.500
Error	7	0.0000576	0.0000576	0.0000082		
Total	15	0.0003105				

S = 0.00286759 R-Sq = 81.46% R-Sq(adj) = 60.27%

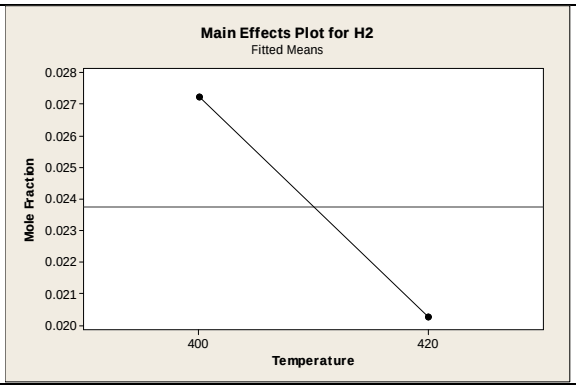

Factor	Type	Levels	Values
Pressure	fixed	2	200, 400
Rep(Pressure)	random	4	2, 4, 1, 3
Temperature	fixed	2	400, 420
Feed Rate	fixed	2	4, 7

Analysis of Variance for CO, using Adjusted SS for Tests

Source	DF	Seq SS	Adj SS	Adj MS	F	P
Pressure	1	0.0051043	0.0051043	0.0051043	7.96	0.106
Rep(Pressure)	2	0.0012828	0.0012828	0.0006414	2.61	0.142
Temperature	1	0.0092517	0.0092517	0.0092517	37.63	**0.000**
Feed Rate	1	0.0004264	0.0004264	0.0004264	1.73	0.229
Pressure*Temperature	1	0.0013720	0.0013720	0.0013720	5.58	**0.050**
Pressure*Feed Rate	1	0.0000083	0.0000083	0.0000083	0.03	0.860
Temperature*Feed Rate	1	0.0001965	0.0001965	0.0001965	0.80	0.401
Error	7	0.0017208	0.0017208	0.0002458		
Total	15	0.0193627				

S = 0.0156790 R-Sq = 91.11% R-Sq(adj) = 80.96%

Unusual Observations for CO

Obs	CO	Fit	SE Fit	Residual	St Resid
1	0.503428	0.478471	0.011759	0.024956	2.41 R

R denotes an observation with a large standardized residual.

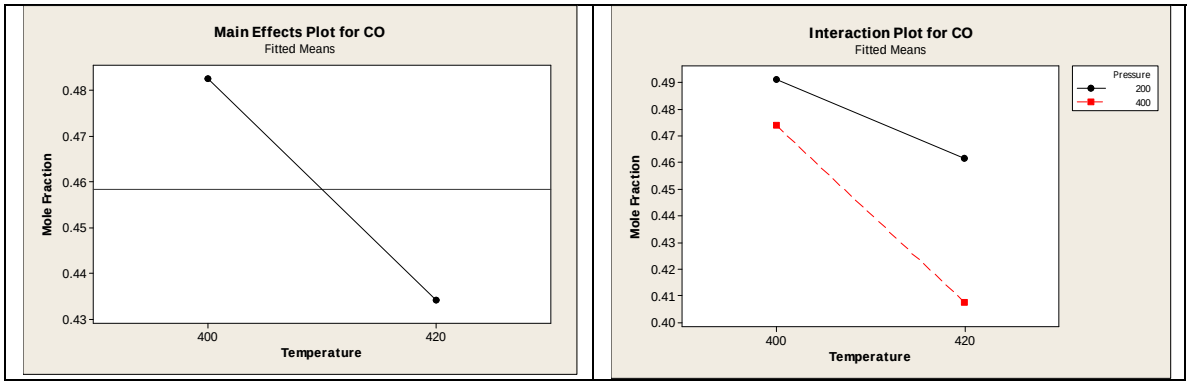

Factor	Type	Levels	Values
Pressure	fixed	2	200, 400
Rep(Pressure)	random	4	2, 4, 1, 3
Temperature	fixed	2	400, 420
Feed Rate	fixed	2	4, 7

Analysis of Variance for Methane, using Adjusted SS for Tests

Source	DF	Seq SS	Adj SS	Adj MS	F	P
Pressure	1	0.0003888	0.0003888	0.0003888	1.09	0.406
Rep(Pressure)	2	0.0007133	0.0007133	0.0003566	5.43	0.038
Temperature	1	0.0018172	0.0018172	0.0018172	27.67	**0.001**
Feed Rate	1	0.0003310	0.0003310	0.0003310	5.04	0.060
Pressure*Temperature	1	0.0000002	0.0000002	0.0000002	0.00	0.963
Pressure*Feed Rate	1	0.0000417	0.0000417	0.0000417	0.63	0.452
Temperature*Feed Rate	1	0.0000933	0.0000933	0.0000933	1.42	0.272
Error	7	0.0004598	0.0004598	0.0000657		
Total	15	0.0038451				

S = 0.00810455 R-Sq = 88.04% R-Sq(adj) = 74.38%

Unusual Observations for Methane

Obs	Methane	Fit	SE Fit	Residual	St Resid
12	0.107001	0.095647	0.006078	0.011355	2.12 R

R denotes an observation with a large standardized residual.

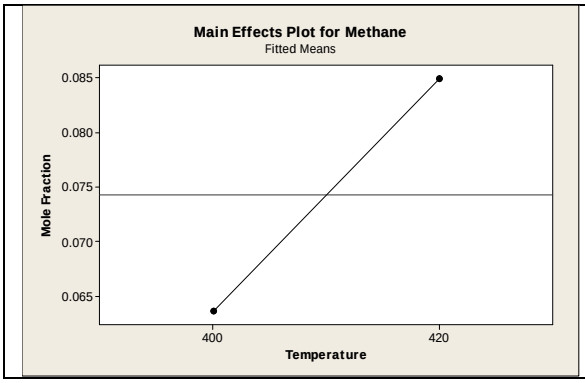

Factor	Type	Levels	Values
Pressure	fixed	2	200, 400
Rep(Pressure)	random	4	2, 4, 1, 3
Temperature	fixed	2	400, 420
Feed Rate	fixed	2	4, 7

Analysis of Variance for CO2, using Adjusted SS for Tests

Source	DF	Seq SS	Adj SS	Adj MS	F	P
Pressure	1	0.0007585	0.0007585	0.0007585	3.71	0.194
Rep(Pressure)	2	0.0004093	0.0004093	0.0002047	22.94	0.001
Temperature	1	0.0067936	0.0067936	0.0067936	761.57	**0.000**
Feed Rate	1	0.0000730	0.0000730	0.0000730	8.18	**0.024**
Pressure*Temperature	1	0.0003043	0.0003043	0.0003043	34.11	**0.001**
Pressure*Feed Rate	1	0.0000076	0.0000076	0.0000076	0.85	0.387
Temperature*Feed Rate	1	0.0000000	0.0000000	0.0000000	0.00	0.972
Error	7	0.0000624	0.0000624	0.0000089		
Total	15	0.0084087				

S = 0.00298671 R-Sq = 99.26% R-Sq(adj) = 98.41%

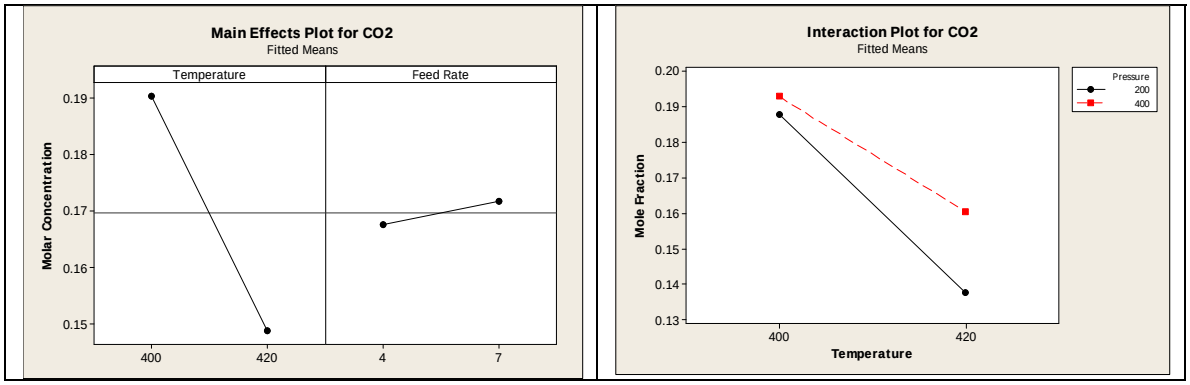

Factor	Type	Levels	Values
Pressure	fixed	2	200, 400
Rep(Pressure)	random	4	2, 4, 1, 3
Temperature	fixed	2	400, 420
Feed Rate	fixed	2	4, 7

Analysis of Variance for Ethylene, using Adjusted SS for Tests

Source	DF	Seq SS	Adj SS	Adj MS	F	P
Pressure	1	0.0001800	0.0001800	0.0001800	185.66	**0.005**
Rep(Pressure)	2	0.0000019	0.0000019	0.0000010	0.77	0.498
Temperature	1	0.0000137	0.0000137	0.0000137	10.89	**0.013**
Feed Rate	1	0.0000040	0.0000040	0.0000040	3.16	0.119
Pressure*Temperature	1	0.0000015	0.0000015	0.0000015	1.21	0.308
Pressure*Feed Rate	1	0.0000000	0.0000000	0.0000000	0.01	0.924
Temperature*Feed Rate	1	0.0000002	0.0000002	0.0000002	0.14	0.719
Error	7	0.0000088	0.0000088	0.0000013		
Total	15	0.0002101				

S = 0.00112144 R-Sq = 95.81% R-Sq(adj) = 91.02%

Unusual Observations for Ethylene

Obs	Ethylene	Fit	SE Fit	Residual	St Resid
16	0.020931	0.019430	0.000841	0.001501	2.02 R

R denotes an observation with a large standardized residual.

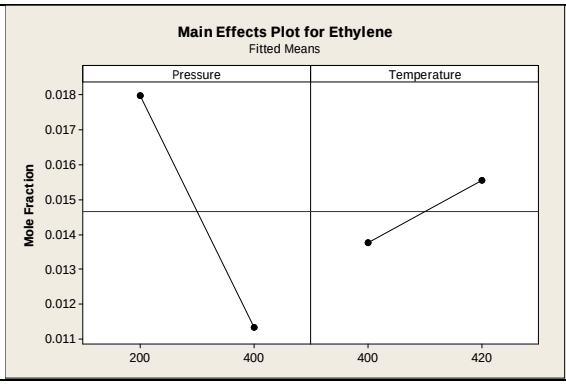

Factor	Type	Levels	Values
Pressure	fixed	2	200, 400
Rep(Pressure)	random	4	2, 4, 1, 3
Temperature	fixed	2	400, 420
Feed Rate	fixed	2	4, 7

Analysis of Variance for Propane, using Adjusted SS for Tests

Source	DF	Seq SS	Adj SS	Adj MS	F	P
Pressure	1	0.0006050	0.0006050	0.0006050	177.46	**0.006**
Rep(Pressure)	2	0.0000068	0.0000068	0.0000034	0.06	0.941
Temperature	1	0.0004673	0.0004673	0.0004673	8.41	**0.023**
Feed Rate	1	0.0000194	0.0000194	0.0000194	0.35	0.573
Pressure*Temperature	1	0.0000064	0.0000064	0.0000064	0.11	0.745
Pressure*Feed Rate	1	0.0000018	0.0000018	0.0000018	0.03	0.862
Temperature*Feed Rate	1	0.0000080	0.0000080	0.0000080	0.14	0.716
Error	7	0.0003889	0.0003889	0.0000556		
Total	15	0.0015035				

S = 0.00745319 R-Sq = 74.14% R-Sq(adj) = 44.58%

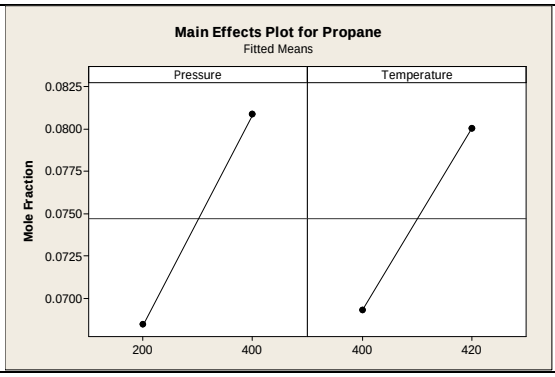

Factor	Type	Levels	Values
Pressure	fixed	2	200, 400
Rep(Pressure)	random	4	2, 4, 1, 3
Temperature	fixed	2	400, 420
Feed Rate	fixed	2	4, 7

Analysis of Variance for Propylene, using Adjusted SS for Tests

Source	DF	Seq SS	Adj SS	Adj MS	F	P
Pressure	1	0.0000122	0.0000122	0.0000122	1.45	0.352
Rep(Pressure)	2	0.0000168	0.0000168	0.0000084	0.19	0.833
Temperature	1	0.0028396	0.0028396	0.0028396	63.10	**0.000**
Feed Rate	1	0.0000479	0.0000479	0.0000479	1.06	0.336
Pressure*Temperature	1	0.0000380	0.0000380	0.0000380	0.84	0.389
Pressure*Feed Rate	1	0.0000734	0.0000734	0.0000734	1.63	0.242
Temperature*Feed Rate	1	0.0000124	0.0000124	0.0000124	0.28	0.616
Error	7	0.0003150	0.0003150	0.0000450		
Total	15	0.0033553				

S = 0.00670816 R-Sq = 90.61% R-Sq(adj) = 79.88%

Unusual Observations for Propylene

Obs	Propylene	Fit	SE Fit	Residual	St Resid
1	0.059906	0.070914	0.005031	-0.011008	-2.48 R

R denotes an observation with a large standardized residual.

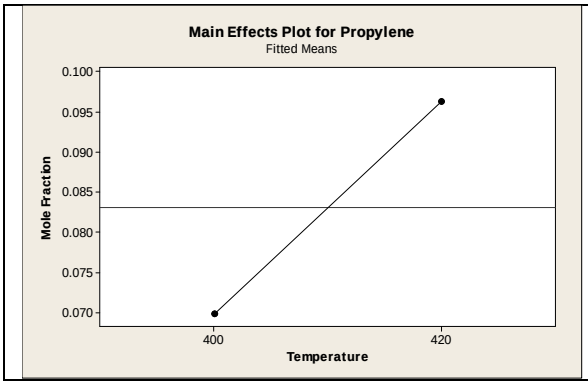

Factor	Type	Levels	Values
Pressure	fixed	2	200, 400
Rep(Pressure)	random	4	2, 4, 1, 3
Temperature	fixed	2	400, 420
Feed Rate	fixed	2	4, 7

Analysis of Variance for Butene, using Adjusted SS for Tests

Source	DF	Seq SS	Adj SS	Adj MS	F	P
Pressure	1	0.0000760	0.0000760	0.0000760	3.66	0.196
Rep(Pressure)	2	0.0000415	0.0000415	0.0000207	0.44	0.658
Temperature	1	0.0014238	0.0014238	0.0014238	30.51	**0.001**
Feed Rate	1	0.0000068	0.0000068	0.0000068	0.15	0.714
Pressure*Temperature	1	0.0000719	0.0000719	0.0000719	1.54	0.255
Pressure*Feed Rate	1	0.0000603	0.0000603	0.0000603	1.29	0.293
Temperature*Feed Rate	1	0.0000007	0.0000007	0.0000007	0.02	0.906
Error	7	0.0003266	0.0003266	0.0000467		
Total	15	0.0020076				

S = 0.00683106 R-Sq = 83.73% R-Sq(adj) = 65.13%

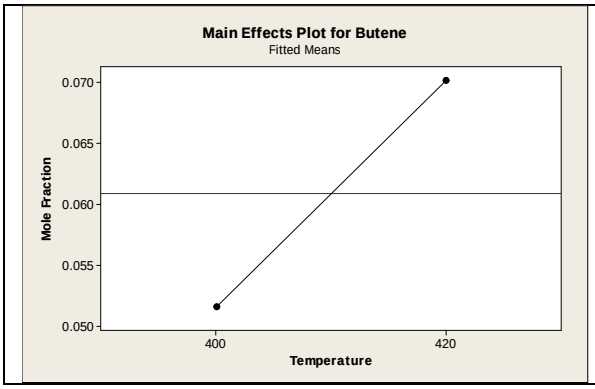

Factor	Type	Levels	Values
Pressure	fixed	2	200, 400
Rep(Pressure)	random	4	2, 4, 1, 3
Temperature	fixed	2	400, 420
Feed Rate	fixed	2	4, 7

Analysis of Variance for Pentane, using Adjusted SS for Tests

Source	DF	Seq SS	Adj SS	Adj MS	F	P
Pressure	1	0.0000007	0.0000007	0.0000007	0.04	0.859
Rep(Pressure)	2	0.0000362	0.0000362	0.0000181	0.46	0.648
Temperature	1	0.0005721	0.0005721	0.0005721	14.58	**0.007**
Feed Rate	1	0.0000120	0.0000120	0.0000120	0.31	0.597
Pressure*Temperature	1	0.0000055	0.0000055	0.0000055	0.14	0.718
Pressure*Feed Rate	1	0.0000427	0.0000427	0.0000427	1.09	0.332
Temperature*Feed Rate	1	0.0000047	0.0000047	0.0000047	0.12	0.740
Error	7	0.0002746	0.0002746	0.0000392		
Total	15	0.0009486				

S = 0.00626337 R-Sq = 71.05% R-Sq(adj) = 37.96%

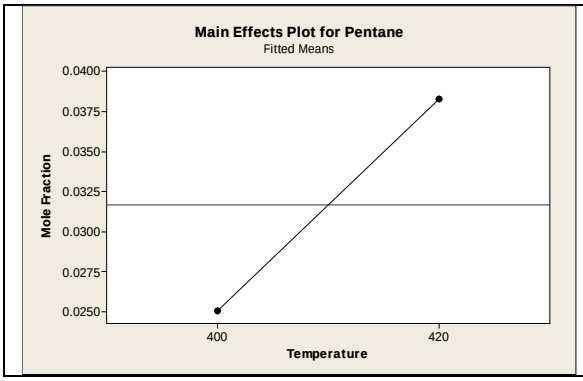

Factor	Type	Levels	Values
Pressure	fixed	2	200, 400
Rep(Pressure)	random	4	2, 4, 1, 3
Temperature	fixed	2	400, 420
Feed Rate	fixed	2	4, 7

Analysis of Variance for Hexane, using Adjusted SS for Tests

Source	DF	Seq SS	Adj SS	Adj MS	F	P
Pressure	1	0.0000026	0.0000026	0.0000026	1.10	0.405
Rep(Pressure)	2	0.0000047	0.0000047	0.0000024	0.40	0.686
Temperature	1	0.0000930	0.0000930	0.0000930	15.64	**0.005**
Feed Rate	1	0.0000009	0.0000009	0.0000009	0.15	0.714
Pressure*Temperature	1	0.0000025	0.0000025	0.0000025	0.42	0.535
Pressure*Feed Rate	1	0.0000000	0.0000000	0.0000000	0.01	0.943
Temperature*Feed Rate	1	0.0000011	0.0000011	0.0000011	0.19	0.676
Error	7	0.0000416	0.0000416	0.0000059		
Total	15	0.0001465				

S = 0.00243839 R-Sq = 71.59% R-Sq(adj) = 39.12%

Unusual Observations for Hexane

Obs	Hexane	Fit	SE Fit	Residual	St Resid
2	0.014414	0.010884	0.001829	0.003530	2.19 R

R denotes an observation with a large standardized residual.

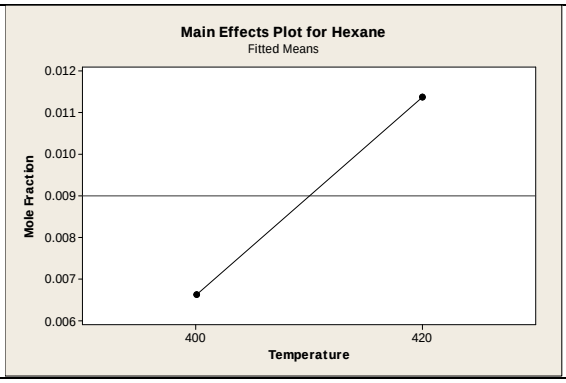

APPENDIX L

SPLIT-PLOT DOE - LIQUID PRODUCT STATISICAL ANALYSIS

Soybean Oil Split-Plot DOE, Organic Liquid Product (OLP) Yield and Acid Number												
Std	Run	Center	Rep	Pressure	Temperature	Feed Rate	Experiment	Yield (Wt% of Oil Fed)				Acid No.
Order	Order	Pt		(psig)	(°C)	(L/hr)	ID	OLP<150	150<OLP<250	OLP>250	OLP Total	(mg KOH/g OLP)
1	4	1	1	400	400	4	A	3.9%	8.0%	81.7%	93.7%	121.7
2	2	1	1	400	420	4	B	9.2%	17.5%	60.1%	86.8%	114.0
3	3	1	1	400	400	7	C	3.0%	5.9%	85.4%	94.3%	103.0
4	1	1	1	400	420	7	D	5.7%	13.0%	72.2%	90.9%	112.7
5	6	1	2	200	400	4	E	4.0%	10.1%	79.6%	93.7%	125.1
6	7	1	2	200	420	4	F	9.8%	22.2%	48.5%	80.4%	108.4
7	5	1	2	200	400	7	G	3.5%	7.4%	82.4%	93.3%	115.3
8	8	1	2	200	420	7	H	3.9%	14.5%	68.1%	86.5%	97.0
9	15	1	3	400	400	4	AA	2.2%	9.1%	85.3%	96.6%	107.3
10	14	1	3	400	420	4	BB	10.0%	17.5%	60.9%	88.4%	117.4
11	16	1	3	400	400	7	CC	2.9%	7.1%	86.5%	96.4%	106.6
12	13	1	3	400	420	7	DD	6.8%	12.7%	71.6%	91.1%	105.9
13	11	1	4	200	400	4	EE	4.7%	10.7%	77.2%	92.6%	116.9
14	12	1	4	200	420	4	FF	10.3%	21.3%	52.7%	84.3%	105.3
15	10	1	4	200	400	7	GG	2.1%	5.4%	85.6%	93.1%	104.2
16	9	1	4	200	420	7	HH	5.9%	17.7%	67.6%	91.2%	106.7

Factor	Type	Levels	Values
Pressure	fixed	2	200, 400
Rep(Pressure)	random	4	2, 4, 1, 3
Temperature	fixed	2	400, 420
Feed Rate	fixed	2	4, 7

Analysis of Variance for OLP, using Adjusted SS for Tests

Source	DF	Seq SS	Adj SS	Adj MS	F	P
Pressure	1	0.0033171	0.0033171	0.0033171	5.20	0.150
Rep(Pressure)	2	0.0012757	0.0012757	0.0006378	2.60	0.143
Temperature	1	0.0182487	0.0182487	0.0182487	74.27	**0.000**
Feed Rate	1	0.0025952	0.0025952	0.0025952	10.56	**0.014**
Pressure*Temperature	1	0.0002492	0.0002492	0.0002492	1.01	0.347
Pressure*Feed Rate	1	0.0002287	0.0002287	0.0002287	0.93	0.367
Temperature*Feed Rate	1	0.0022930	0.0022930	0.0022930	9.33	**0.018**
Error	7	0.0017199	0.0017199	0.0002457		
Total	15	0.0299276				

S = 0.0156750 R-Sq = 94.25% R-Sq(adj) = 87.68%

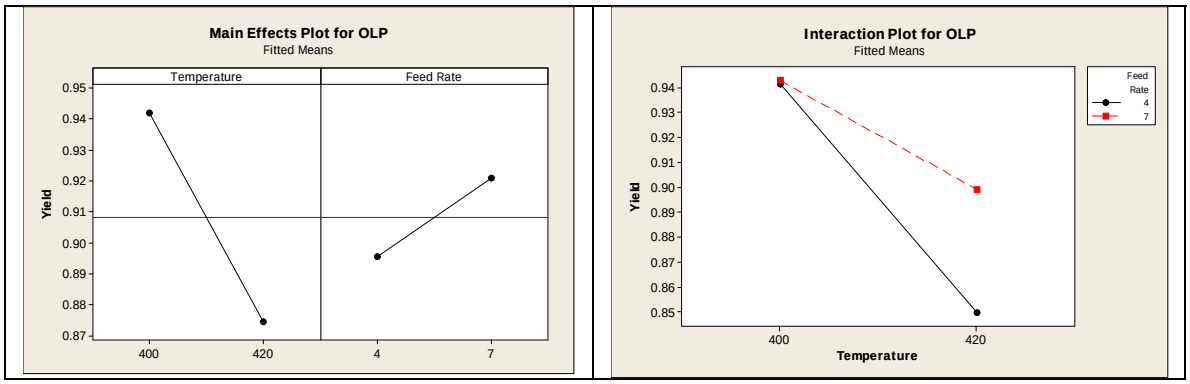

Factor	Type	Levels	Values
Pressure	fixed	2	200, 400
Rep(Pressure)	random	4	2, 4, 1, 3
Temperature	fixed	2	400, 420
Feed Rate	fixed	2	4, 7

Analysis of Variance for OLP<150, using Adjusted SS for Tests

Source	DF	Seq SS	Adj SS	Adj MS	F	P
Pressure	1	0.0000015	0.0000015	0.0000015	0.06	0.828
Rep(Pressure)	2	0.0000481	0.0000481	0.0000241	0.32	0.738
Temperature	1	0.0077730	0.0077730	0.0077730	102.65	**0.000**
Feed Rate	1	0.0025673	0.0025673	0.0025673	33.91	**0.001**
Pressure*Temperature	1	0.0000942	0.0000942	0.0000942	1.24	0.302
Pressure*Feed Rate	1	0.0002527	0.0002527	0.0002527	3.34	0.110
Temperature*Feed Rate	1	0.0011671	0.0011671	0.0011671	15.41	**0.006**
Error	7	0.0005300	0.0005300	0.0000757		
Total	15	0.0124339				

S = 0.00870177 R-Sq = 95.74% R-Sq(adj) = 90.87%

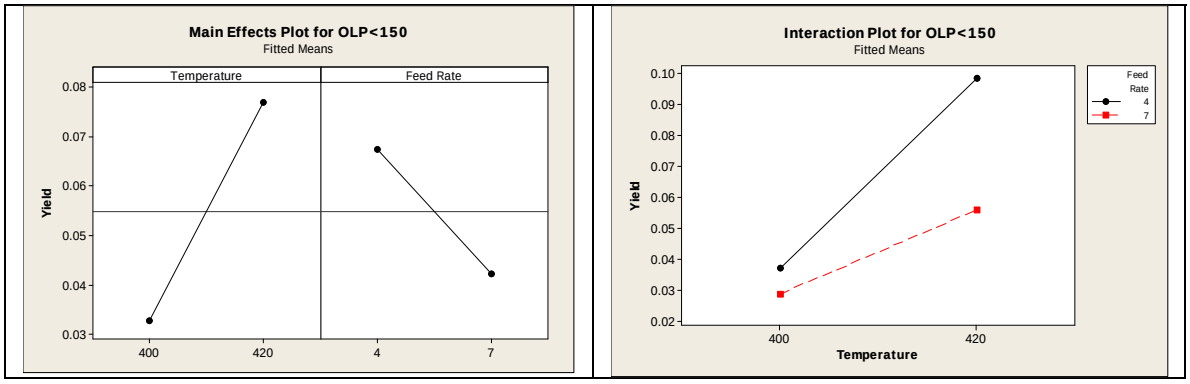

Factor	Type	Levels	Values
Pressure	fixed	2	200, 400
Rep(Pressure)	random	4	2, 4, 1, 3
Temperature	fixed	2	400, 420
Feed Rate	fixed	2	4, 7

Analysis of Variance for 150<OLP<250, using Adjusted SS for Tests

Source	DF	Seq SS	Adj SS	Adj MS	F	P
Pressure	1	0.0021103	0.0021103	0.0021103	70.73	**0.014**
Rep(Pressure)	2	0.0000597	0.0000597	0.0000298	0.25	0.788
Temperature	1	0.0331407	0.0331407	0.0331407	274.00	**0.000**
Feed Rate	1	0.0066943	0.0066943	0.0066943	55.35	**0.000**
Pressure*Temperature	1	0.0008296	0.0008296	0.0008296	6.86	**0.034**
Pressure*Feed Rate	1	0.0002019	0.0002019	0.0002019	1.67	0.237
Temperature*Feed Rate	1	0.0004416	0.0004416	0.0004416	3.65	0.098
Error	7	0.0008467	0.0008467	0.0001210		
Total	15	0.0443247				

S = 0.0109978 R-Sq = 98.09% R-Sq(adj) = 95.91%

Unusual Observations for 150<OLP<250

Obs	150<OLP<250	Fit	SE Fit	Residual	St Resid
16	0.176753	0.160856	0.008248	0.015897	2.19 R

R denotes an observation with a large standardized residual.

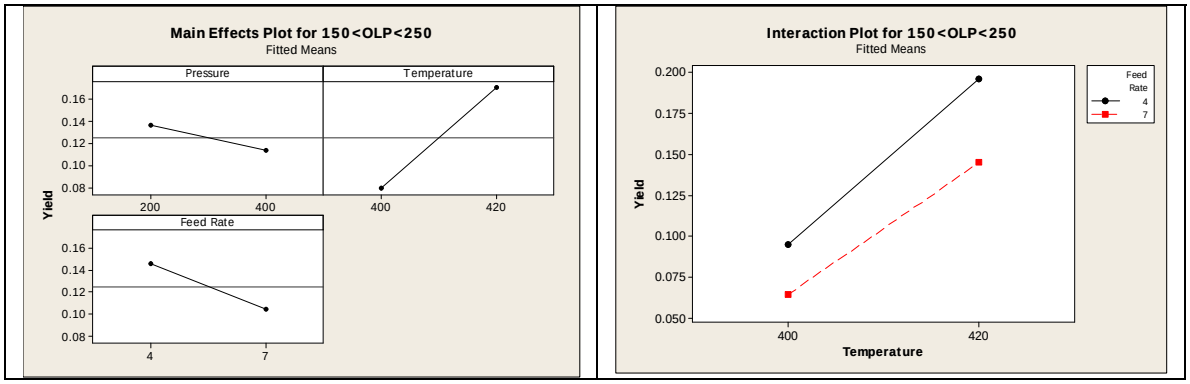

Factor	Type	Levels	Values
Pressure	fixed	2	200, 400
Rep(Pressure)	random	4	2, 4, 1, 3
Temperature	fixed	2	400, 420
Feed Rate	fixed	2	4, 7

Analysis of Variance for OLP>250, using Adjusted SS for Tests

Source	DF	Seq SS	Adj SS	Adj MS	F	P
Pressure	1	0.010972	0.010972	0.010972	39.14	**0.025**
Rep(Pressure)	2	0.000561	0.000561	0.000280	0.95	0.430
Temperature	1	0.164267	0.164267	0.164267	558.78	**0.000**
Feed Rate	1	0.033647	0.033647	0.033647	114.46	**0.000**
Pressure*Temperature	1	0.001217	0.001217	0.001217	4.14	0.081
Pressure*Feed Rate	1	0.002045	0.002045	0.002045	6.96	**0.034**
Temperature*Feed Rate	1	0.010622	0.010622	0.010622	36.13	**0.001**
Error	7	0.002058	0.002058	0.000294		
Total	15	0.225388				

S = 0.0171457 R-Sq = 99.09% R-Sq(adj) = 98.04%

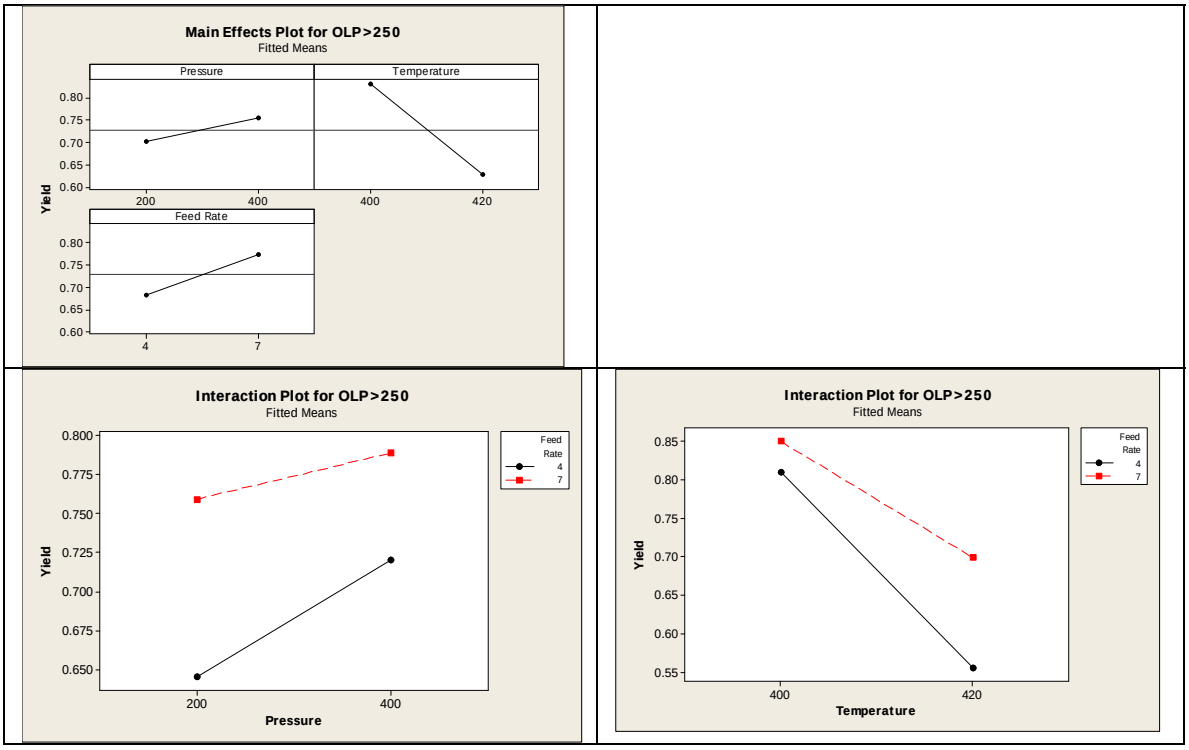

Factor	Type	Levels	Values
Pressure	fixed	2	200, 400
Rep(Pressure)	random	4	2, 4, 1, 3
Temperature	fixed	2	400, 420
Feed Rate	fixed	2	4, 7

Analysis of Variance for Acid No., using Adjusted SS for Tests

Source	DF	Seq SS	Adj SS	Adj MS	F	P
Pressure	1	5.84	5.84	5.84	0.26	0.663
Rep(Pressure)	2	45.51	45.51	22.76	0.66	0.547
Temperature	1	66.67	66.67	66.67	1.93	0.208
Feed Rate	1	260.53	260.53	260.53	7.53	**0.029**
Pressure*Temperature	1	192.73	192.73	192.73	5.57	0.050
Pressure*Feed Rate	1	0.01	0.01	0.01	0.00	0.990
Temperature*Feed Rate	1	22.57	22.57	22.57	0.65	0.446
Error	7	242.04	242.04	34.58		
Total	15	835.90				

S = 5.88029 R-Sq = 71.04% R-Sq(adj) = 37.95%

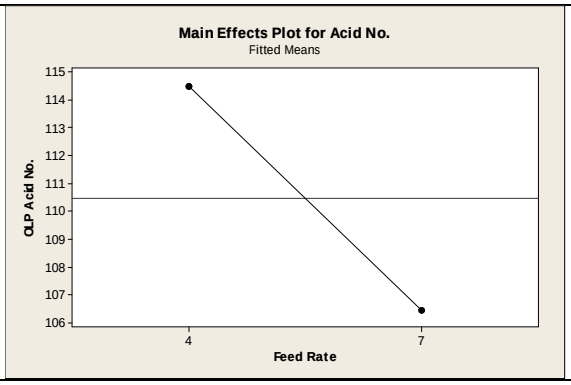

REFERENCES

[1] Swapnil Gandhi, "Catalytic Cracking of Soybean Oil to Produce a Biojet Fuel Similar to that of Aviation Fuel JP-8," University of North Dakota, Grand Forks, Thesis 2008.

[2] Yan Luo, "Evaluation of Thermal Cracking Conditions for Biojet Fuel Generation from Canola Oil/CME," University of North Dakota, Grand Forks, Thesis 2006.

[3] Institute of Shortening and Edible Oils, "Food Fats and Oils," July 7, 2006. [Online]. http://www.iseo.org/foodfats.htm

[4] United States Department of Agriculture, "Oilseeds: World Markets and Trade," Foreign Agricultural Service, Circular Series FOP 12-10 2010.

[5] K.D Maher and D.C. Bressler, "Pyrolysis of triglyceride materials for the production of renewable fuels and chemicals," *Bioresource Technology*, pp. 2351-2368, 2007.

[6] Ayhan Demirbas, "Progress and recent trends in biodiesel fuels," *Energy Conversion and Management*, pp. 14-34, 2009.

[7] James G Speight and Baki Ozum, *Petroleum Refining Processes*. New York: Marcel Dekker, Inc., 2002.

[8] Raphael O Idem, Sai P Katikaneni, and Narendra N Bakhshi, "Thermal Cracking of Canola Oil: Reaction Products in the Presence and Absence of Steam," *Energy & Fuels*, vol. 10, pp. 1150-1162, 1996.

[9] A. Kossiakoff and F.O. Rice, "Thermal Decomposition of Hydrocarbons, Resonance Stabilization and Isomerization of Free Radicals," *J. Am. Chem. Soc.*, vol. 65, pp. 590-595, 1943.

[10] Farhad Khorasheh and Murray R. Gray, "High-Pressure Thermal Cracking of n-Hexadecane," *Ind. Eng. Chem. Res.*, vol. 32, pp. 1853-1863, 1993.

[11] C C Change and S W Wan, "Chinas Motor Fuels from Tung Oil," *Ind. Eng. Chem.*, vol. 39, no. 12, pp. 1543-1548, 1947.

[12] J. W. Alencar, P. B. Alves, and A. A. Craveiro, "Pyrolysis of Tropical Vegetable Oil," *J. Agric. Food Chem.*, vol. 31, pp. 1268-1270, 1983.

[13] A. W. Schwab, G. J. Dykstra, E. Selke, S. C. Sorenson, and E. H. Pryde, "Diesel Fuel from Thermal Decomposition of Soybean Oil," *JAOCS*, vol. 65, no. 11, pp. 1781-1786, November 1988.

[14] Alena Kubatova et al., "Triacylglyceride Thermal Cracking: Pathways to Cyclic Hydrocarbons," *Energy & Fuels*, no. 26, pp. 672-685, 2012.

[15] Guozhong Wu, Yosuke Katsumura, Chihiro Matsuura, and Kenkichi Ishigure, "Comparison of Liquid-Phase and Gas-Phase Pure Thermal Cracking of n-Hexadecane," *Ind. Eng. Chem. Res.*, vol. 35, no. 12, pp. 4747-4754, 1996.

[16] K.D. Maher, K.M. Kirkwood, M.R. Gray, and D.C. Bressler, "Pyrolytic Decarboxylation and Cracking of Stearic Acid," *Ind. Eng. Chem. Res.*, pp. 5328-5336, 2008.

[17] Carl Branan, *Rules of Thumb for Chemical Engineers*, 4th ed.: Gulf Professional Publishing, 2005.

[18] Mohinder L. Nayyar, Ed., *Piping Handbook*, 6th ed.: McGraw-Hill, Inc, 1992.

[19] Don W. Green, Ed., *Perry's Chemical Engineers' Handbook*, 8th ed. New York: McGraw-Hill, 2008.

[20] Ayhan Demirbas and Huseyin Kara, "New Options for Conversion of Vegetable Oils to Alternative Fuels," *Energy Sources*, pp. 619-626, 2006.

[21] K.M. Doll, B.K. Sharma, P.A.Z. Suarez, and S.Z. Erhan, "Comparing biofuels obtained from pyrolysis, of soybean oil or soapstock, with traditional soybean biodiesel: density, kinematic viscosity, and surface tensions," *Energy & Fuels*, pp. 2061-2066, 2008.

[22] Gael D. Ulrich, *Chemical Engineering Process Design and Economics: A Practical Guide*, 2nd ed. Durham: Process Publishing, 2004.

[23] B. M. Fabuss, J. O. Smith, and C. N. Satterfield, "Rapid Thermal Cracking of n-Hexadecane at Elevated Pressures," *Adv. Pet. Chem. Refin.*, vol. 1, no. 4, pp. 293-299, October 1962.

[24] Feng Shubo, Sun Liming, and Lou Qiangkun, "A study on coke deposition and coking inhibitors during AGO pyrolysis in pulsed micro-reactor system," *Journal of Analytical and Applied Pyrolysis*, vol. 65, pp. 301-312, 2002.

[25] United States Department of Agriculture, "World Agricultural Production ," Foreign Agricultural Service, Circular Series WAP 12-10 2010.

[26] Evguenii Kozliak et al., "Non-catalytic cracking of jojoba oil to produce fuel and chemical by-products," *Industrial Crops and Products*, no. 43, pp. 386-392, 2013.